Fluorescent Ionene-Dye Nanoparticles by Electrostatic Self-Assembly

Dissertation

zur Erlangung des Grades

"Doktor der Naturwissenschaften"

am Fachbereich Chemie und Pharmazie der

Johannes-Gutenberg-Universität

in Mainz

Ümit Hakan YILDIZ

born in Ankara, Turkey

Mainz 2009

Contents

1 Introduction

"Supramolecular structures" fulfill many functions and posses a variety of architectures in nature. Due to versatility and potential, there has been a desire to study concepts for the synthetic design of supramolecular structures. "Supramolecular structure" here means a connection of multiple small building units by non-covalent interactions. Different types of interactions can be the origin for such non-covalent assemblies, both in natural and synthetic systems. Assemblies based on hydrophobic interactions are well-known, ranging from lipid-bilayer membranes over surfactant micelles to more complex variations. This classical "hydrophobic interaction" is based on the increase of entropy of water molecules when hydrophobic molecules or molecule parts associate rather than being molecularly distributed in the solution.[1,2] The shape of such supramolecular structures is determined by minimizing the interface energy under the constraint of the building block architecture. Further forces that can be the basis for the formation of assemblies are hydrogen bonding or metal coordination, which can be used to build a variety synthetic structure. Herein, the terms "supramolecular structure" or "assembly" usually are used to indicate a somehow defined object (narrowly distributed either in size and/or shape), while an "aggregate", which also consists of small building blocks, can be either defined or broadly distributed. In this thesis, nomenclature will be used accordingly.

Ionic interaction is the origin of assemblies such as DNA-histone complexes in biologic systems. Synthetically, solid self-assembled structures based on ionic interactions include polyelectrolyte surfactant complexes or dye surfactant complexes, that is, are formed due to a combination of electrostatic interaction between polyelectrolyte (or dye) and surfactant head group and hydrophobic interactions in-between surfactant tails. Due to microphase separation of ionic and hydrophobic moieties in the solid material, a variety of morphologies can thereby be created. Properties and applications discussed for such materials include coatings with ultra-low surface tension or special optical, electrical and mechanical properties. Thus, in this case the initial aggregation of molecules in solution is comparable to assemblies mentioned above, however, aggregation does not lead to finite sized objects but to solid bulk materials. (forces that stabilize finite sized assemblies will

be discussed below). The term polyelectrolyte surfactant "complex" and dye-surfactant "complex" we here used in reference to literature on those systems, where this is the common nomenclature. However, as this is not connected to the typical "complex formation" like in coordination chemistry of ions in solution, in the following we will rather refer to "aggregation" rather than "complex formation".

Two major types of ionic polyelectrolyte aggregates that “directly” form in solution by mixing the components and are stable in aqueous solution have been investigated in detail: Polyelectrolytes with multivalent inorganic salts show aggregation due to intermolecular bridging at high salt concentration while size and coordination capability of the counterion (e.g. whether Cu^{2+} or of Ca^{2+} is applied) play an additional decisive role. Further, aggregation of two oppositely charged polyelectrolytes yields aggregates that have been described as ladder-like for small molecular weight components and scrambled-egg-like for high molecular weight components. Upon further addition of counterions, e.g. Ca^{2+} ions to polyacrylic acid, precipitation occurs. (more details on interaction forces in these systems see chapter background..) In both cases, polyelectrolytes with multivalent inorganic ions and inter-polyelectrolyte complexes, possibilities to direct the structure are limited and the size distribution of the aggregates is usually broad.

Aggregate formation using polyelectrolytes may have certain advantages in tuning physical properties of the supramolecular assemblies through variation of charge density, flexibility and hydrophobicity of the polyelectrolyte and the oppositely charged molecules. For an aggregation not to lead to broadly distributed aggregates, but assemblies of a defined size and/or shape, building blocks however need to be able to influence the structure of the aggregate or even induce a certain structure. Simple small metal ions and flexible linear polymer chains, evidently, are not capable to realize that. Thus, in these cases aggregate formation may rather be seen in analogy to a precipitation due to decreased solvent quality. "Decreased solvent quality" is caused by the counterion associating with the polyelectrolyte due to electrostatics, so called "counterion condensation" and thereby neutralizing the charges. In certain cases, a thereby neutralized, that is less charged, polymer chain my show a lower solubility. However, it was shown that also for systems that remain hydrophilic such aggregation is observed and

it was shown that this process is endothermic. Thus, it is also not a pure electrostatic effect, but again entropically driven. This can again be due to the change in entropy of water molecules. The interplay of energetic and entropic effects in such aggregation was for example discussed by Muthukumar [3]

Recently it was shown that assemblies with narrow size distribution and with different shapes can be formed using polyelectrolytes of certain architectures in combination with stiff, multivalent organic counterions.[4,5] This was called "electrostatic self-assembly", in analogy to the term "self assembly" being commonly used for the formation of micelles from surfactants and in addition indicating that the main driving force is electrostatic in nature, that is, the attraction of polyelectrolyte and counterion due to opposite charge. This is thus different to the "electrostatic self assembly" that refers to the above mentioned layer-by-layer deposition. Although the same term is used for that method in literature, we here stay with the classical definition of self-assembly: that is, assemblies being formed by simply adding the building blocks in solution (one type or multiple types of building blocks) with no further external forces, alternating treatment or likewise. It was found that in this type of “electrostatic self-assembly” the interplay of electrostatic interaction between counterion and macroion and additional mutual secondary interaction of the counterions can yield narrowly distributed assemblies in solution. Association of poly(amidoamine) (PAMAM) dendrimers with the two isomeric naphthalene dicarboxylic acids resulted in cylindrical and spherical aggregates. Association of the dendrimer macroions with oppositely charged dyes yielded cylindrical aggregates with narrow size distribution. These aggregates could be switched “off” by changing the pH such that the dendrimer amine groups became uncharged and “on” again by re-charging the dendrimer through pH. In a similar system, rather than secondary interaction, the geometry of counterion and polyelectrolyte also yielded aggregates of different shapes.[6] Interestingly, these are stable in aqueous solution, at least for certain molar ratios of the components. It was concluded that this is due to these aggregates carrying charges and thereby being stabilized in analogy to a charged colloid. (More details see within this thesis).

It is thus highly interesting to investigate in how far also “simple” linear homo-polyelectrolytes can be used for the formation of defined assemblies in aqueous solution.

Association of linear polyelectrolytes with charged aromatic dye molecules was already studied many years ago by UV-VIS measurements.[7-11] These studies along these lines followed, usually however focusing on spectroscopic properties rather than the structures formed.

In this work we employ electrostatic self-assembly to form polyelectrolyte-dye complexes and to characterize the aggregation behavior of dye molecules and colloidal properties of resulting complexes. For this purpose four different 1,4 Diazabicyclo[2.2.2] octane based polyionenes with various spacer groups, have been synthesized. Sodium pyrenetetrasulfonate (PY) has been chosen as anionic probe. Influence of various parameters such as polyelectrolyte architecture, addition of salt, composition of components have been investigated through light scattering, UV-Vis, fluorescence spectroscopy, confocal and atomic force microscopy.

2 Theory and Background

One particular feature of polyelectrolytes is their ability to form complexes with oppositely charged species. This phenomenon has been known from the precipitation behavior of proteins.[12,13] The contribution of Micheals and Miekka was the first systematic research about polyelectrolyte complex formation using synthetic polyelectrolytes.[14,15] Scientific and industrial interest in polyelectrolyte complexes followed.[16-22] Polyelectrolyte complexes can be classified into complexes of cationic and anionic polyelectrolytes (PECs) and complexes of polyelectrolytes and surfactants (PE-surf). Although there are numerous procedures to form a complex, the easiest way of PEC or PE-surf preparation is to mix aqueous solutions of two the oppositely charged species. The various methods in complex preparation protocols brings unique advances in the field of applications of PECs. The well-known layer-by-layer technique or in other words "electrostatic self-assembly" yields multilayer films.[23] Recent advances on multilayer assemblies show that hollow nanospheres and capsules may be obtained effectively by this method as well.[24,25]

The mechanism of complex formation of PECs and PE-surf is governed self-assembly processes. In particular, in PE-surf complex formation, the cooperative binding effects are predominant. (Binding is cooperative if the affinity of ligands increases with the amount of ligand already bound.) Due to cooperative binding, highly ordered mesophase structures are obtained from PE-surf complexes.[26-28] In contrast to this case, the resultant complex morphology in PECs is rather disordered.

This chapter primarily reviews the theoretical background of complex formation and synthesis of polyelectrolyte (Section 2.1 and 2.2). The fundamentals of conjugated polymers will be discussed in Section 2.3 serving as introduction for chapter 6. Subsequent sections 2.3.1 and 2.3.2 mainly deal with the theoretical background of the characterization methods.

2.1 Polyelectrolyte Complexes

2.1.1 Polyelectrolyte-Polyelectrolyte Complexes

PEC formation is the consequence of fast reactions between oppositely charged molecules. Due to the possibility to vary preparation conditions and components, complex formation results in a variety of structures. As borderline cases for the resulting structures of PECs two models were suggested i) the ladder like structure and ii) the scrambled egg model. PEC formation between polyions with weak ionic groups (such as carboxylic acid groups) and significantly different molecular weights in non stoichiometric systems results in soluble complexes, which are structured according to the ladder model, consisting of hydrophilic single stranded and hydrophobic double-stranded segments. Such systems were comprehensively studied by the groups of Tsuchida[29,30] and Kabanov.[31,32] However, in most examples PEC formation was carried out under conditions, which lead to highly aggregated systems (scrambled egg model) and often to macroscopic flocculation. Complex formation between polyanions and polycations with strong ionic groups (such as sulfonic acid moities) and/or comparable high molecular weight result in such structures. Because of high cooperativity of the ionic binding PEC formation take place far from the thermodynamic conditions even in the presence of salt. The aggregation is mainly controlled by the concentration of the component solutions. In highly diluted solutions ($< 10^{-4}$ g / ml) gel like particles of a colloidal nature are formed.

2.1.1.1 Mechanism of PECs Formation

Mixing solutions of polyanions and polycations leads to a spontaneous aggregation under release of the counterions (Figure 2.1). Complex formation can take place between polyacids and polybases and also between their neutralized metal and halogenide salts, respectively. For free polyelectrolytes, with high charge densities, because of the counterion condensation effect some amount of the counterions is located near the macroions. The driving force of the complex formation is mainly the gain in

entropy due to liberation of low molecular mass counterions. However, other interactions such as hydrogen bonding or hydrophobic ones and the enthalpy of the water molecules may play an additional role. The reaction of the polyelectrolyte complex formation can be described by the equation

$$(>-A^{-}c^{+})_n + (>-C^{+}a^{-})_m \Leftrightarrow (>-A^{-}C^{+})_x + (>-A^{-}c^{+})_{n-x} + (>-C^{+}a^{-})_{m-x} + xa^{-} + xc^{+}$$

where A^- and C^+ are the charged groups of the polyelectrolytes, a^- and c^+ the counterions

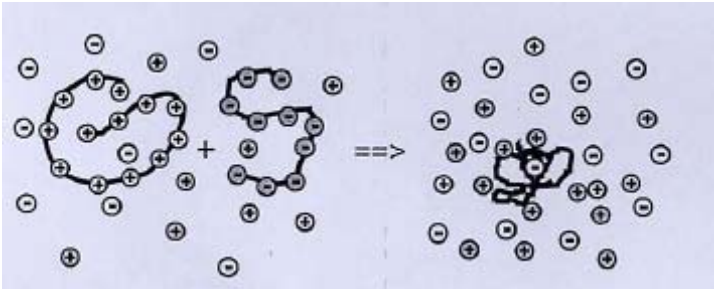

Figure 2.1.Scheme of polyelectrolyte complex formation.[33]

n and *m* the number of the anionic and cationic groups in the solution, *n/m* or *m/n* = X molar mixing ratio, $\theta = x/n$, $n < m$ or $\theta = x/m$, $m<n$, and θ the degree of conversion.

The degree of conversion describes in how far the ionic sites of the component in deficiency are completely bound by the oppositely charged polyelectrolyte or low molecular counterions remain partly in the complex. Another characteristic quantity of a PEC is its end point stoichiometry, i.e., the molar ratio $f_E = [A^-]_E / [C^+]_E$ at the end of the complex formation reaction. However, this ratio may be different at other mixing ratios *X* so that we have to introduce the stoichiometric factor $f(X) = [A^-]_x / [C^+]_x$ to describe the overall composition of the PEC structures at any mixing ratio.

The resultant morphology of PECs depends on the characteristic of the component and external reaction conditions (temperature, pH, ionic strenght). Two models were suggested for resulting structures[34] i) the ladderlike structure, in which molecular level complex formation takes place via conformational adaptation ii) the scrambled egg model where many chains are incorporated into a particle (Figure 2.2)

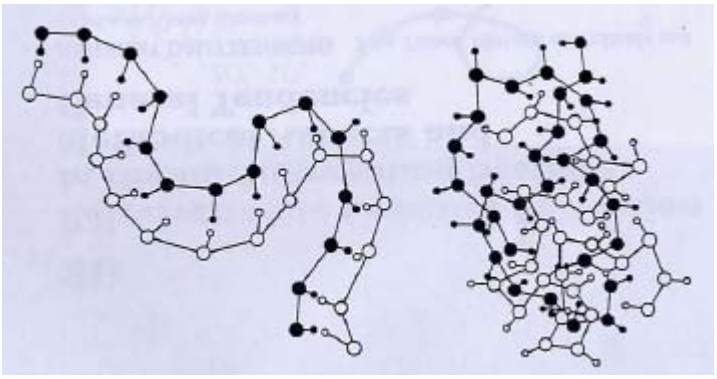

Figure 2.2. Structure models: ladder and scrambled egg structure.[33,34]

2.1.2 Polyelectrolyte-Surfactant Complexes

The complexation of polyelectrolytes with surfactants has been intensively investigated for many years. Solution structures were reviewed by Goddard.[35] Starting with work by Antonietti[36] polyelectrolyte surfactant complexes (PE-surf) in the solid state have also become of increasing interest.

2.1.2.1 PE-Surfs in Solid State

The principle of PE-suf complexation allows the design and simple synthesis of a variety of ordered structures.[37-42] The variation of polyelectrolyte properties (backbone, tacticity, distance between charges, hydrophobicity) as well as surfactant properties (length and number of tails, disk geometry, fluorinated surfactants) enables fine tuning of phase morphologies as well as of the related mechanical, electrical and optical properties. Due to the surfactants the PE complex consist of a polar backbone (a string of ion pairs) on the one hand and the hydrophobic tails on the other hand and demixing in the solid state and mesophase formation are to be expected (surface acive agents exhibit a number of ordered phases which are the basis of the structure-forming abilities of the polyelectrolyte-surfactant complexes).

The resulting structure type (cubic, lamellar or cylindrical) is determined by the delicate balance of the volume fractions of ionic and alkyl-mesophase, the interface (determined by number of the surfactant), the curvature of the interface, and several other factors

related to the molecular geometry of both surfactant and polyelectrolyte. A typical example of the order phenomena in solid PE-surfs is provided by the complex between polyacrylic acid and dodecyltrimethylammonium counterions (PAA-C_{12})[36]. Although completely amorphous, on local length scale PAA-C_{12} exhibits a set of extremely narrow small angle scattering peaks which can be indexed according to the face centered cubic (FCC) lattice. According to the orientation dependent mechanical and optical properties of these polymer phase were proposed as cylindrical domains (Figure 2.3 a).

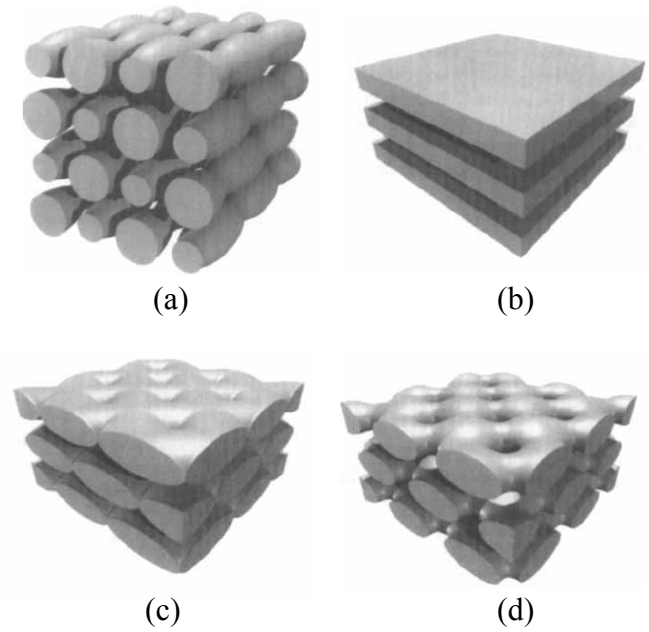

Figure 2.3. a) Computer model of the phase morphology of PAA-C_{12}. The ionic phase consists of cylinders with a diameter of ca. 2 nm. Cubic undulations occur due to a mismatch of packing of molecules and interface area, b) Simple lamellar (PSS-C_{14}), c) "Mattress"- phase (PSS-C_{18}), d) "Perforated layer"- phase (PSS-C_{20})[36]

In addition to a cylindrical phase cubic and lamellar morphologies are also observed. They are often not easily distinguished since the fundamental symmetry and the symmetry of the undulations frequently belong to the different classes as seen for PAA-C_{12}. A good example for different lamellar modifications is given by in the examination of a series of complexes between polystyrenesulfonate (PSS) and various commercially available alkyltrimethylammonium counterions (C_{12}-C_{18}). All these

complexes exhibit basically a lamellar morphology, but show different interface undulations which are fine-tuned by the relative volume fractions of both phases, i.e., the resulting spontaneous curvature of the interface. PSS-C_{14} is plainly lamellar whereas for PSS-C_{18} the undulations of the interface are big enough to localize to an FCC arrangement of the maxima which are still embedded in lamellar layers ("mattress-phase"). The next homologue, PSS-C_{20}, shows that its morphology characterized by a regular piercing of the ionic layers by the alkyl phase ("perforated layer phase"). Figure 3b-d shows the computer model of the phase morphology of corresponding PSS-C_x complexes.

2.1.2.2 PE-Surf in the Solution

Interactions between polymers and surfactants in aqueous solutions have attracted significant interest because of their widespread application and relatively complex behaviors. Numerous studies have been devoted to advancing the fundamental understanding of the physics governing these interactions.[43-56] For oppositely charged polyelectrolytes and surfactant systems, the strong electrostatic attraction between the charged groups is clearly observable and occurs at concentrations several orders of magnitude below the critical micelle concentration (cmc). The interaction is generally regarded as an ion-exchange process where the electrostatic forces of interaction are enhanced by the aggregation of alkyl chains of the bound surfactant molecules. Although the numbers of variables which affect the binding mechanisms are countless, modern calorimetric methods such as the micro calorimetric technique[44-49, 54, 56] are sensitive enough to monitor heat changes. Isothermal titration calorimetry (ITC) can be used to extract the thermodynamic parameters such as enthalpy (ΔH), entropy (ΔS), Gibbs energy (ΔG), of the complex formation and heat capacity (C_p) which are critical to understanding of polymer/surfactant interactions.

The current understanding on the interaction between fully ionized polyelectrolyte such as polyacrylic acid (PAA) and cationic surfactant, dodecyltrimethylammonium bromide (DTAB), is that the polymer chains induce the formation of bound micelles. The surfactant binds to the polymer independently from the

degree of neutralization (α) of polymer. However the biding mechanism varies with α. When α is lower than a critical value (α_c), the hydrocarbon chains DTAB cooperatively bind to the polar segment of PAA driven by hydrophobic interaction at very low DTAB concentration ($C_{DTAB} < 0.2$ mM). In this binding region the ITC profile exhibits a significant exothermic peak and the mixture precipitates, which is attributed to the inter-chain complexation via hydrogen bonding induced by the binding. The precipitate is soon resolubilized with further addition of surfactant as more DTAB micelles are bound on the polymer backbones with their ionic head groups extending outwards. When $\alpha > \alpha_c$, the hydrophobic binding ceases as the polymer is progressively ionized and DTAB binds to the charged polymer chains driven by the electrostatic attraction. The counterions condensed on the charged polymer chains are released via the ion exchange process, resulting in an endothermic minimum on the ITC profile. The value of α_c determined from ITC is approximately 0.3, which is reasonably close to the theoretical value derived from Mannig's counterion condensation theory (approximately 0.35).The thermodynamic parameters derived from ITC measurements suggest that the electrostatic binding is an endothermic process driven by entropy. The positive entropy is attributed to the recovery of translational entropy of released counterions by the bound surfactant.

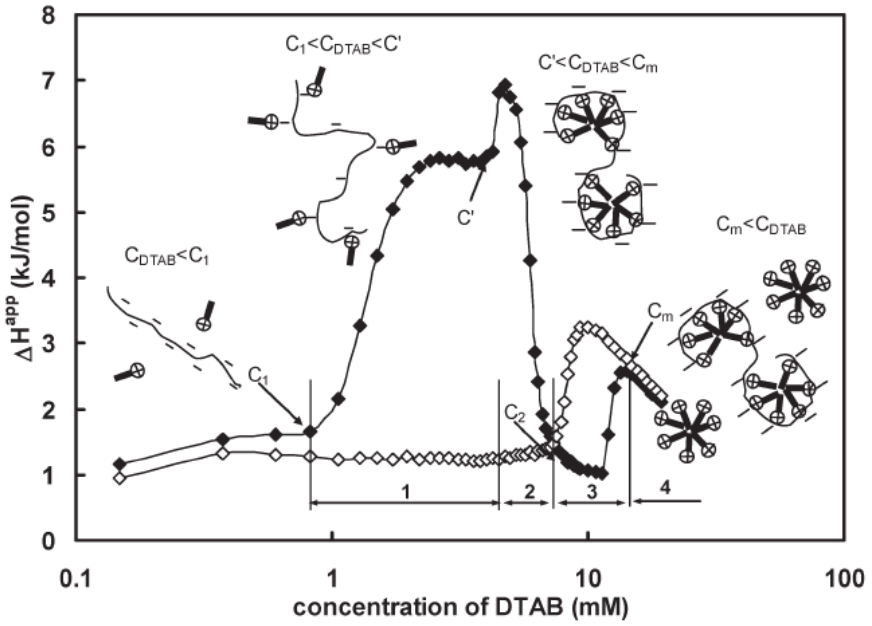

Figure 2.4.Classification of binding regime and schematic binding mechanism of the PA/DoTab system (◆) binding isotherm in 0.1 M NaCl solution (◊) dilution curve in 0.1 M NaCl solution.[56]

The ITC curves for the titrations performed in different salt conditions show that addition of salt screens the electrostatic repulsion between the surfactant head group and attraction between oppositely charged polymer chains and surfactant molecules. This favors the formation of free micelles, which weakens the binding of the surfactant onto the polymers. The ITC thermogram and proposed structures during the binding interaction are shown in Figure 2.4.

2.1.3 Polyelectrolyte-Dye Complexes

Recently, efforts have been devoted to the complex formation of DNA-dye[57]and polyelectrolyte-dye[58-62] couples and investigation of their optical, photo physical applications in solid state. The polyelectrolyte enhanced dye aggregation has strengthened and diversified the functionality and applicability of ultra thin films or multi

layer systems for surface coating and patterning applications.[63-66] Beside the efforts regarding polyelectrolyte-dye complexes at solid phase, investigation of solution properties of these systems have received considerable attention as well. Basically polyelectrolyte-dye complexes provide useful information about the nature and the mechanism of the binding process. Binding of small molecules to the polyelectrolyte has been investigated in the light of cooperative binding mechanism[78]. In particular the interactions between water-soluble dyes and bio or synthetic polyelectrolytes have been interpreted from the point of view of cooperative binding[127-130.] Although electrostatic forces are a major contributor for the formation of polyelectrolyte-dye complexes, overall binding is the result of orchestrating of π–π interactions (π–π stacking) and electrostatic forces. Understanding the fundamentals of polyelectrolyte-dye complexes in solution enables to deduce binding and transport mechanism of more complicated systems such as DNA-surfactant, DNA-amphiphiles and protein-surfactant complexes not only in vitro conditions but also in living systems.[131-137] Recent advances reveal that self-assembly with oppositely charged molecules might provide functional materials such as chemo-biosensors,[70,71] nanowires,[72-75] light harvesting complexes.[76,77] Although synthetic methods to obtain well defined supramolecular complexes have been revealed still there are some challenges which are not fulfilled yet such as size control of complexes and facile synthetic procedures.

2.2 System Components

2.2.1 Ionenes

The generic name "ionene" is used for polymeric quaternary ammonium compounds that contain quaternary nitrogen atoms in the macromolecular main chain. The first report about the self condensation of (ω-bromoalkyl) diethylamine to produce linear cationic polyelectrolytes via a step growth polymerization is from 1933.[79,80] Since then, ionenes can be synthesized by either the Menschutkin reaction[81,82] of alkyl dihalide and ditertiary amine or by the reaction of an aminoalkylhalide with itself to form the linear quaternary polyelectrolyte. Rembaum et al. used the Menschutkin reaction to synthesize ionenes with a variety of methylene spacers.[83-85] The '*x,y-ionene*' notation is commonly used to name ionenes, in this notation x and y represent the number of methylene units of diamine and dihalide monomers respectively. No polymer is formed when the integers *x* and *y* are less than 3 and various parameters such as polarity of the solvent,[86-88] steric hindrance of substituents,[89,90] nucleophilicity[91,92] and mobility of leaving groups[93] have predominant effect on polymerization reactions and resultant ionenes. When *x* and *y* are 3 or larger one could obtain polymers with a weight-average molecular mass up to M_W = 40,000 g/mol. One of the highest molecular masses was achieved with 3-4ionene (from the reaction of *N,N,N',N'*-tetramethyl-1,3-propanediamine with 1,4-dibromobutane). Similar results and highest charge density were obtained with 3,3-ionene which also can be prepared from 3,3-dimethylaminopropyl chloride. Intercharge distances can be tailored within a wide range.

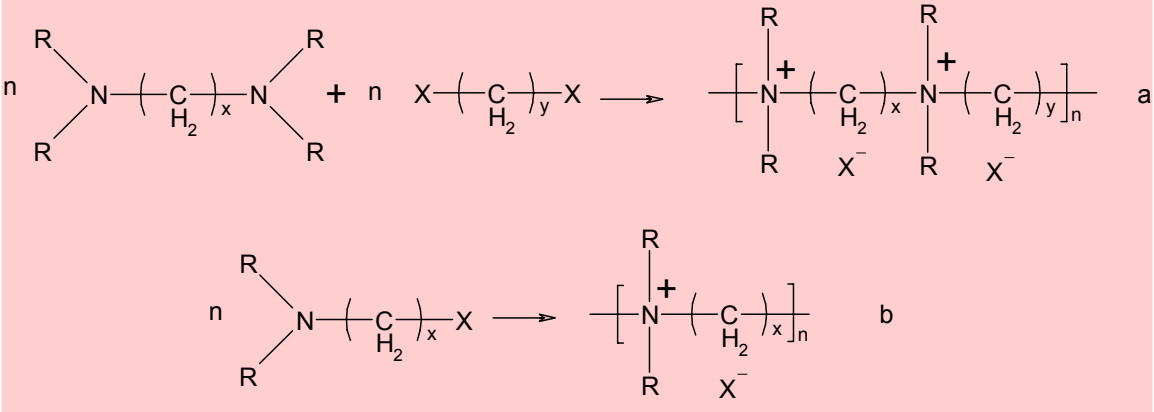

Scheme 2.1. a) Synthesis of ionenes by polyaddition of di-*tert*-amines and dihalides b) and by reaction of aminoalkylhalides.

The reaction of epichlorohydrin with bifunctional secondary amines leads to linear cationic polyelectrolytes with quaternized nitrogen in the backbone too (see Scheme 2.2 a). The polymers have number-average molecular masses of about M_n = 10,000 g/mol. Novel ionenes were obtained from the reaction of bispyrylium salts with diamines (see Scheme 2.2b).[94]

Ionenes can also be synthesized by ring opening polymerization of suitable quaternary salts or betaines of *N*-alkylazetidines. Solution polymerization of polymerization of N,N-dialkylazetidinium salts leads to ionenes via Menschutkin reaction of the intermediate N,N-dialkyl-3-haloprpylamine (see Scheme 2.2c). These polymers are soluble in polar organic solvent. Furthermore, ring opening azetidinium sulfobetadines in the bulk yields zwitterionic ionenes with pendent SO_3^- groups (see Scheme 2.2d) which are soluble in organic solvent but insoluble in water.

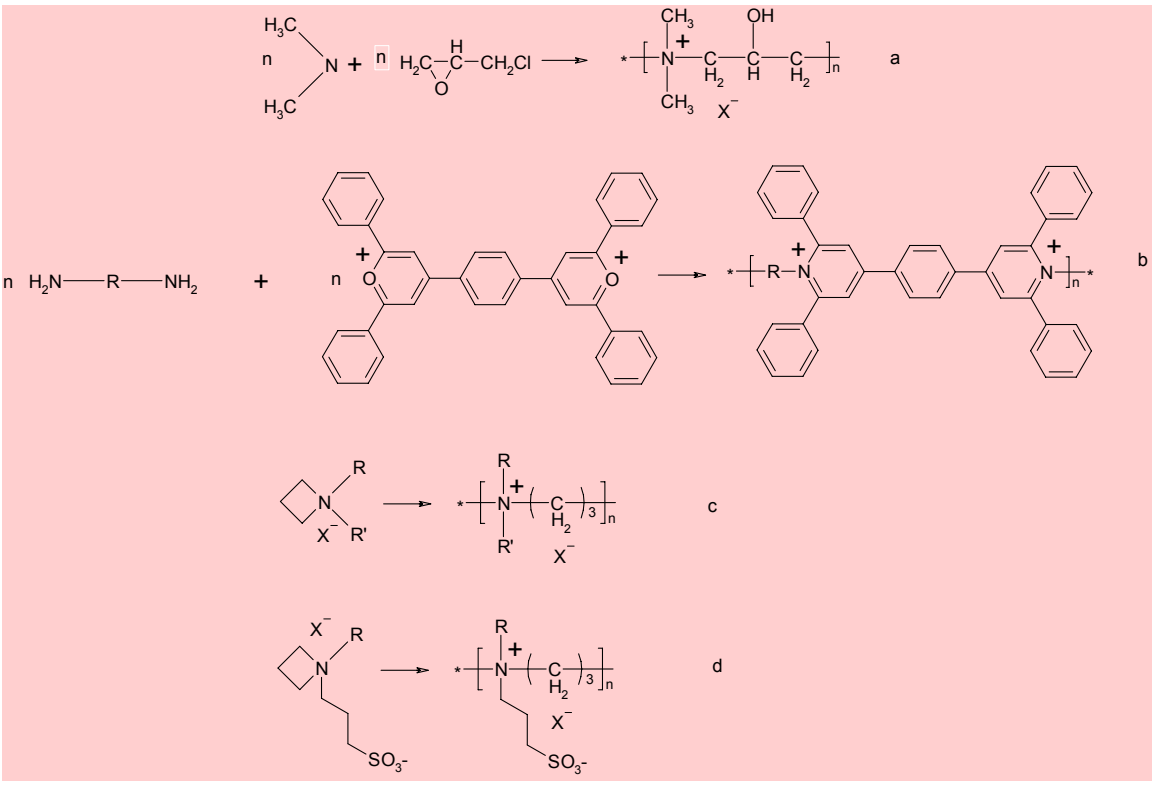

Scheme 2.2. a) Polyaddition of dimethylamine and epichlorohydrin b) synthesis of ionenes from bispyrylium salts c, d) synthesis of cationic and ampholytic ionenes by ring-opening polymerization.

The polymerization reaction which involves the synthesis of the above mentioned ionenes, is a step-growth polymerization reaction. A step-growth polymerization is characterized as a reaction of at least bifuntional monomers, which react stepwise and independent via stable intermediates. Contrary to chain-growth polymerization, these intermediates possess the same reactivity as the monomers. Therefore there is no need to distinguish mechanistically between different elementary reactions. In the course of chain-growth polymerization, addition of monomers as well as reaction of oligomers and macromolecules with each other, proceed simultaneously. In the reaction mixture, monomers, oligomers and polymers coexist in equilibrium. Step-growth polymerization proceeds with multifunctional monomers, each containing one type of functional group, or by reaction of one monomer containing different functional groups. The formation of linear macromolecules needs bifunctional monomers. Any intermediate product may react with each other or with the monomer. All quantitative treatments are based on the

assumption that the reactivity of the functional group at a chain end is independent of the length of the chain. Experimentally this is an excellent assumption for degrees of polymerization larger than five. Step-growth results in linear macromolecules only at higher conversion. As an example, to yield macromolecules with a degree of polymerization $P_n = 100$ a conversion of 99% must be achieved. This condition limits the possibility of obtaining very high molecular mass polymers by step growth polymerization. Such polymers are available with tri or multifunctional monomers resulting in branched macromolecules before extended cross-linking takes place. Step-growth polymerization can proceed as a condensation reaction with splitting of a low molecular weight compounds (Examples are the formation of ester or amide linkages from the reaction of a carboxylic group with an amine or hydroxyl group). Furthermore, step-growth polymerization can proceed as a polyaddition by stepwise addition of cyclic or double bond containing monomers. The polymer building reaction is combined with the movement of a hydrogen atom. A further process is stepwise alkylation.

Step-growth polymerization leads to different equilibria:

1. An exchange equilibrium between starting materials and polymers, e.g., for a polyamide.

$$K = \frac{[amide][H_2O]}{[NH_2][COOH]}$$

2. An exchange equilibrium between polymers, where the chain segments will be exchanged, e.g

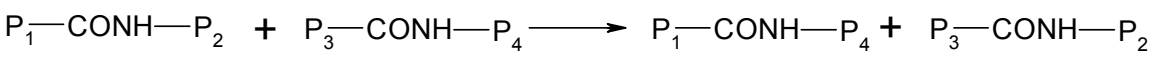

These exchange reactions lead to a molecular mass distribution with a low polydispersity.

Chain propagation is often accompanied by cyclization reactions. Intramolecular cyclization often takes place with monomers of the type A-B. The content of cyclic oligomers in polycaprolactam (nylon-6) is well known.

2.2.2 Polythiophene Based Polyelectrolytes

Many conductive polymers have been synthesized to provide certain electronic features (e.g. band gap, electron affinity). The monomer repeat units are often based on five-or six membered (benzene) cabon ring systems including polypyrrole, polythiophene, polyphenylenevinylene and polyaniline. Such polymers generally show lower electrical conductivity than polyacetylene; however they can have the advantage of high stability and processability. The Chemistry Nobel Prize 2000 was given to Alan Heeger, Alan McDiarmid and Hideki Shirakawa for their work on conducting and conjugated polymers. The first conducting polymer synthesized was polyacetylene.[95,96] Polyacetylene is the simplest conjugated polymer. Since the first electrical conducting polymer, polyacetylene, was discovered in 1977, several conjugated polymers have been investigated over the last two decades.[97]Much of the research efforts of industrial and academic researchers have been directed to the development of new materials that are stable, in the conducting state. These new conducting materials such as polythiophene, [99] polyfuran,[99] polypyrrole,[100] polyphenylene,[101] poly(phenylenevinylene),[102] polyfluorene,[103] polyaniline[104] have attracted great attention.

2.2.2.1 Theory of Conducting Polymers

In polyacetylene the valance band or π band is normally filled with electrons while the conduction band or π* band is normally empty. Like silicon the conductivity of polyacetylene can be changed by the addition impurity atoms. However the term doping is a misnomer as it tends to imply the use of minute quantities parts per million or less, of impurities introduced into crystal lattice. In the case of conductive polymers, typically 1% to 50% by weight of chemically oxidising (electron withdrawing) or reducing (electron donating) agents are used to alter physically the number of π-electrons on the polymer backbone, leaving oppositely charged counterions alongside the polymer chain. These process are redox chemistry. For example, halogen doping process that transforms polyacetylene to a good conductor is oxidation.

$$[CH]_n + \frac{3x}{2} I_2 \rightarrow [CH]_n^{x+} + xI_3^-$$

Reductive doping (n-doping) is also possible, e.g. using an alkali metal.

$$[CH]_n + xNa \rightarrow [CH]_n^{x-} + xNa^+$$

In both cases, the doped polymer is a salt. The counterions I_3^- or Na^+ are fixed in the position while charges on the polymer backbone are mobile and contribute to the conductivity. The doping effect can be achieved because of π electron can be removed (or added) without destroying the σ backbone of the polymer so that charged polymer remains intact. The increase in conductivity can be as much as eleven orders of magnitude.

The electrical properties of semiconductive organic polymers are not directly comparable to those of silicon. An important material parameter is the mobility of the charge carriers μ. This determines the (additional) velocity that a charge carrier (an electron or hole) acquires because of an applied electric field, and defined by

$$\mu = \frac{v_d}{E}$$

where v_d is the drift velocity of the carrier and E is the electric field. The mobility may be further related to the electrical conductivity σ by the expression

$$\sigma = |q| n \mu$$

where n is the density of the charge carriers and $|q|$ is the magnitude of their charge. The carrier mobility provides an indication of how quickly the carriers react to the field (i.e. the frequency response of the material). The greater the degree of electron delocalisation, the larger the width of the bands (in energy terms) and the higher the mobility of the carriers within the band.

Electrical conduction in polymers not only requires carrier transport along the chains but some kind transfer, or *hopping* between these chains, which tend to lie tangled up like a plate of spaghetti. The charge carrier mobilities in organic polymers are therefore quite low.

2.2.2.2 Synthesis of Conducting Polymers

Many conducting polymers can be synthesized form appropriate monomers both by chemical or electrochemical polymerization methods. Otherwise different synthesis routes have been suggested such as photopolymerization, solid state polymerization, methathesis polymerization and pyrolysis.[106,107]

2.2.2.2.1 Chemical Synthesis of Conducting Polymers

Conducting polymers can be prepared by chemical polymerization. Fe^{3+} and Fe^{2+} salts are useful as catalyst for the chemical polymerization of conducting polymers such as polypyrrole (PPy) and polyaniline (PAni), and also oxygen, ozone and H_2O_2 are suitable oxidizing agents. $FeCl_3$ and other Lewis acids can also be used for heterocyclic monomers.[108-110] For the Fe^{3+} catalyzed chemical polymerization, the small amount of Fe^{3+} first oxidizes the pyrrole monomer to give PPy and Fe^{3+} ions are reduced to Fe^{2+} ions. Thus Fe^{3+} acts as a catalyst in the synthesis to promote the growth of PPy. Other types of iron salts, such as $FeCl_2$, $Fe(ClO_4)_3$, $Fe(ClO_4)_2$ and $FeSO_4$, can also be used to produce similar polymers. Chemical oxidation of monomer by using such kind of oxidation agent, supply the formation of conducting polymer in doped state. By performing strong reducing agent such as ammonium hydroxide or hydrazine, neutral polymer (undoped) can be achieved.

2.2.2.2.2 Electrochemical Synthesis of Conducting Polymers

Although conducting polymers can be prepared by chemical oxidation methods, the most effective and widely used method is the electrochemical oxidation. The main advantage of electrochemical polymerization is to control the reaction rate and the doping process. Besides it is a simple, selective, reproducible method and control of film thickness and molecular weight is easy. The major disadvantage of this route is the resulting insoluble material by this way.

An electro polymerization reaction occurs by the oxidation of a monomer in supporting electrolyte solution. Reactive radical cations are generated by applying an external potential. After an initial oxidation step two ways are possible to the formation of polymer. The first way, a radical cation of monomer can couple with a neutral monomer to form a dimer and in the second way, coupling of two radical cations form a dimer. Then, dimer is oxidized again and proceeds up to formation of electroactive polymer.

A schematic representation of the proposed electro polymerization mechanism of heterocyclic monomers is shown in Figure 2.8. Pyrrole and thiophene are the most typical heterocyclic monomers.[111] First step is the oxidation of monomer to form a radical cation, second step is the coupling of two radical cations to form a dimer. Then, the radical form of the dimer that is more easily oxidized than monomer undergoes coupling with other radicals to keep on polymerization. Polymer chains carry a charge for every fixed units of heterocyclic rings. Oxidation level depends on the nature of polymer not supporting electrolyte or other electrolysis parameters.

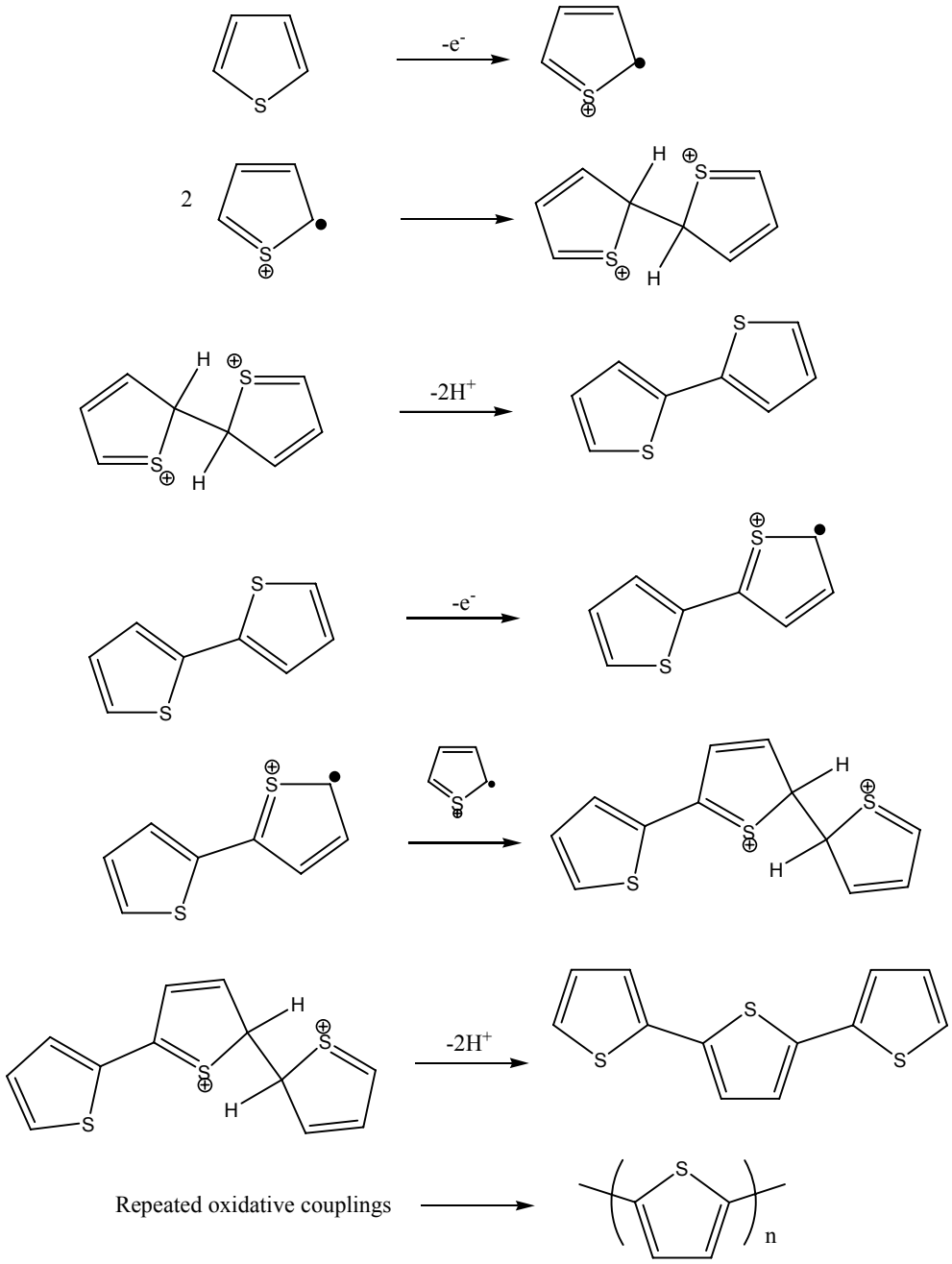

Figure 2.8. Proposed mechanism for the electrochemical polymerization

2.3 Characterization Techniques

2.3.1 Microscopic Techniques

2.3.1.1 Atomic Force Microscopy

The atomic force microscope, which was invented in 1986, permits to detect individual atoms on both conducting and insulating surfaces. In this procedure, a flexible force-sensing cantilever scans in a raster pattern over the surface of the sample. The force acting between the cantilever and the sample surface causes deflection of the cantilever, which is detected by optical means. The motion of the tip, or sometimes sample, is achieved with a piezoelectric tube. During a scan, the force on the tip is held constant by the up-and-down motion of the tip, which then provides the topographic information. One of advantages of the atomic force microscope is that it is applicable to nonconducting samples.

Figure 2.9 schematically shows the most common method for detecting the deflection of the cantilever holding the tip. A laser beam is reflected from a spot on the cantilever to a segmented photodiode that detects the motion of the probe. The output from the photodiode then controls the force applied to the tip so that it remains constant. The movement system is a tubular piezoelectric device that moves the sample in an x, y and z direction under the tip. The signal from the laser beam is then fed back into the sample piezoelectric transducer, which causes the sample to move up and down to maintain a constant force between tip and the sample.

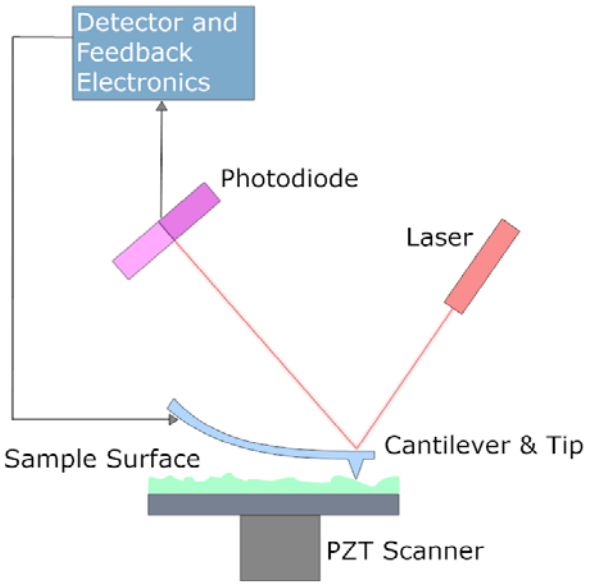

Figure 2.9. Schematic representation of atomic force microscopy*

Two modes are usually used in AFM investigations: i) contact mode ii) tapping mode. As indicated by the name, the tip is in constant contact with the sample in the contact mode. One of the disadvantages of the contact mode scanning is that the tip in constant contact with the surface of the sample may cause damage to the sample surface and a distortion of the image is the consequence. This problem is particularly expressed with soft materials, such as biological samples, polymers but also some seemingly hard materials such as silicon wafers.

It has been found that the problem of surface damage can be largely overcome by a process in which the tip contacts the surface for only a brief time periodically and then is removed from the surface. In this tapping mode operation, the cantilever is oscillated at a frequency of a few hundred kilohertz. The oscillation is driven by a constant driving force and the amplitude is monitored continuously. The cantilever is positioned so that the tip touches the surface only at the bottom of each oscillation cycle. This technique has been used successfully to image wide variety materials that have been difficult or impossible to image by a ordinary constant contact mode.

* The image has reprinted from http://en.wikipedia.org/wiki/Image:Atomic_force_microscope_block_diagram.png

2.3.1.2 Fluorescence Microscopy

In fluorescence microscopy, the sample desired to study is itself the light source. The technique is used to study specimens, which can be made to fluoresce. The fluorescence microscope is based on the phenomenon that certain material emit energy detectable as visible light when irradiated with the light of a specific wavelength. The sample can either be fluorescing in its natural form like chlorophyll and some minerals, or stained with fluorescing chemicals.

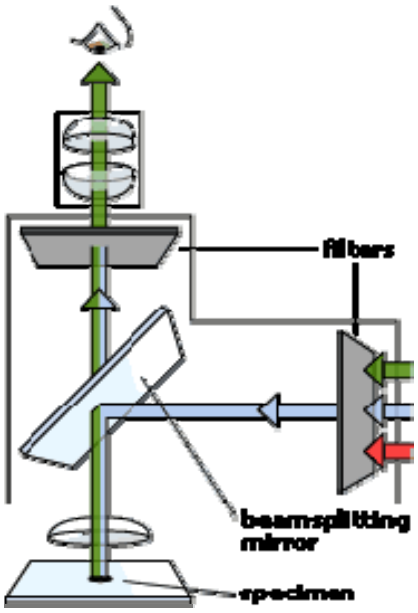

Figure 2.10. Schematic representation of fluorescence microscopy *

* Image has reprinted from:http://nobelprize.org/educational_games/physics/microscopes/fluorescence/

The basic function of the fluorescence microscope is to expose to specimen excitation light radiate and then sort out the much weaker emitted light to create the image. First, the microscope has a filter that only lets through radiation with the desired wavelength that matches the fluorescing material. The radiation collides with the atoms in the specimen and electrons are excited to a higher energy level. When they relax to a lower level, they emit light. To become visible, the emitted light is separated from the much brighter excitation light in a second filter. Here, the fact that the emitted light is of lower energy and has a longer wavelength is used. The fluorescing areas can be observed in the microscope and shine out against a dark background with high contrast (see Figure 2.10). Fluorescence microscopy is a rapidly expanding technique, both in the medical and biological sciences. The technique has made it possible to identify cells and cellular components with a high degree of specificity. For example, certain antibodies and disease conditions or impurities in inorganic material can be studied with the fluorescence microscopy.

2.3.2 Scattering Techniques

2.3.2.1 Light Scattering

In the determination of molecular weights of polymers, light scattering is one of the most frequently used methods. In addition, light scattering on polymers has gone beyond molecular weight determination. In particular, the wide scope of applicability of the light scattering technique makes it one of the most informative and practical methods in the investigation of static and dynamic properties of macromolecules. The basics of scattering phenomena have been well documented in literature.[112-114,116-118] Here we assume that scattered light exhibits the same wavelength as the primary light source, or so called elastic scattering takes place. Two types of scattering experiments may be performed. If the average scattering intensity depending on the angle is measured, a static light scattering experiment is performed. Contrary to static light scattering, in dynamic light scattering experiments, the time dependent scattering intensity measured and correlated.

2.3.2.1.1 Static Light Scattering

According to the fluctuation theory, light scattering arises from the fluctuation of the polarizibility α of the scattering medium. In simple fluids, small fluctuations of α arise from density fluctuations and the scattering intensity is usually small. In the case of polymer solutions the major effect usually originates from concentration fluctuations. Since the contribution of solvent scattering intensity is eliminated by subtraction from the total scattering intensity, the effect of density fluctuations can be neglected. Replacing the change in the polarizibility by the change in the refractive index n, yields at the important result:

$$\frac{i_\theta}{I_0} \sim c\left(\frac{dn}{dc}\right)^2\left(\frac{\delta\mu}{\delta c}\right)_{T,P}^{-1} \qquad 1$$

where i_θ is the excess scattering intensity, $i_\theta = (i_{(solution)} - i_{(solvent)})$, I_0 the primary intensity, dn /dc the refractive index increment (contrast), and $\delta\mu/\delta C$ the local fluctuation of the

chemical potential with concentration. Since $(\delta\mu / \delta C)_{T, P} = (\delta\pi / \delta c)_{T, P}$ and applying the virial expansion of osmotic pressure π, one obtains

$$\frac{i_\theta}{I_0} \sim c\left(\frac{dn}{dc}\right)^2 \left(M^{-1} + 2A_2c + \ldots\right)^{-1} \qquad 2$$

or in a more convenient form,

$$\frac{Kc}{R_\theta} = \frac{1}{M} + 2A_2c + 3A_3c + \ldots \qquad 3$$

where the K is an optical constant given by

$$K = 4\pi^2 n_0^2 \left(\frac{dn}{dc}\right)^2 / (N_A \lambda_0^4) \qquad 4$$

where n_0 is refractive index of the medium, λ_0 is the wavelength of the primary beam in *vacuo* and R_θ the Rayleigh ratio:

$$R_\theta = r^2\left(\frac{i_\theta}{I_0}\right) \qquad 5$$

where r is the distance of the detector from the scattering volume. Since the determination of the absolute value the primary intensity is rather elaborate, a light scattering instrument is calibrated by standard of known scattering power (usually benzene or toluene). The Rayleigh ratio is then derived as

$$R_\theta = \frac{i(solution) - i(solvent)}{i(toluene)} I_{abs}(toluene) \qquad 6$$

where I_{abs} (toluene) is 1.346 x 10^{-3} m^{-1} (for λ = 638 nm)

Equation 3 represents the basic relation for the determination of the molecular mass. For polydisperse systems the weight average molecular mass is measured, because

$$R_\theta / K = \sum c_i M_i \qquad 7$$

Dividing both sides by $c = \Sigma c_i$ yields

$$\frac{R_\theta}{Kc} = \frac{\sum c_i M_i}{\sum c_i} = M_w \qquad 8$$

The derivation of eqn. 3 shows that light scattering and osmotic pressure measurements yield identical second virial coefficients A_2 for monodisperse samples. The effect of polydispersity on A_2 is theoretically unclear and not believed to be very significant. Generally, the Rayleigh ratio R_θ depends on the scattering vector q defined as (see Figure 2.11)

$$q = \frac{4\pi n}{\lambda}\sin(\theta/2) \qquad 9$$

where λ is the wavelength of the light in the medium and θ the scattering angle. This q-dependence originates from the fact that different scattering centers in the solution may exhibit a phase relation and accordingly interfere. This interference is described by the static structure factor

$$S(q) = \sum_i^x \sum_j^x \left\langle \exp(iqr_{ij}) \right\rangle \qquad 10$$

where x represents the number of point scatterers in the scattering volume and

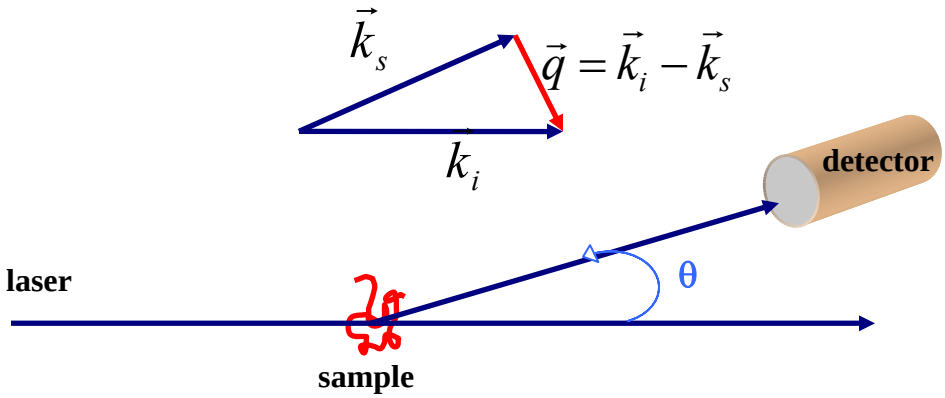

Figure 2.11. Block diagram of light scattering experiment set up, including sketch of scattering vector q and scattering angle θ.

$r_{ij} = r_i - r_j$ the distance vector between the scattering elements i and j. In diluted solutions one can separate S(q) due to pure intramolecular interference, and P(q), commonly known as the form factor or particle scattering factor:

$$P(q) = \frac{S(q)}{S(0)} = \frac{1}{N^2}\sum_i^N \sum_j^N \left\langle \exp(iqr_{ij}) \right\rangle \qquad 11$$

where N is the number of scattering elements per molecule.

Implementing P(q) in to eqn. 3, one yields,

$$\frac{Kc}{R_\theta} = \frac{1}{M_w P_z(q)} + 2A_2 c + 3A_3 c^2 + \ldots \qquad 12$$

where the subscript z denotes the z-average of P(q), defined as

$$P_z(q) = \frac{\sum m_i M_i P_i(q)}{\sum m_i M_i} \qquad 13$$

m_i being the mass fraction of particle I with molecular weight M_i. The form factor P(q) depends on the geometry of the scattering particles, as shown in Figure 2.12.

For small values of q, P(q) can be expanded as

$$P_z(q) = 1 - \frac{1}{3} q^2 \left\langle R_G^2 \right\rangle_z + \ldots \qquad 14$$

and allows the determination of the z-average mean square radius of gyration $\left\langle R_G^2 \right\rangle_z$. It is defined as the average squared distance of all polymer segments from the center of mass:

$$\left\langle R_G^2 \right\rangle_z = \frac{1}{N}\sum |S_i|^2 \ldots \qquad 15$$

$$\left\langle R_G^2 \right\rangle_z = \frac{\sum m_i M_i \left\langle R_G^2 \right\rangle_i}{\sum m_i M_i} \qquad 16$$

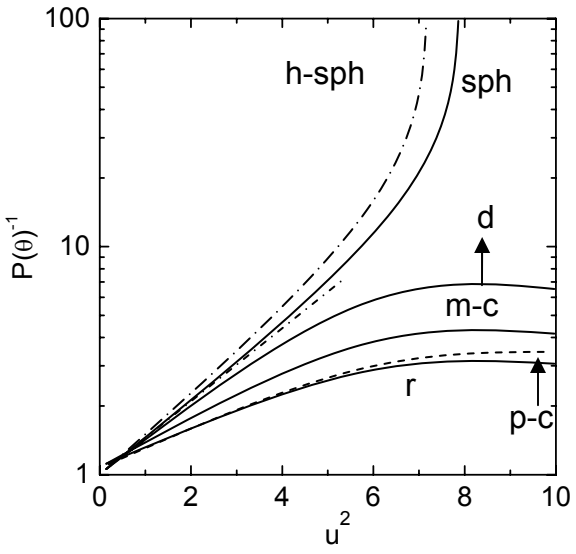

Figure 2.12. Particle scattering factor for various structures. hollow sphere (h-sph), sphere (sph), disc (d), monodisperse coils (m-c), polydisperse coils (p-c), rigid rods (r).[115]

where S_i is the distance of segment I to the center of mass. Combination of equation 14 and 12 gives the well known Zimm relation:

$$\frac{KC}{R_\theta} = \frac{1}{M_w}(1 + \frac{1}{3}q^2\left\langle R_G^2\right\rangle_z + ...) + 2A_2C + ... \qquad 17$$

from which the molecular mass M_w, the mean square radius of gyration $\left\langle R_G^2\right\rangle_z$ and the second virial coefficient A_2 are derived by plotting KC/R_θ vs. $(q^2 + kC)$ (Zimm plot) with k a suitable constant.

2.3.2.1.2 Dynamic Light Scattering

In dynamic light scattering the detected photons are not time-averaged but correlated. The intensity-time correlation function g_2 (t) is defined as:

$$g_2(t) = \left\langle i(0)i(n.\tau)\right\rangle \qquad 18$$

The time t is given by $t = n\tau$, with n the number of delay channels separated by sample time τ. Of theoretical interest is the correlation function g_1 (t) of the electric field, which is given by

$$g_1(t) = S(q,t)/S(q) \qquad 19$$

where S(q) is the static structure factor defined by eqn. 10 and S(q,t) the dynamic structure factor,

$$S(q,t) = \sum_{i}^{x}\sum_{j}^{x}\left\langle \exp(iqr_{ij}(t))\right\rangle \qquad 20$$

Experimentally, $g_1(t)$ is derived from the measured correlation function $g_2(t)$ by the Siegert relation:

$$g_1 = \left[(g_2(t) - A)/A\right]^{1/2} \qquad 21$$

with A being the experimentally determined baseline. The relation between $g_1(t)$ and the Doppler broadening S(ω) is given according to the Wiener-Khintchine theorem as a Fourier transformation.:

$$g_1(t) \sim \int_0^{\infty} S(\omega)\exp(-iq\omega t)d\omega \qquad 22$$

Since the polymers in solution move rather slowly, the spectrum broadening is very small and cannot be resolved sufficiently by current spectrum analyzers. Therefore the intensity time correlation function $g_2(t)$ is measured instead. This is possible since fast computers and highly monochromatic light sources (lasers) are available. The correlation procedure is illustrated by Figure 2.13 where the fluctuating scattering intensity I(q) is plotted vs. time t. Performing the correlation I(0)(I (t = τ)), I(0)I(t = 2 τ),..,I(0)(I (n τ)), and repeating this procedure over a longer period of time (minutes to hours) yields the autocorrelation function $g_2(t)$, which decays from $\left\langle I(t)^2\right\rangle$ to $\left\langle I(t)\right\rangle^2$. For monodisperse small particles the correlation function decreases as a single exponential function,

$$g_1(t) = B\exp(-q^2 Dt), \qquad 23$$

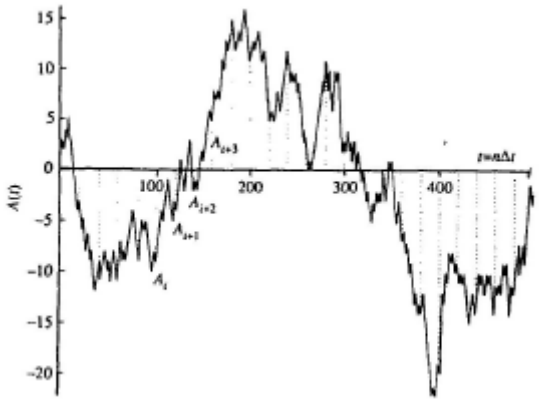

Figure 2.13. Fluctuation of scattering intensity.[120]

The decay constant yields the translational diffusion coefficient D; here B is the signal-to-noise ratio and depends on the optical set up of the experiment. For polydisperse small particles $g_1(t)$ is given by

$$g_1(t) = B\frac{\sum m_i M_i \exp(-q^2 D_i t)}{\sum m_i M_i} \qquad 24$$

the initial slope of which yields the z-average diffusion coefficient D_z:

$$\left[-\frac{d(\ln)}{dt}\right]_{t=0} = q^2 \frac{\sum m_i M_i D_i}{\sum m_i M_i} \equiv q^2 D_z \qquad 25$$

For large nonspherical particles $g_1(t)$ also depends on internal motions, e.g. on the rotational diffusion coefficient for rods or on the Zimm relaxation modes for flexible coils. For example, for the latter case Percora derived

$$g_1(t) = \exp(-q^2 Dt)(P_0 + P_{21}\exp(-2t/\tau_1) + P_{12}\exp(-t/\tau_2) + P_{22}\exp(-2t/\tau_2) + P_4\exp(-4t/\tau_1) + \ldots) \qquad 26$$

P_{ij} being the q-dependent amplitudes and τ_j the Rouse or Zimm relaxation times. Equation 26 has been employed to determine the first two relaxation times, τ_1 and τ_2, of polystyrene under theta conditions. However, the results show considerable scatter because the proper evaluation of decay constants represents a non-trivial problem.

One generally accepted way of coping with a multi-exponential decay of $g_1(t)$ is to apply a cumulant fit to the logarithmic correlation function:

$$\ln(g_1(t)) = -\Gamma t + \frac{\mu_2}{2}\Gamma^2 t^2 - \frac{\mu_3}{6}\Gamma^3 t^3 + \ldots \qquad 27$$

and to define an apparent diffusion coefficient $D_{app}(q)$ from the initial slope Γ as

$$D_{app}(q) = \frac{\Gamma}{q^2} \qquad 28$$

According to eqns 24 and 25 one obtains in the limit of small q,

$$\lim_{q \to 0} \frac{\Gamma}{q^2} D_z \qquad 29$$

The higher cumulants μ_2 and μ_3 represents a qualitative measure of the polydispersity when the effect of internal modes can be neglected. This is usually achieved at small q values. As indicated by eqn. 28 reduced initial slope Γ/q^2 of $g_1(t)$ depends on q. For low q values, $D_{app}(q)$ can always be expanded and yields

$$D_{app}(q) = D_z(1 + C\left\langle R_G^2 \right\rangle_z q^2 + ...) \qquad 30$$

The dimensionless slope C depends on the structure of the polymer and has been calculated for various models as shown Figure 2.14. The experimental evaluation of C is rather difficult and calculate because C is for zero time. This is difficult to achieve experimentally, owing to the limited resolution of correlator, which is determined by the smallest available sample time. Therefore only a few experimental values C have been reported.

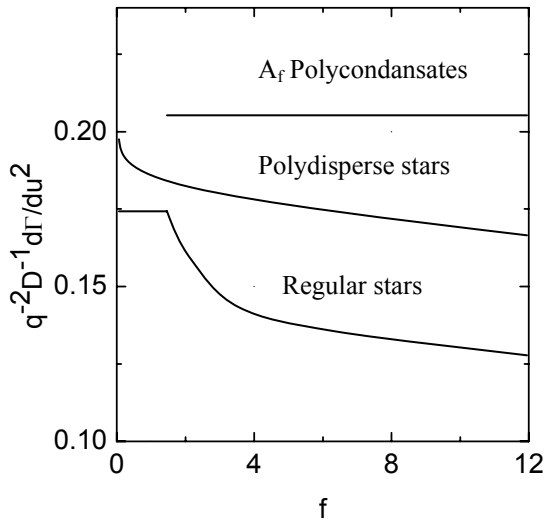

Figure 2.14 Coefficient C for three different branching models vs. branching density[121]

The concentration-dependence of the diffusion coefficient D_z is usually written as

$$D = D_0(1 + k_D C + ...) \quad 31$$

where k_D is related by irreversible thermodynamics to the second virial coefficient A_2 and the concentration-dependence of the friction coefficient,

$$f = f_0(1 + k_f C + ...) \quad 32$$

as

$$k_D = 2A_2 - k_f - \tilde{\nu}_2 \quad 33$$

where $\tilde{\nu}_2$ is the partial molar volume of the polymer. Some theoretical effort has been made to calculate k_f with various approximations. Since k_f is always positive it follows eqn. 33 that k_D is negative for theta conditions, and becomes eventually positive as the solvent quality increases.

Equation 30 and 31 are combined

$$D_{app}(q,c) = D_z(1 + C\left\langle R_G^2 \right\rangle_z q^2 + ...)(1 + k_D C + ...) \quad 33$$

which is formally in analogy to equation 17, the Zimm equation for the static scattering intensity. It has been suggested that eqn. 33 can be plotted as "dynamic zimm plot", i.e $D_{app}(q,c)$ vs. $(q^2 + kC)$.

3 Synthesis and Characterization of Ionenes

The ionenes which have been used in this work have been synthesized according to Menschutkin reaction which is a classical nucleophilic bimolecular substitutuion (S_N2) reaction. As it has been discussed above, the reaction between diprimary alkyl halide and

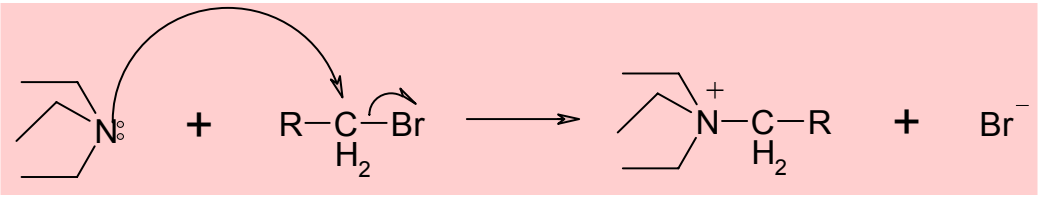

Scheme 3.1. Menchutkin reaction mechanism

a ditertiary amine yields polymeric quaternary salt (see Scheme 3.1). Rembaum et. al.[122,123] have reported that the synthesis of ionenes with a weight average molecular mass of 10,000-15,000 g / mol was usually obtained when the spacer alkyl chains were longer than three.[124] In the case of a number of carbon atoms less than three either cyclic compounds or unexpected linear compounds normally resulted.

In order to reduce the possibility of cyclization and to obtain a high nucleophilicity, 1,4-diaza [2.2.2]bicycle-octane (DABCO) has been used as a di-tertiary amine. The bicyclic di-tertiary amine DABCO is analogous to the acyclic di-tertiary amine *N,N,N',N'*-tetramethylethylene-diamine. However, because of its rigid structure, the nitrogen lone-pair electrons should be fully exposed. This would be expected to enhance the nucleophilicity of DABCO relative to its nonrigid analog in much the same fashion as has been noted in the greater reactivity of the bicyclic amine quinuclidine with methyl iodide, in comparison to the reactivity of triethylamine.[125]

Based on these effects, it was anticipated that ionene polymers could readily be prepared from DABCO. Furthermore the utilization of this diamine could lead the polycation with a higher positive charge density than that prepared from previously reported Menschutkin reactions, since the rigid structure in the former case would lead to a greater proximity of positively charged sites.

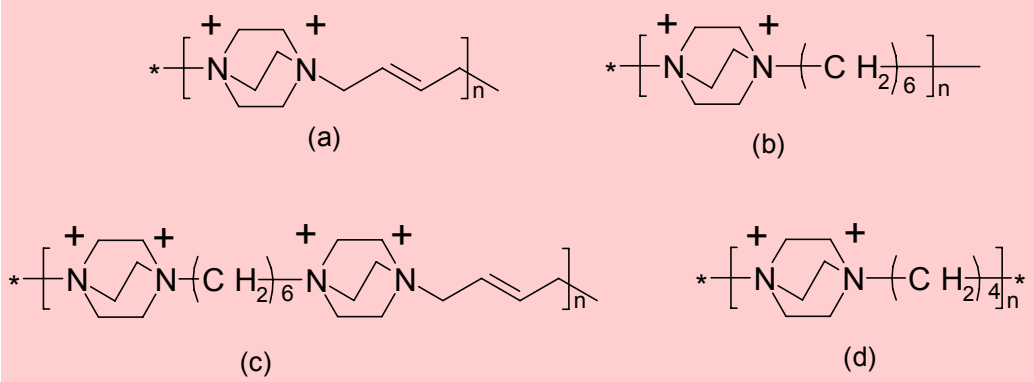

Scheme 3.2. Chemical structures of polyionen a) PD4, b) PD6, c) PD4coPD6 d) PD4-2

Water-soluble ionenes PD4, PD6, PD4coPD6 and PD4-2 were successfully synthesized via Menschutkin reaction[122,126] from 1-4-diazabicyclo[2.2.2] and dibromides as indicated in Scheme 3.2. ^{1}H and ^{13}C NMR spectroscopy results are in good agreement with the structure. It has been observed that in Figure 3.1 the peak labeled with **b** and in Figure 3.3 the peak labeled with **a,** have shoulders. These shoulders can be attributed to end group protons which are placed in α position with respect to the bromine atom. As shown in Table 3.1, number average molecular masses of ionenes were determined as 7800 g mol^{-1}, 7200 g mol^{-1} and 19200 g mol^{-1} for PD4, PD6 and PD4coPD6, respectively, by size exclusion chromatography (SEC) (eluent: 0.1 M trifluoroacetic acid solution, coloumn: Novema, standart: pullulan, PSS Company Mainz). The polydispersities and range of the molecular mass of obtained ionenes were consistent with the synthesis of other polyelectrolytes of the same calls described in literature[122-126]. Moreover, molar masses of ionenes have been double checked by end group analysis (via NMR spectroscopy) and it shows that results are in good agreement for both methods.

Unlike PD6, one particular feature of the SEC elugram of PD4 and PD4coPD6 are the multi modal peaks. In accordance with the kinetics of addition polymerization, such distribution is unusual. However, precipitation of ionene from the polymerization medium may cause such inhomogenity in molar mass distribution due to the insolubility of product.

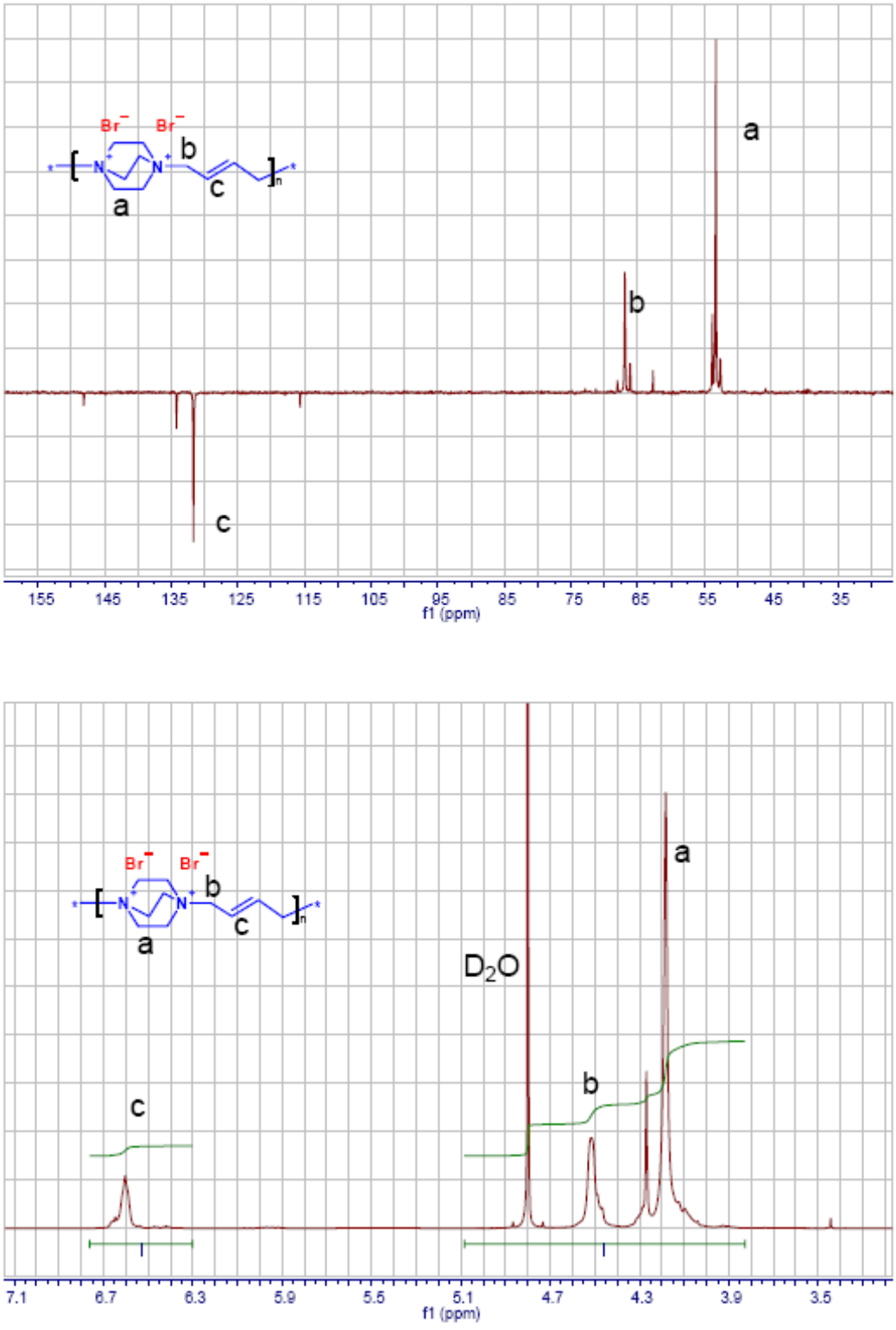

Figure 3.1. ^{1}H and ^{13}C NMR of PD4.

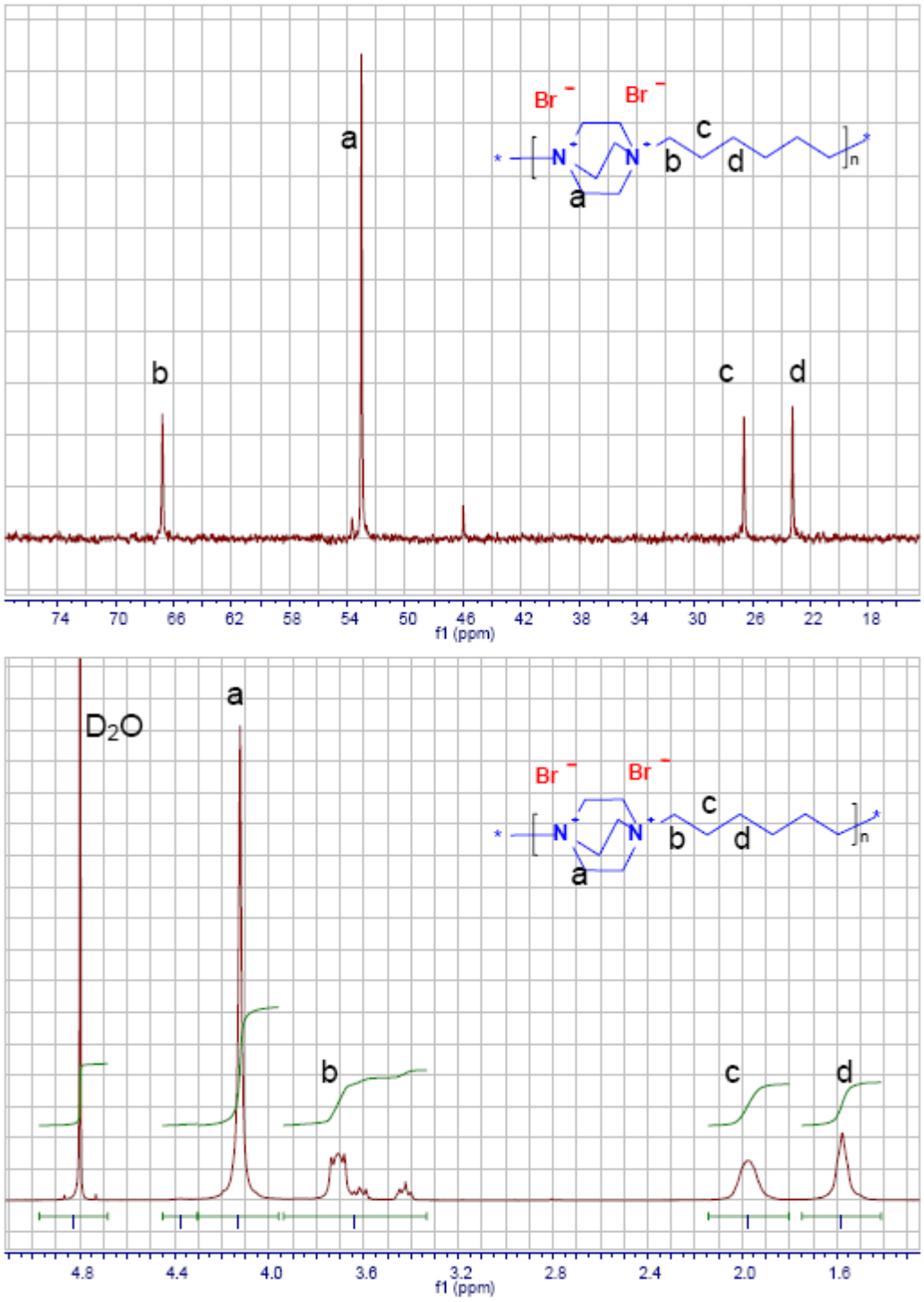

Figure 3.2. ^{1}H and ^{13}C NMR of PD6

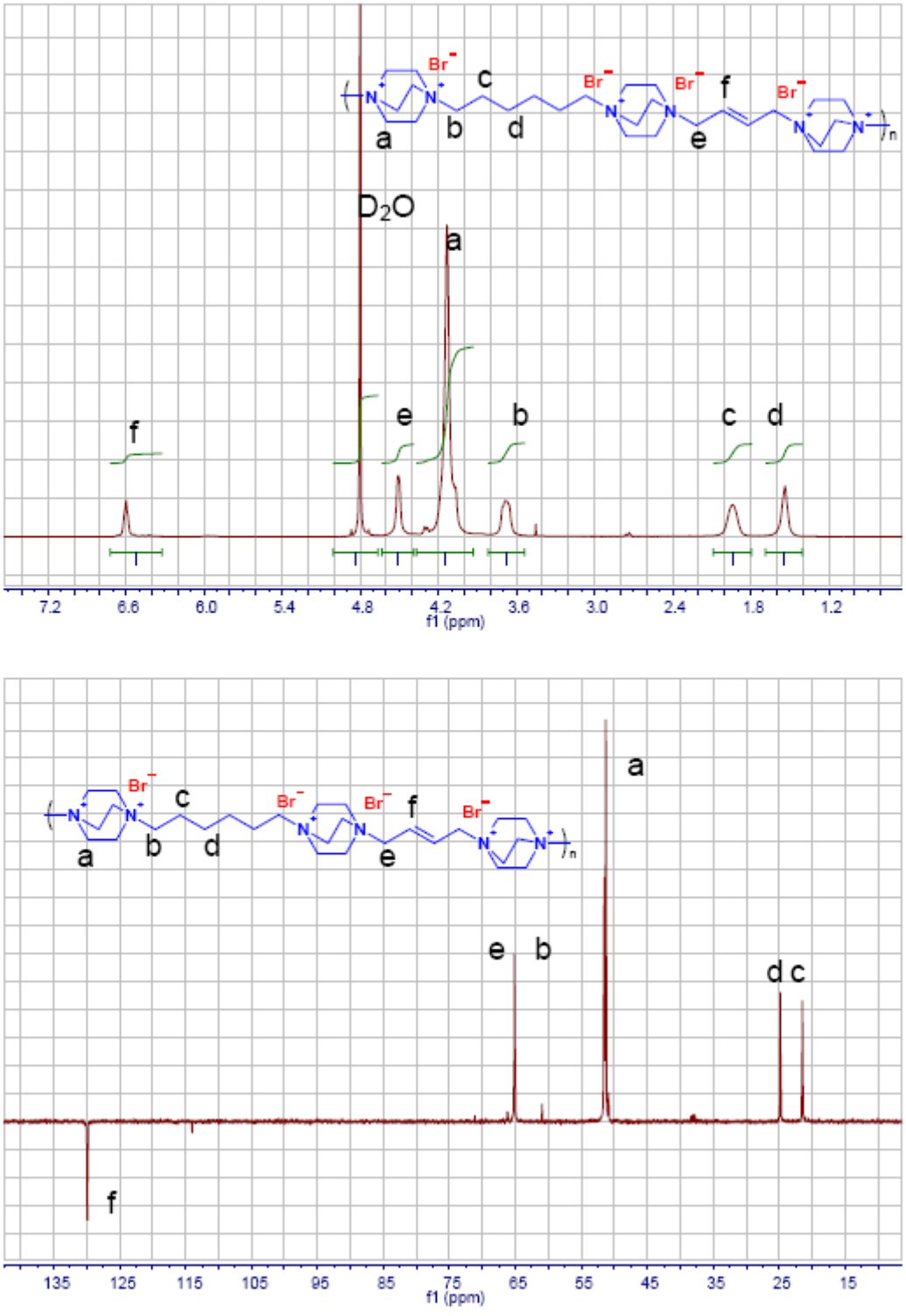

Figure 3.3. ^{1}H and ^{13}C NMR of PD6coPD4.

Table 3.1. Molecular weight of ionenes

polyionen	M_n /gmol$^-$	M_w / gmol$^-$	D(M_w/M_n)
PD6	7865	18941	2.41
PD4	7261	20198	2.78
PD4coPD6	19180	66403	3.45
PD4-2	3000	-	-

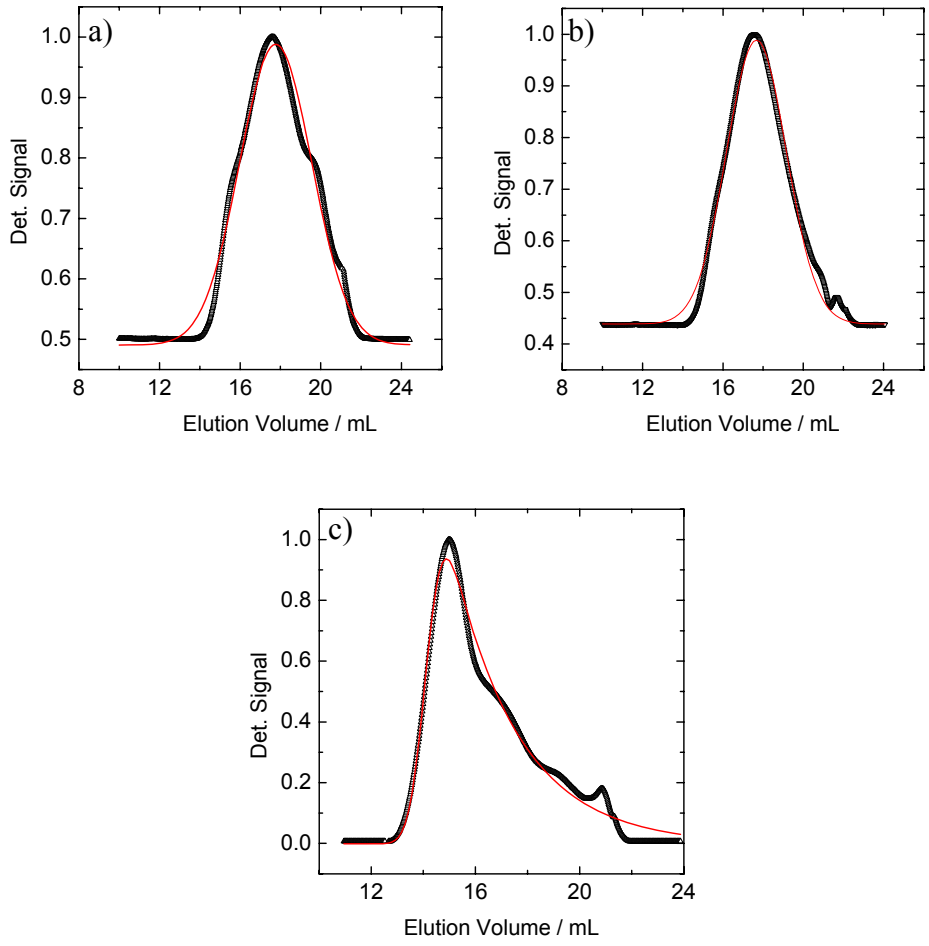

Figure 3.4. SEC elugrams of a) PD4 b) PD6 and c) PD4coPD6.

4 Ionenes-Dye Complexes

Understanding the fundamentals of polyelectrolyte-dye complexes in solution enables to deduce binding and transport mechanism of more complicated systems such as DNA-surfactant, DNA-amphiphiles and protein-surfactant complexes not only in vitro conditions but also in living systems.[131-137] Current literature reveals that self-assembly of oppositely charged molecules might provide materials such as chemo-biosensors,[70,71] nanowires,[72-75] light harvesting complexes[76-77] due to their facile preparation procedures. Recent studies reported the formation of nano-sized aggregates in solution[138-143] presumably held together via electrostatic forces. It would be desirable to allow for systematic comparison in order to get more information about possible size and structural control on the synthesis of polyelectrolyte-dye complexes in solution.

In this chapter electrostatic self-assembly of a series of linear model polyelectrolytes of varying structure is investigated: specifically, four different 1,4 diazabicyclo[2.2.2]octane based ionenes (PD4, PD6, PD4-2 and PD4coPD6), that is varying in the charge distance (four, six or alternatingly four and six carbons) and type of polymer chain (form in variant). These were combined with pyrenetetrasulfonate (PY), as example for a multivalent counterion with the capability for mutual $\pi-\pi$ interactions. Chemical structures of these building units are displayed in Scheme 4.1. It should be noted that the positive charges of the polyelectrolytes originate from quartenized nitrogens, while counterions are bromide ions. Thus effects of weak acid/bases are avoided for this type of polyelectrolytes and "counterion condensation" can selectively be studied. The sodium salt of the PY is used.

The inherent formation of sodium chloride upon complex formation is desired, as it is expected to screen interactions somewhat and thereby makes the structure analysis easier, while the structure formation is based on tetravalent ions the ionic interaction of which is expected to be strong. The association of these building units will be first followed by UV-VIS and fluorescence spectroscopy. Assemblies formed were investigated by

confocal microscopy, by AFM after drop casting on silicon surfaces and by static and dynamic light scattering in solution.

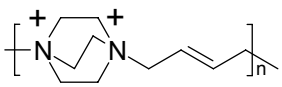

PD4

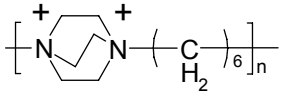

PD6

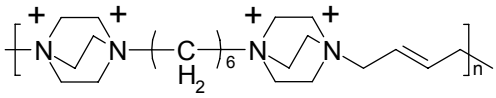

PD4coPD6

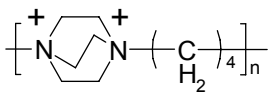

PD4-2

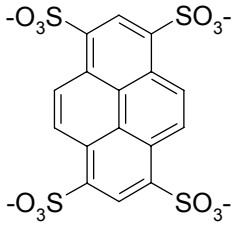

PY

Scheme 4.1. Chemical structures of ionenes PD4, PD6, PD4coPD6 and PD4-2 and the tetravalent dye counterion PY (pyrenetetrasulfonate). The bromide salt of ionenes and sodium salt of PY was used.

4.1 UV-Vis and Fluorescence Spectroscopy

The effect of the ionenes on the absorption and emission properties of pyrenetetrasulfonate was determined by UV-Vis and fluorescence measurements. Sodium pyrenetetrasulfonate (PY) was titrated spectrophotometrically with ionenes. For parametrization we here use the charge ratio λ that is defined as

$$\lambda = \frac{c(N^+ \text{of polyionene})}{c(SO_3^- \text{of dye})}$$

where c ($N^+$of ionenes) and c(SO_3^- of dye) are the molar concentrations of ammonium groups of the polyiones and sulfonic acid residuals of pyrenetetrasulfonate, respectively.

UV-Vis spectroscopy of PY is shown in Figure 4.1. In the absence of ionenes, the spectrum exhibits two main maxima one at 283 nm (35445 cm^-) which corresponds to $S_2 \leftarrow S_0$ transitions and one at 375 nm (26670 cm^-) which corresponds to $S_1 \leftarrow S_0$ transitions. The absorption spectrum also reveals that three vibronic bands at 270nm (36760 cm^-), 335nm (29530 cm^-), 355 nm (28190 cm^-).

Upon addition of PD6 solution to PY solution the absorption maximum ($S_2 \leftarrow S_0$ transition) of PY gradually red shifted until λ = 1 and then remained at 288 nm (34610 cm^{-1}) and 380 nm (26250 cm^-) for λ > 1 (Figure 4.2). Isosbestic points in the spectra can be attributed to the existence of two species in equilibrium. These two species are considered to be free PY dye in solution and PY associated with PD6.

The behavior with the polyelectrolyte PD4 under otherwise same conditions is different (Figure 4.3): Upon addition of PD4 solution to PY solution, the absorption maximum of the dye shifted slightly to the red and in particular decreased.

The UV-titration of PY with PD4-2 is presented by Figure 4.4. Qualitatively it resembles more the behavior with PD4 rather than PD6, however with clear differences, that is, more shift to red up to λ = 1 and less decrease of peak maximum.

Further Figure 4.5 shows results for the copolymer PD4coPD6. Spectra of this system have mainly similar characteristics as PD6. For all polyelectrolyte-dye systems no significant changes have been observed at λ > 1.

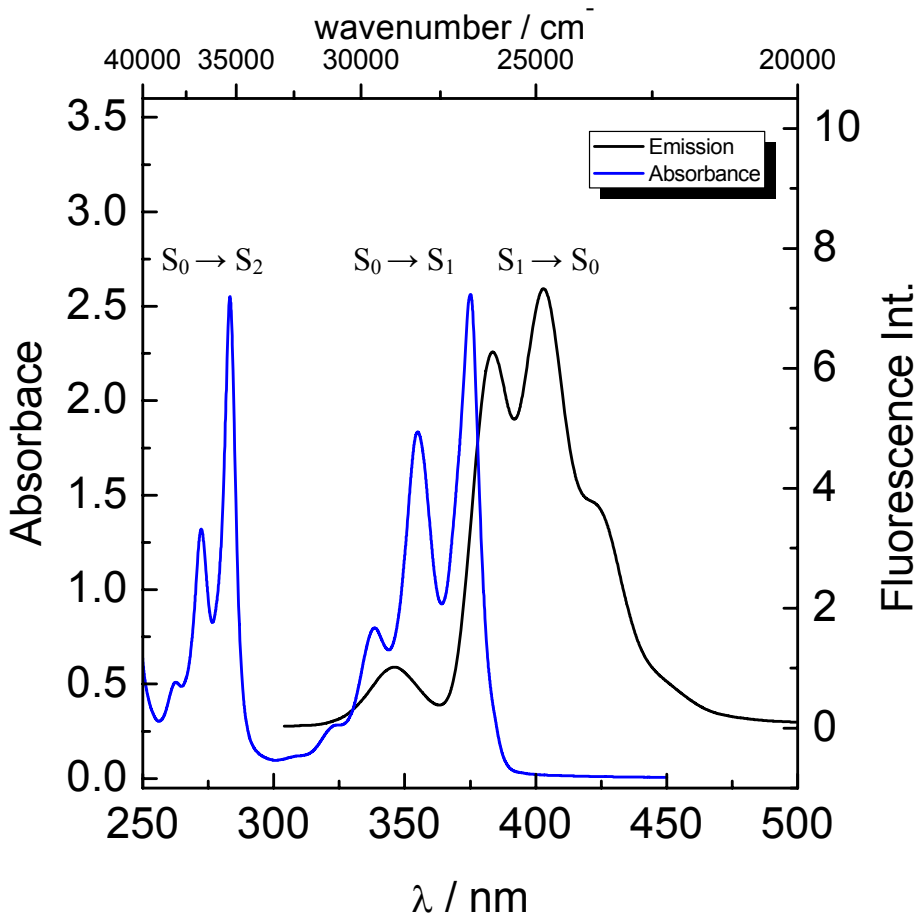

Figure4.1. Absorption and emission spectrum of pyrenetetrasulfonate in water

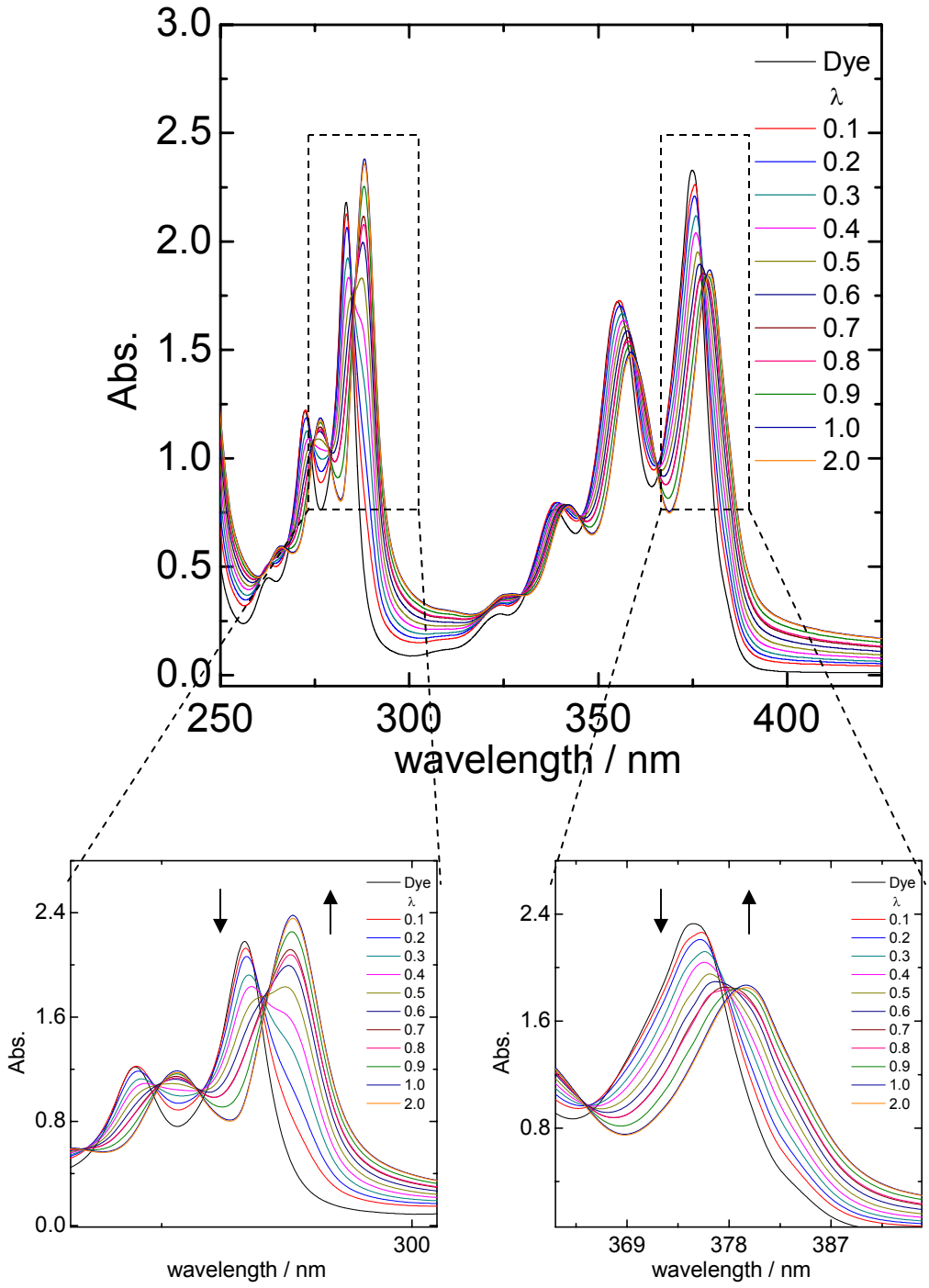

Figure 4.2. Absorption spectra of PY ($1.8\ 10^{-4}$ M) titrated with PD6

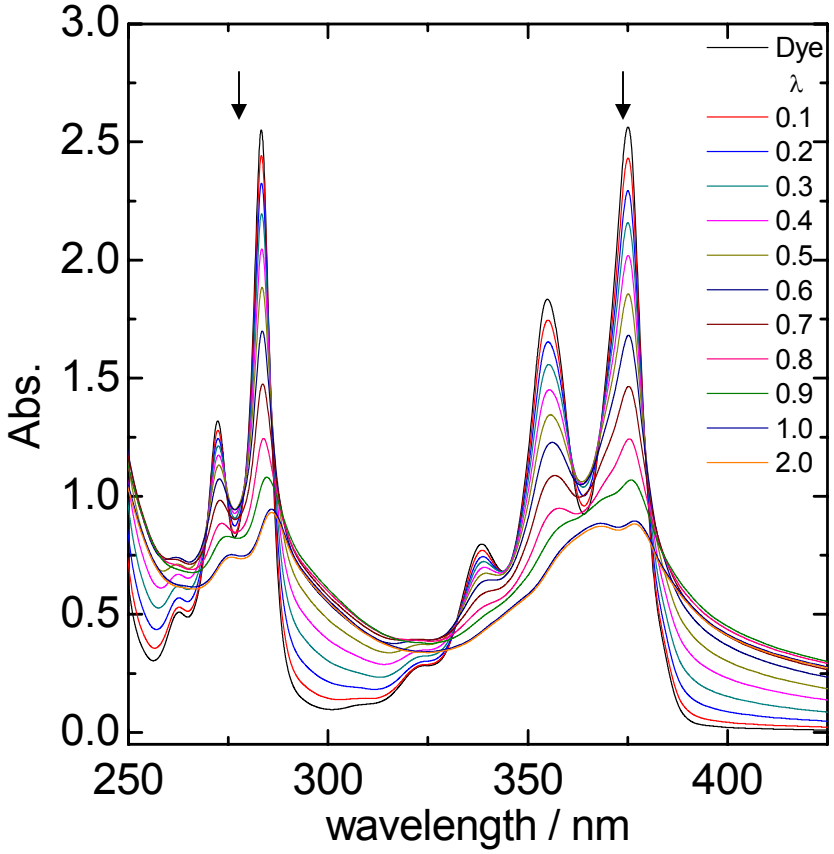

Figure 4.3. Absorption spectra of PY ($1.8\ 10^{-4}$ M) titrated with PD4

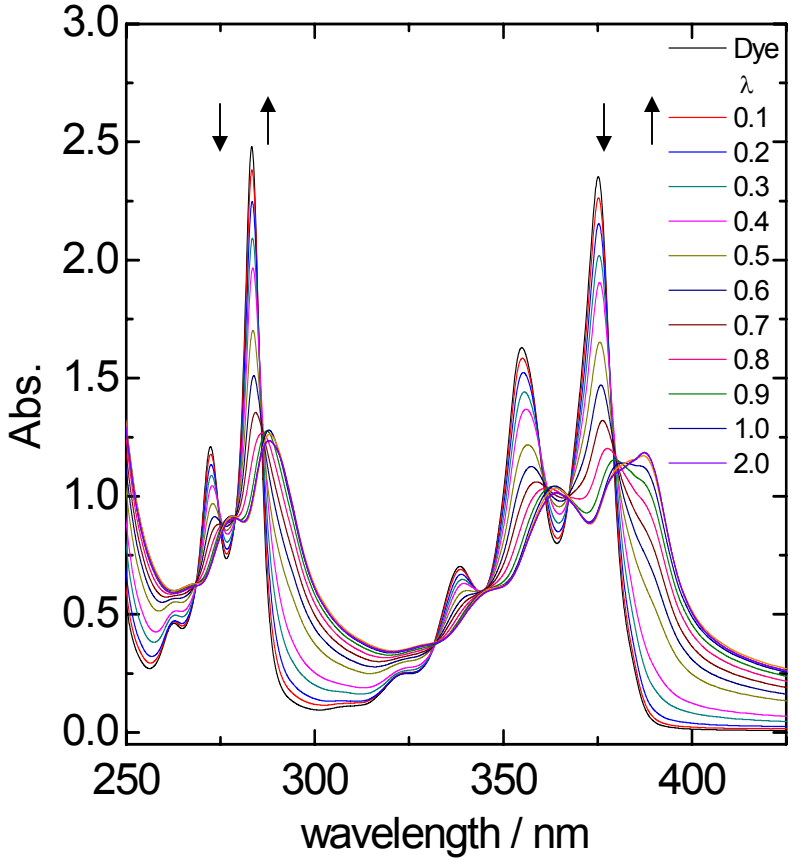

Figure 4.4. Absorption spectra of PY ($1.8\ 10^{-4}$ M) titrated with PD4-2

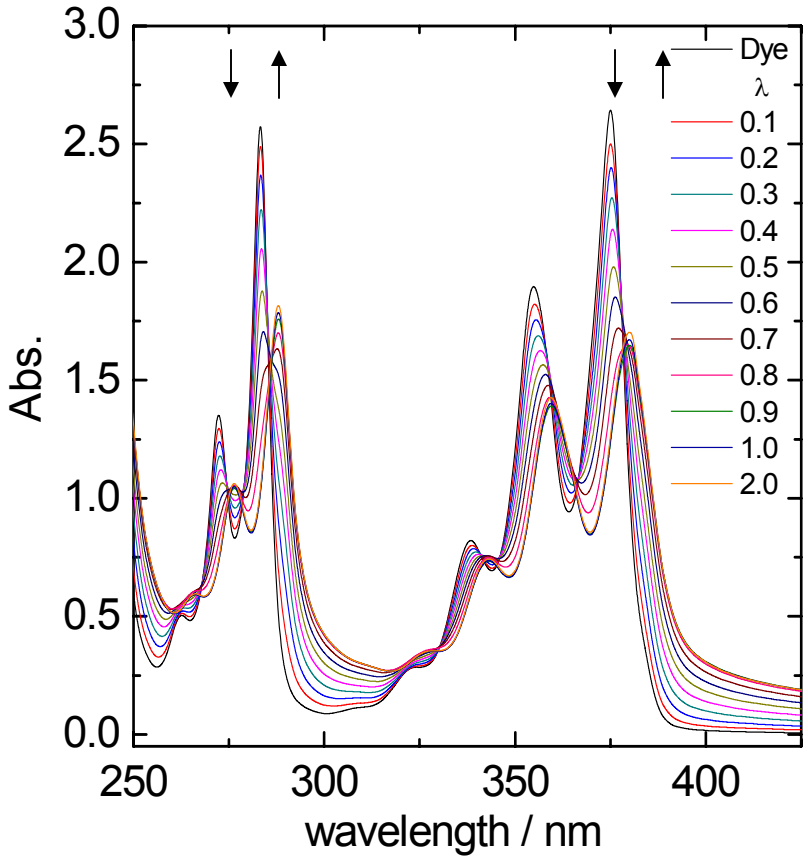

Figure 4.5. Absorption spectra of PY (1.8 10^{-4} M) titrated with PD4coPD6

In all absorption spectra, one clear indication of pyrene association is the broadening of the absorption bands, compared to the absorption in very dilute solution without addition. The broadening of the absorption bands were accompanied by the small red shifts in the positions of the maxima and by the decrease of the intensity of the peak. As pointed out by Winnik; the magnitude of the red shift (2 nm and 5-7nm in the presence of PD4 and PD6, PD4- 2, PD4coPD6 respectively) gives a qualitative measure of the extent of the pyrene aggregation.[144] According to the observed red shift in absorption maximum it could be concluded that while PD4 induces the dimerization of PY, the rest of the ionenes induces the formation of higher PY aggregates. This result considers that association of PY molecules to polyelectrolytes is clearly influenced by the polyion structure. In particular the mutual interaction of the dye molecules may

predominantly be effected the by intercharge distances of ionenes. The long distances between the positive centers of PD6, with respect to the PD4 and PD4-2 may limit the interaction of PY molecules and induces formation of lower aggregates.

Based on the UV-Vis results dye binding abilities of all ionenes can be generalized as follows: Both the red shifts and the hypochromism clearly prove the ground state association of PY molecules and existence of pyrene dimers and aggregates. Charge distances correspondingly charge densities of the ionenes chain enhance the PY-PY interactions and induce formation of higher PY ground state aggregate.

To understand the binding characteristics and actual state of bound pyrene molecules on ionenes backbone, fluorescence titration experiments were carried out. The fluorescence spectrum of PY at low concentration (10^{-6} M) in pure water exhibits the characteristic monomeric emission where the emission maxima are located at 385 nm and 403 nm (Figure 4.1 black line). Figure 4.7 shows the PY titration with PD6, the only detectable change was quenching of the monomer emission (This decrease may be because of concentration quenching, page 111 Figure A6). In contrast, addition of PD4 (Figure 4.8) induces the onset of the typical excimer emission at 500 nm. At $\lambda \geq 1$ the original monomer emission of PY becomes very weak and only excimer is present.[145-147] While PD4-2 behaves like PD6, the copolymer (Figure 4.9 and 4.10) exhibit weak excimer emission with respect to PD4. These results suggest that the nature or structure of association of PY can be varied by ionenes with different charge separations of their backbone. The inter-charge distance evidently is a significant parameter for pyrene association. The lack of induced excimer emission for PD6-PY complexes as compared to PD4-PY may be because of larger inter-charge distances of PD6 with respect to PD4.[148-150] More explicitly, larger distances between the charges may avoid mutual PY-PY interactions and disrupt the optimum orientation of aromatic rings for excimer formation (see Figure 4.6).

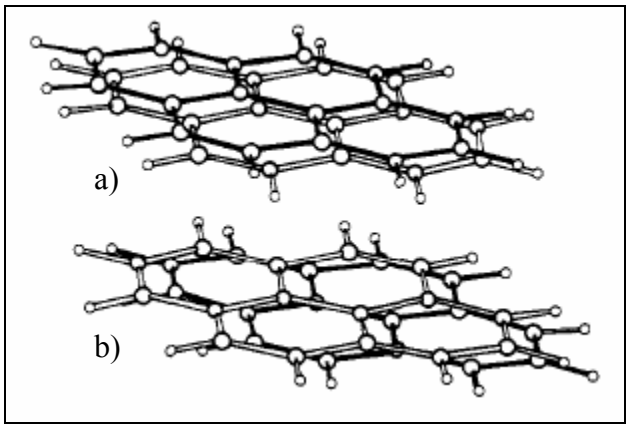

Figure 4.6. Calculated equilibrium geometries of the ground state dimer (a) and the excimer (b). [144]

However this statement is not consistent with our UV-Vis results which unequivocally prove the existence of ground state association PY-PY on PD6 backbone. At this stage it is worth considering the possibility of higher aggregates on the PD6 backbone (or on the PD4-2). When excited, higher order aggregates of pyrene (trimers, tetramer…) can form excimers within the preformed group. An excimer as defined by Birks, is a dimer which is associated in an electronic excited state and which is dissociative in its ground state. However the ability to form an excimer (always involving only two units) depends on the cluster size as well as the excess of vibrational energy[151]. A dimer forms an excimer without excess energy but the higher aggregates require an excess of vibrational energy above a certain minimum value. Presumably the higher cluster of pyrene that exists in the system of PD6-PY and PD4-2-PY are not given any excess vibrational energy to enable them to rearrange and form an emissive sandwich-like structure within the cluster. As a result they are non-emissive or 'dark' aggregates, i.e. not detected in the fluorescent measurement.[151,152]

Both fluorescence and UV-Vis results reveal that inter-charge distances of ionenes play a decisive role on pyrene aggregation; while PD4 likely it is indeed the striucture that plays a role in the interaction here, either directly by electronic interaction or by causing different intercharce distances of the bonds. In any case, it is not alone the charge distance that is decisive. All these observations prove that structure on the backbone of PD4 and PD4coPD6 provides suitable platform for association of pyrene molecules into

dimers and the possible conformational adaptations of the postions of positive centers on PD6 backbone may induce higher order pyrene aggregates.

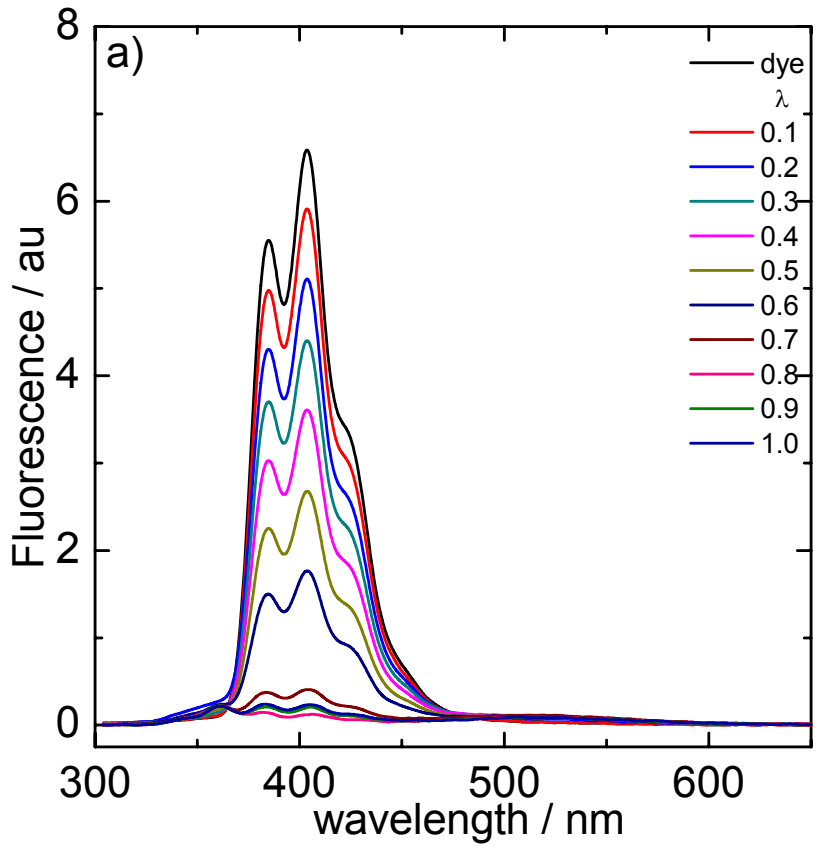

Figure 4.7. Emission spectra of PY (1.8 10^{-4} M) titrated with PD6

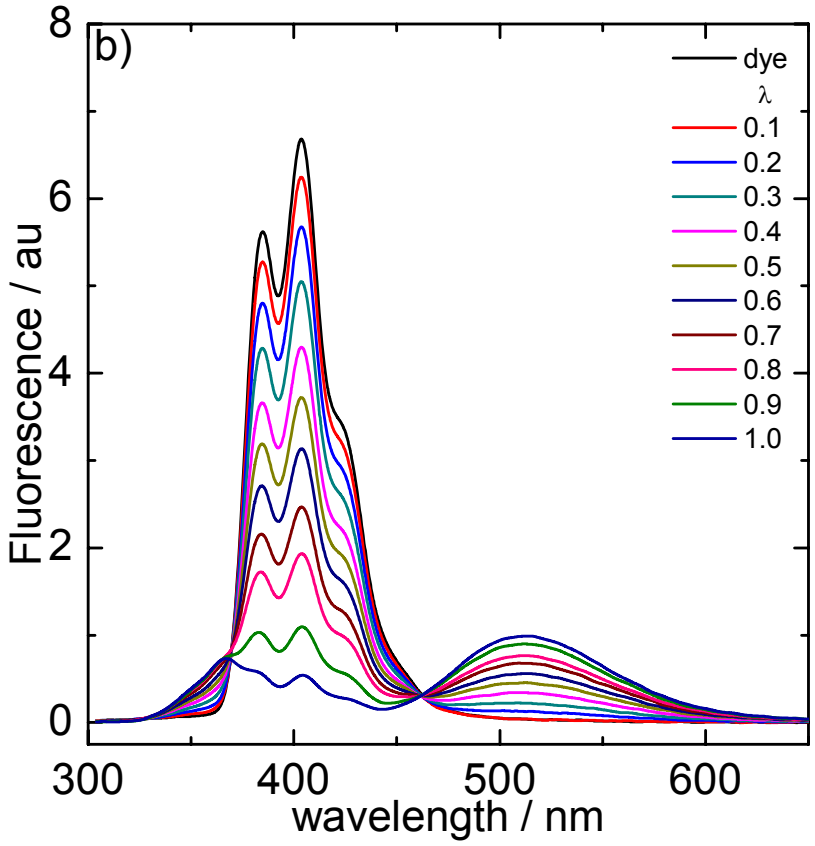

Figure 4.8. Emission spectra of PY (1.8 10^{-4} M) titrated with PD4.

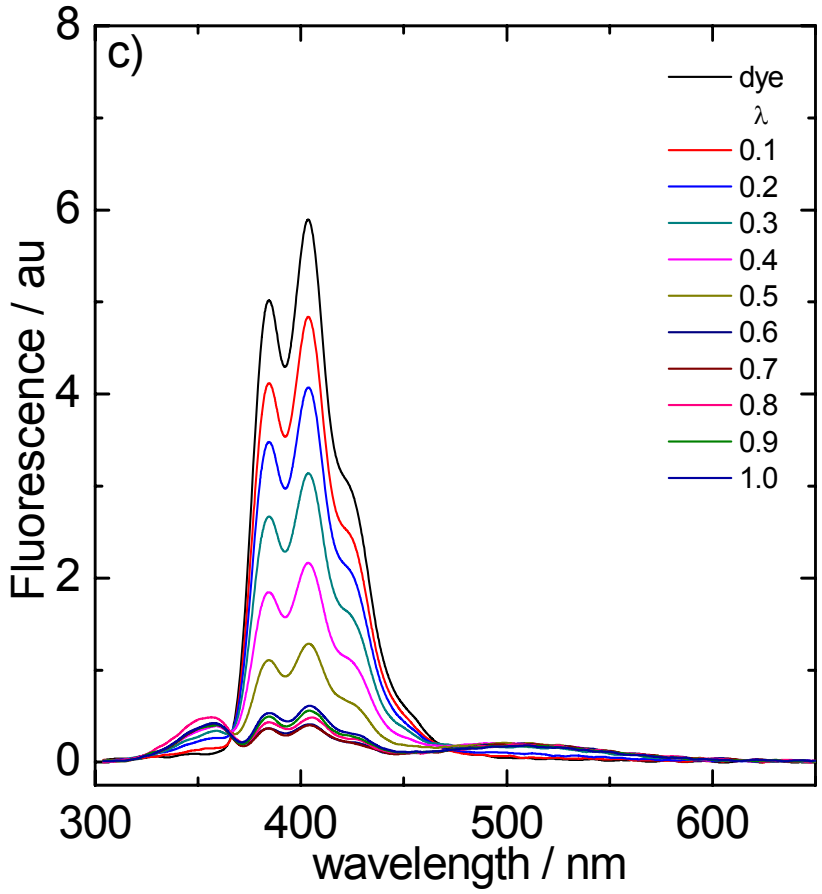

Figure 4.9. Emission spectra of PY (1.8 10^{-4} M) titrated with PD4-2.

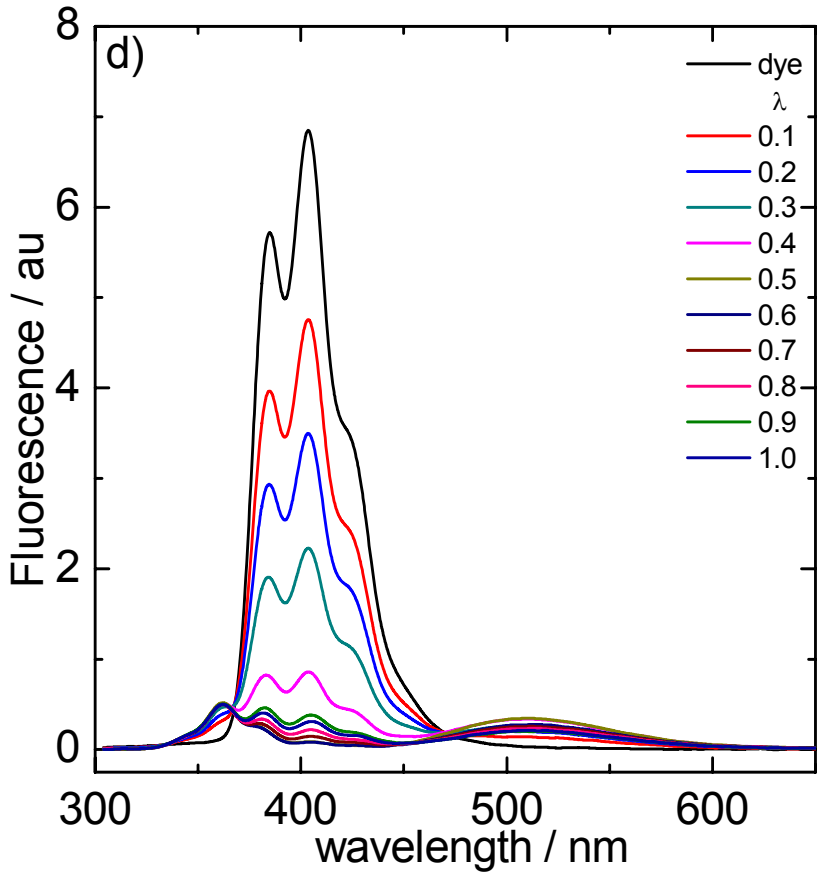

Figure 4.10. Emission spectra of PY ($1.8\ 10^{-4}$ M) titrated with PD4coPD6.

Earlier studies[127-130] showed that the binding mechanism of ionic aromatic dyes to oppositely charged polyelectrolyes is a cooperative process. By considering simple equilibrium constants for dye dimerization and binding of dye to polyelectrolyte, a model for this coopertative binding was developed. By determining extinction coefficients of monomeric dye, dimeric dye and "stacked" dye bound to the polyelectrolyte, UV-VIS spectra as function of charge ratio can thus yield thermodynamic data[78]. According to this model* we determined the fraction of the free dye γ^* (not bound to the polyelectrolyte) as function of polymer to dye ratio (Figure 4.11).

The shape of the curve in Figure 4.11 is typical of cooperative binding behaviour. Analysis yields a cooperative binding constant, that is the equilibrium constant for the binding of one dye to polyelectrolyte adjacently to an already bound dye molecule K = 6.4 x 10^6 M^- ($\pm$ 10^5 M^-) this is two order magnitude larger than the dimerization constant of PY (K_D = 5 x 10^4 M^- ($\pm$ 10^2 M^-) Thus the binding of the dye to polyelectrolyte is much stringer due to ionic interaction and cooperative effects.

* Details about the calculation procedure are documented in Appendix

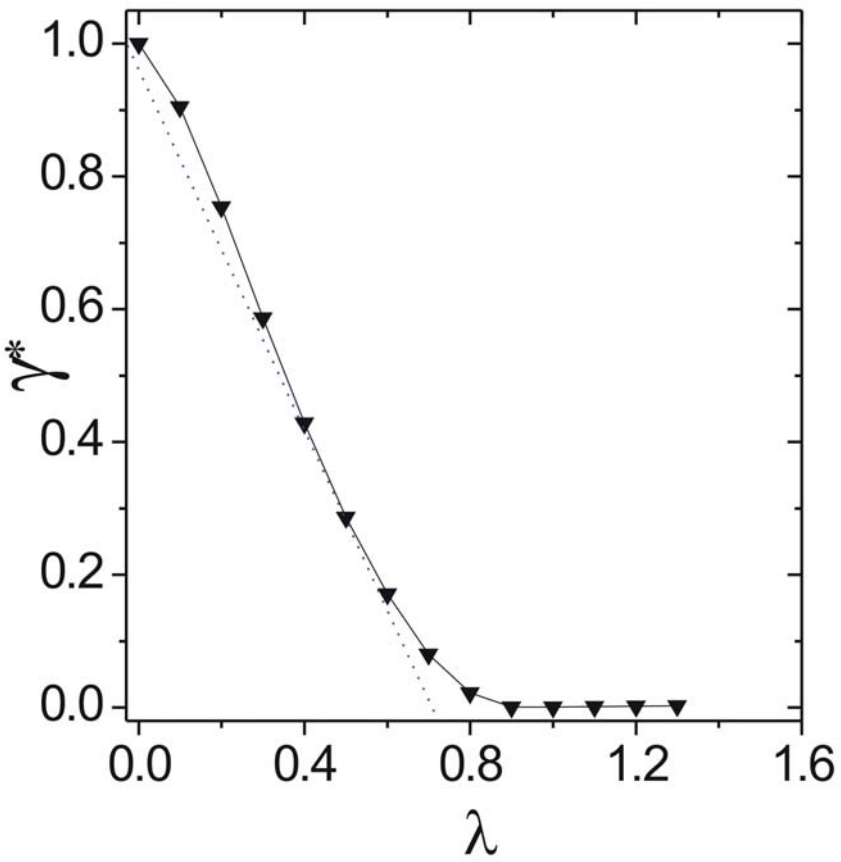

Figure 4.11. PD6-PY system: fraction of free dye (γ^*) as a function of polymer to dye ratio (λ).

4.2 Imaging of Ionene-Dye Aggregates

In the following we focus on the two polyelectrolytes PD4 and PD6 that showed very different association behavior with PY in UV-Vis spectroscopy. An impression of size and geometry of PD4-PY and PD6-PY can be gained from confocal laser scanning microscopy in aqueous solution. Images for aggregates formed at charge stoichiometry are shown in Figure4.12. PD4-PY yields well defined supramolecular spheres which have 300 nm to 400 nm size in diameter (Figure 4.12 b,c,d), on the contrary at same composition PD6-PY aggregates are micrometer sized structureless aggregates (Figure 4.12 a). Thus chemically similar ionenes but with difference in structural details with same dye molecules yield completely different aggregates.

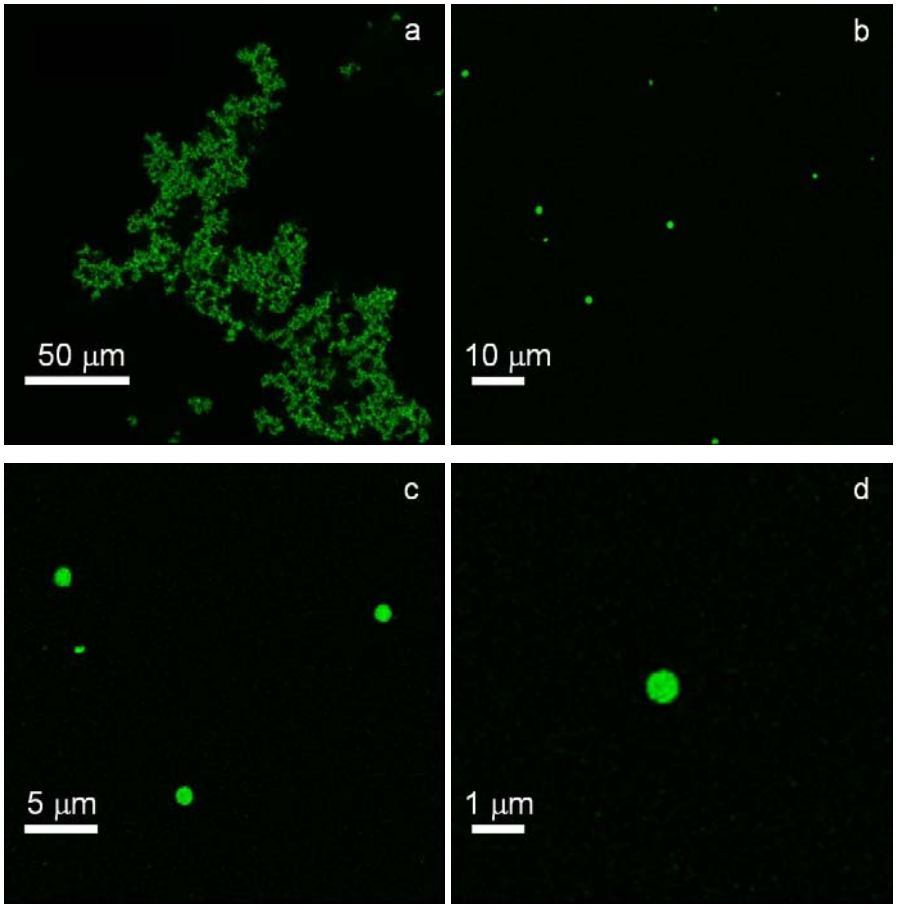

Figure 4.12. Confocal Microscope images of a)PD6-PY b,c,d) PD4-PY

The morphology of aggregates of PD4 and PD6 with PY and pure ionenes was further investigated by atomic force microscopy (see page 116 for sample preparation). The AFM characterization of the PD4 and PD6 ionenes revealed small round shaped flattened particles with 25 nm and 15 nm diameter and 2 nm and 1 nm in height (see Figure 4.13). AFM images of samples with PY are shown in Figure 4.14-17. The result again reveals that the behavior strongly depends on polyions used. Obviously, the structure of an aggregate formed in solution may change substantially upon deposition on a surface. Complementary light scattering results on the solution structures will be discussed in the next section. AFM images show that the PD4-PY has a defined spherical shape while PD6-PY gives randomly interconnected aggregates (in Figure 4.17). Interconnected precipitates (flocculant) which have undefined shape and 5-10 μm in size have been observed. Reasons for the difference between the two systems must again be the variation in the chemical structure of the polyelectrolyte. PD4 may be able to form "closed" aggregates more easily as compared to PD6 with somewhat larger charge distance and charge density.

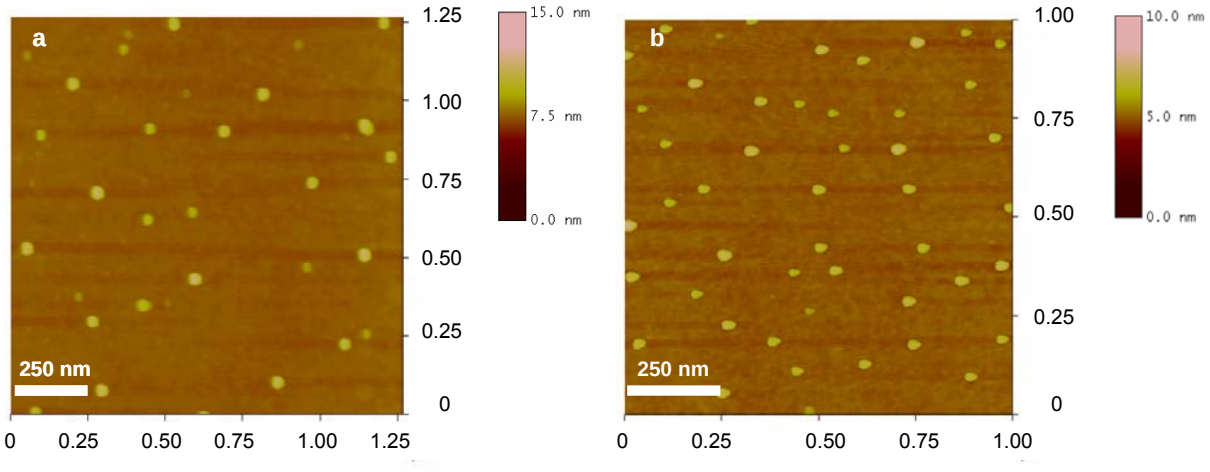

Figure 4.13. AFM images of a) PD4 b) PD6 on Si wafer

AFM images of the PD4-PY aggregates at various λ values, again after deposition on silicon surfaces, are shown in Figure 4.14-16. This investigation shows that PY complexes can be tuned in size by varying λ within certain limits. The complexes that were prepared under conditions of λ = 0.1, which is with pyrene dye in excess, exhibit a diameter of the spherical aggregates on the Si surface in the range from 40 nm to 60 nm

(see Figure 4.14). In the case of $\lambda = 1$ the diameter of the aggregates are 200 nm (± 20 nm) (see Figure 4.15). In contrast, aggregation in excess of polymer ($\lambda > 1$) yields rather undefined particles with no fixed shape and high polydispersity in size. The particle size varies between 30 to 150 nm in this composition also gives range of sizes (Figure 4.16).

The section analysis of the smaller spherical objects reveals that the height of the aggregates is 10-15 nm which may be due to the deformation of the objects on the surface.[158,159] This deformation is even more pronounced in the case of the larger spherical objects (diameter is 200 nm and height is 10 nm to 20 nm). For $\lambda = 1$, nanoparticles are of core-shell type. The core diameter is about 180 nm and its height is (10-15) nm whereas shell diameter is roughly 15 nm with 1 nm height. Nanoparticles formed for $\lambda = 0.1$ do not exhibit this expressed core-shell structure and thus are expected to be solid (soft) sphere-like particles. Spherical nanoparticles may be the consequence of strong ionic interactions between PD4 and PY and stability of the system is may be governed by the combination of the ionic and hydrophobic forces. In a broader sense this is in analogy to the formation of spherical aggregates from polyelectrolyte-surfactant complexes, specifically a poly (ethylene imine)-dodecanoate complex.[41,153]Accordingly, spherical nanoparticles are stabilized as a results of the combination of ionic and steric contributions.[154-157]

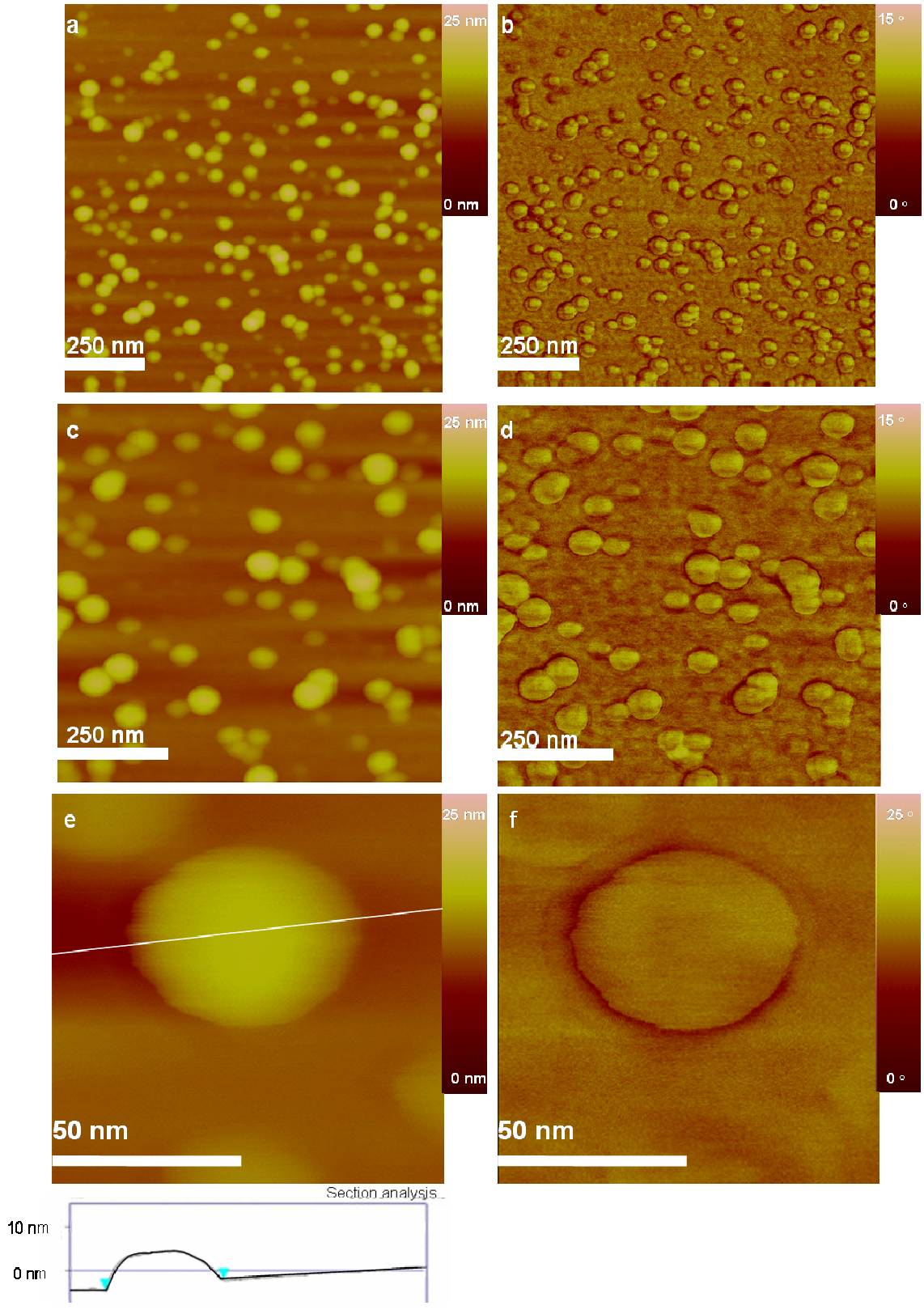

Figure 4.14. PD4-PY aggregates at λ = 0.1 on Si wafer.

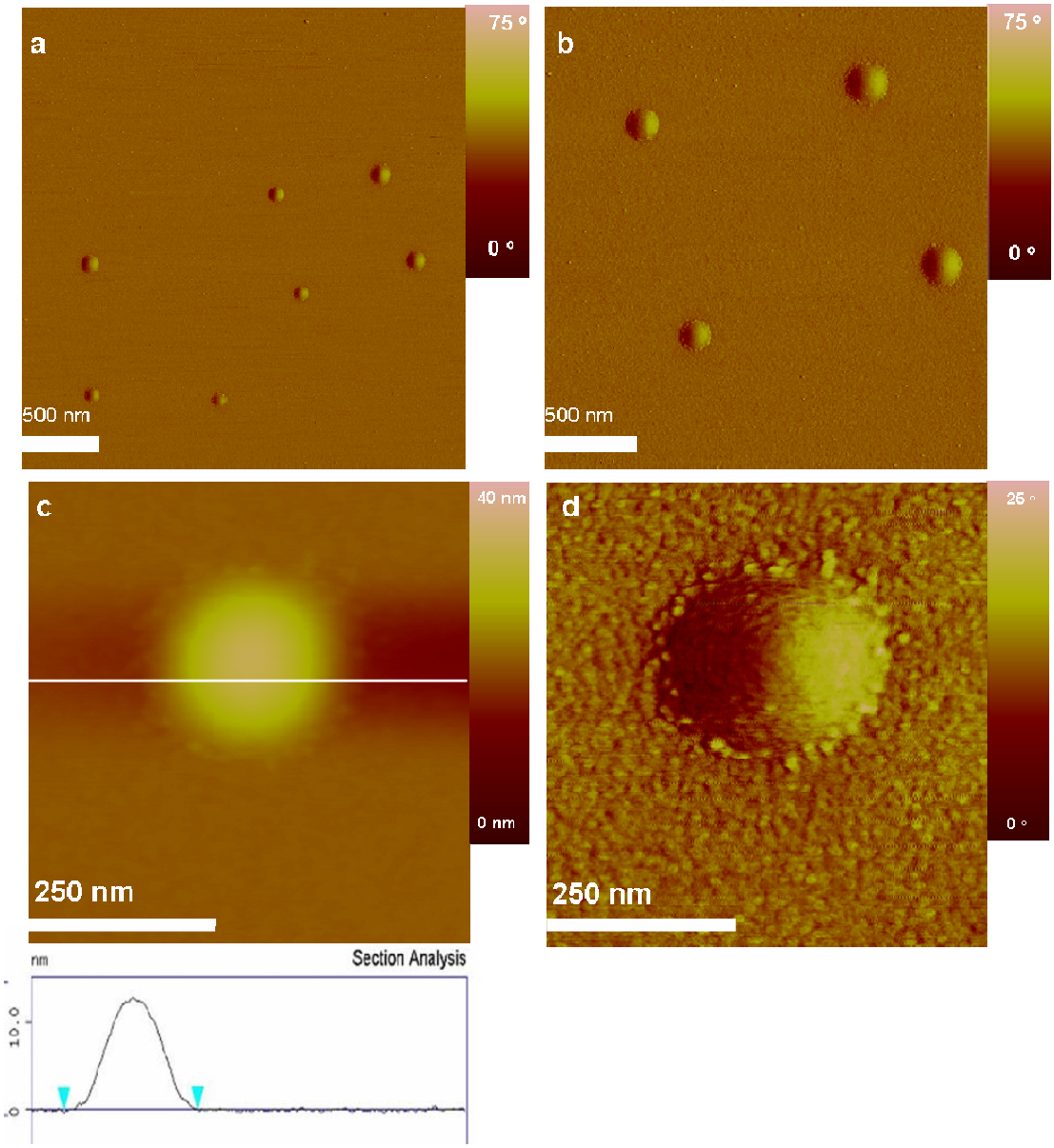

Figure 4.15. PD4-PY aggregates at λ = 1.0 on Si wafer.

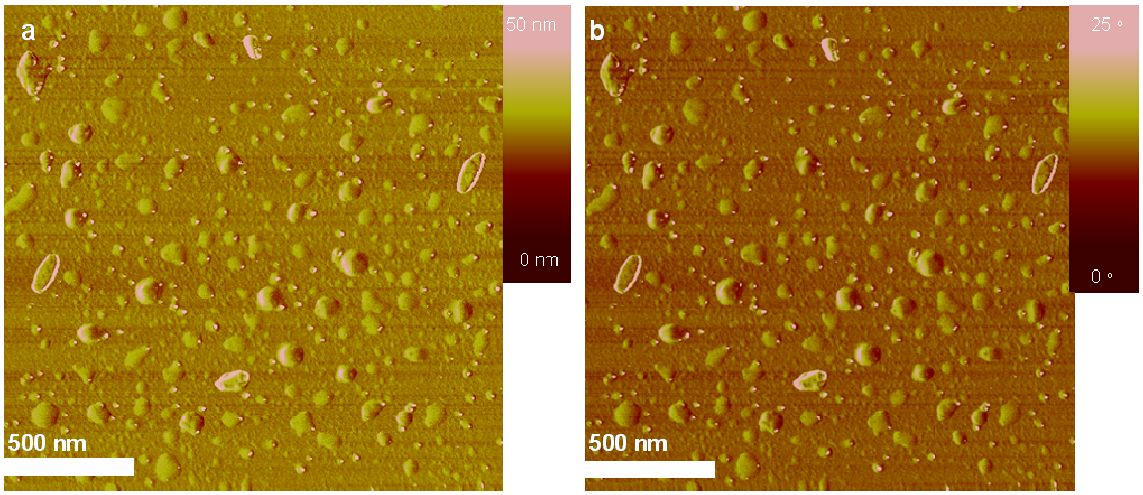

Figure 4.16. PD4-PY aggregtaes at λ = 1.2 on Si wafer.

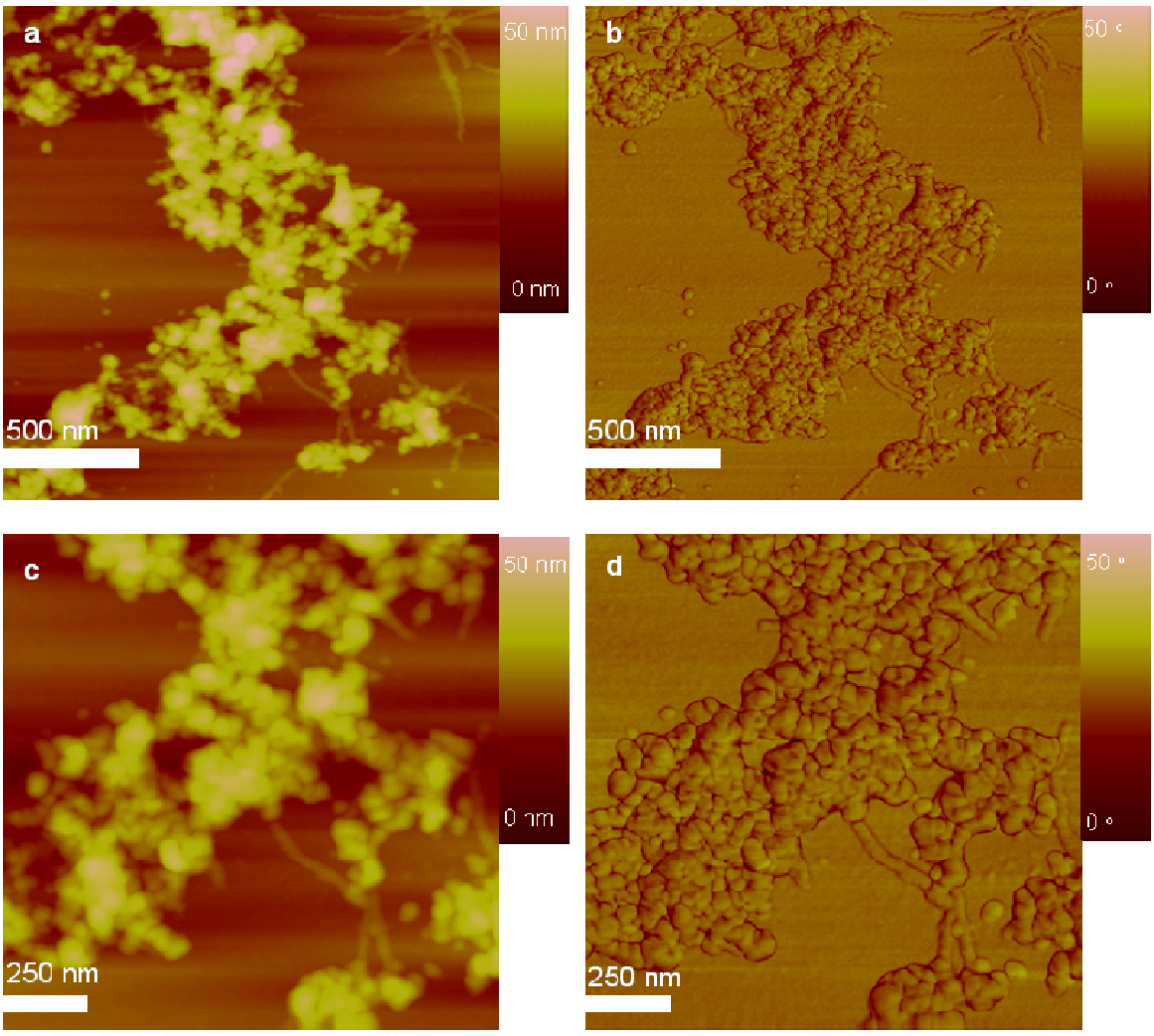

Figure 4.17. PD6-PY aggregates at λ = 1.0 on Si wafer.

As pointed out by Thünemann, such nanoparticles may usually be core-shell type and exhibit a profile with in the corresponding AFM analysis.[153] This behavior is explained by a stoichiometric composition (nearly 1:1) in the core and a non-stoichiometric composition in the shell causing different interaction strength with the surface. The formation of spherical aggregates from poly (ethylene imine)-dodecanoate complex and poly (ethyleneimine)-pyrenetetrasulfonic acid complex have been reported previously.[41,138,153]

The reasons of such a shape persistent nanoparticle formation are ionic and steric contributions in other words, strong ionic binding and high cooperativity between PY molecules provide enough stability against to dissolution (or disintegration) of colloidal particles

4.3 Light Scattering Investigation of Assemblies in Solution

Dynamic and static light scattering were used to measure the particle size of the ionenes and ionenes-dye complexes. Figure 4.18 shows the diffusion coefficient as a function of ionenes concentration in the presence of low molecular mass salt KBr. The apparent hydrodynamic radii (R_H) as determined from the extrapolated diffusion coefficients via Stokes-Einstein equation were 3 nm and 4nm for PD4 and PD6, respectively. Hydrodynamic radii obtained are in agreement with the molecular weight of the corresponding ionenes.

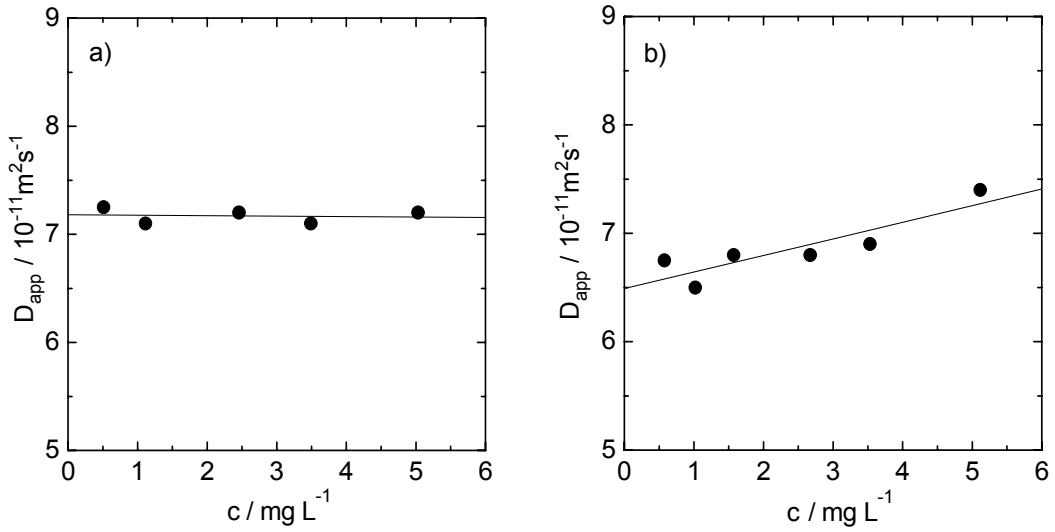

Figure 4.18. Diffusion Coefficient as a function of ionene concentration a) PD4 b) PD6 in 0.4 M KBr solution

4.3.1 PD4-PY Complexes

As previously presented by AFM, topology and size of particles may change as a response to a variation of charge ratio as follows i) when the charge ratio "λ" is lower than 1 (it means dye is in excess) compact spherical nanoparticles are formed, ii) in the case of where "λ" is greater than 1 (it means ionenes are in excess) resultant particles have rather undefined topologies and exhibit significant drop in sizes iii) at $\lambda = 1.0$ significant deviations in surface roughness of particle do occur. These experimental findings are in good agreement with the corresponding light scattering results in a way

that depending on the variation of λ size and the morphology of particles show the same trend.

For PD4-PY, diffusion coefficients for various λ are shown as a function of the scattering vector square in Figure 4.19a. For better visualization all D_{app} distributions at various λ are shown in the same plot. The average diffusion coefficient $\langle D_z \rangle$ which is a z-average was determined by extrapolation of the apparent diffusion coefficient towards zero scattering vector q. Calculated $\langle D_z \rangle$ and corresponding R_H values are tabulated in Table 4.1.

A decrease in diffusion coefficient was observed as λ increases up to λ = 1: for λ = 0.1, the hydrodynamic radius is R_H = 64 nm, whereas at λ = 1.0, it is R_H = 320 nm. This size dependence reverses for λ > 1. The relaxation time distributions for the complexes at various λ values are shown in Figure 4.19c. For λ ≤ 1 distribution are unimodal. Bimodal distributions were observed for λ =1.2 and λ =1.5 (Figure 4.19d). The hydrodynamic radii of the smaller species are around 10 nm. These species are too large to represent individual ionene molecules but may be small nonstiochiometric complexes.

Figure 4.20 exhibits static light scattering results. For the λ ≤1 region, scattering intensity I(q) vs q does not yield linear behavior over an extended q-range (Figure 4.20.a) but a Guinier representation shows initial linear relationship (Figure 4.20b). This confirms the overall globular shape of the particles as observed in AFM and allows determination of the radius of gyration. It is observed that the R_G values are also λ dependent and exhibiting same growth trend as R_H.

Table 4.1. $\langle D_z \rangle$, R_H, R_G and ρ (R_G/R_H ratio) of PD4-PY aggregates at various λ in aqueous solution without added salt.

λ	$\langle D_z \rangle$ / 10^{-12} m^2 s^-	R_H / nm	R_G / nm	ρ
0.1	3.20	64	47	0.75
0.3	1.21	180	130	0.72
0.5	0.94	230	180	0.78
0.7	0.70	290	225	0.77
1.0	0.64	320	190	0.60
1.1	2.4	90	80	0.88
1.5	3.8	55	40	0.72
2.0	4.4	50	40	0.8

R_G of the complex for $\lambda = 0.1$ is $R_G = 47$ nm while at $\lambda = 1.0$, it is $R_G = 190$ nm. The dependence of the ρ ratio, revealing the morphology and microstructure of the complexes, on λ is presented in Figure 4.21. At $\lambda < 1$ ρ is independent of λ and it stays constant as 0.78 which is the characteristic for hard spheres. With regard to AFM images of the complex at $\lambda = 0.1$ rigid morphology can obviously be seen that complexes are in form of solid nanospheres and these findings are in good agreement with light scattering results. However at $\lambda = 1.0$ ρ has been found as 0.60 which is 25% lower than for hard spheres or in other words, aggregates in this region have hydrodynamic radii much larger than the geometric radii. It has already been concluded form AFM investigation that the spherical aggregates at $\lambda = 1.0$ have coronas which are loosely packed with respect to the core of the nanospheres.

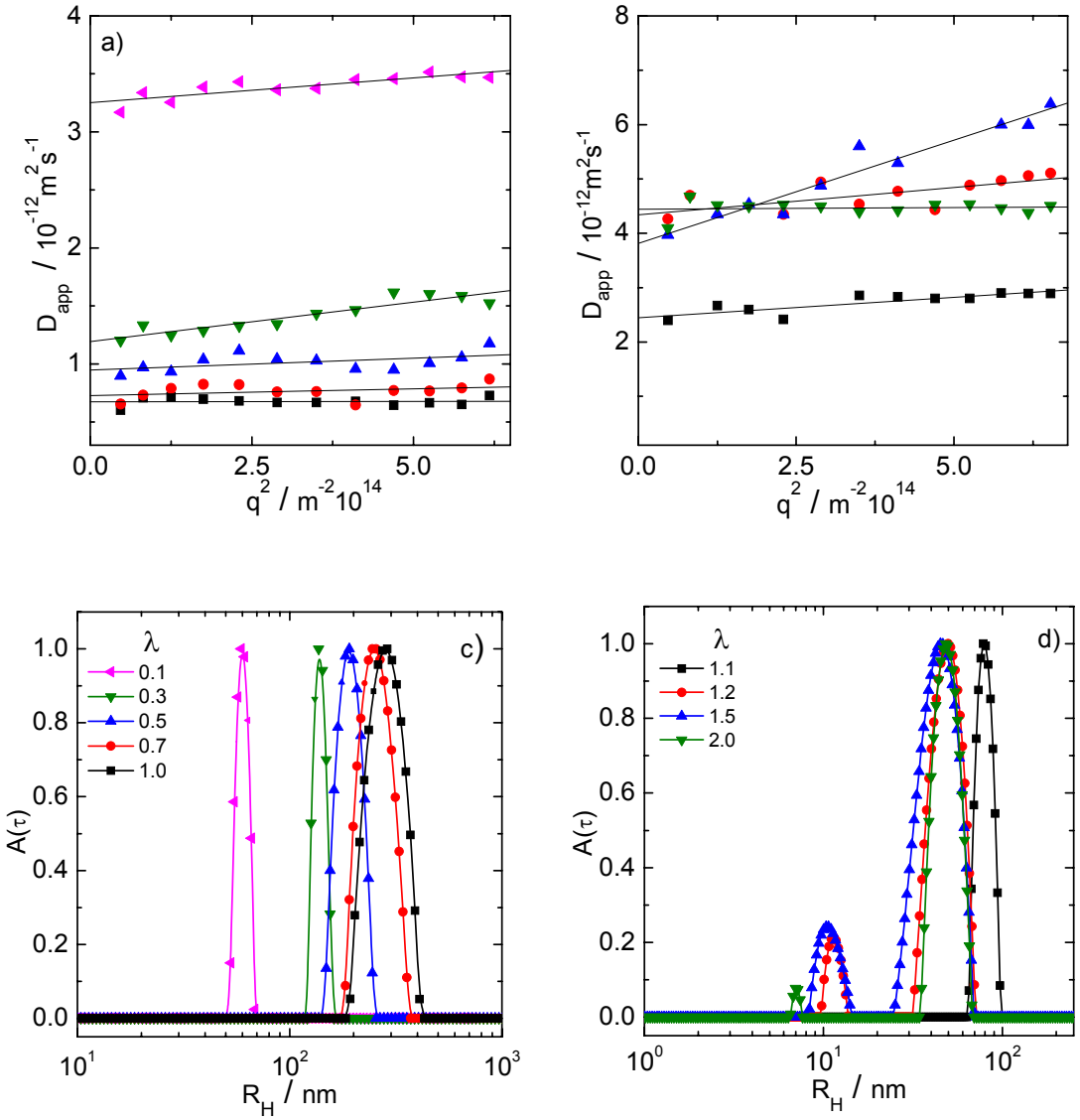

Figure 4.19. Diffusion coefficients of PD4-PY aggregates at as a function of scattering vector square a) λ ≤1 (■:λ=1.0,●:λ=0.7,▼:λ=0.5,▲:λ=0.3,◀:λ=0.1) b) λ > 1 (■:λ=1.1, ●:λ=1.2, ▲:λ=1.5, ▼:λ=2.0) c) Hydrodynamic radius distribution of PD4-PY aggregates at λ≤1 d) Hydrodynamic radius distribution of PD4-PY complexes at λ > 1

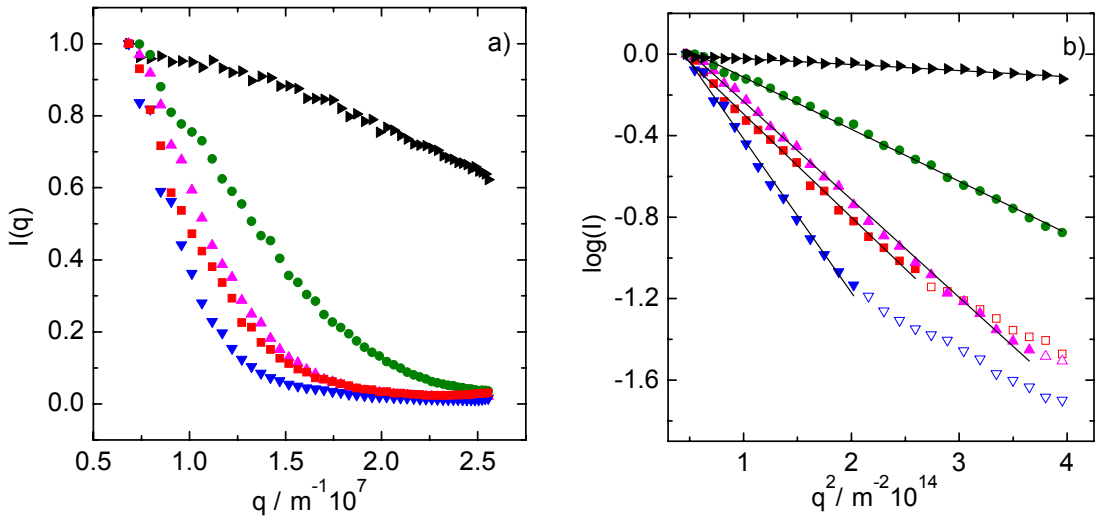

Figure 4.20. a) b) Normalized scattering intensity (I) of PD4-PY aggregates at $\lambda \leq 1$ as a function of scattering vector (q) b) Logarithm of scattering intensity (I) of PD4-PY aggregates at $\lambda \leq 1$ as a function of scattering vector square (q^2)

(■:λ=1.0, ▼:λ=0.7, ▲:λ=0.5, ●:λ=0.3, ►:λ=0.1)

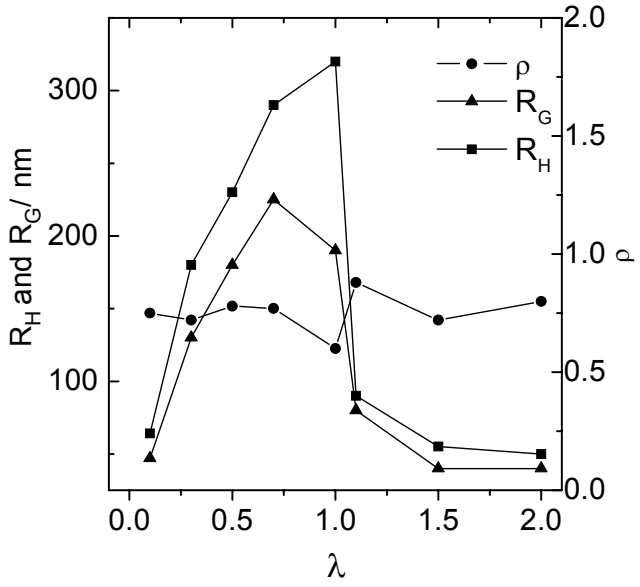

Figure 4.21. R_H, R_G and ρ ratios of PD4-PY complexes at corresponding

In the literature a ρ ratio varying between from 0.49 to 0.58 has been reported for poly (buthlymethacrylate) microgels with spherical geometry.[160] It has been pointed out that possible reason of obtaining such a ρ ratio is the inhomogeneous density or branching profile in center with respect to outer shell of the particles. From the structural point of view from the center to a certain radius a network type structure may be found but more dangling or free chains are present outside. There is a strong analogy between this system and the PD4-PY complexes at $\lambda = 1.0$. As it has already explained in the AFM section; the complex at this λ value is an inhomogeneous sphere consisting of a densely packed core which is made of stoichiometric complex of PD4-PY and corona formed by loosely packed components. Accordingly, PD4-PY nanospheres at this composition yield a hydrodynamic radius much larger than the radius of gyration. In addition the following effect should be considered: non-uniform distribution in morphology allows water incorporation into the loosely packed corona of nanospheres and further expansion of the corona (when comparing LS results to AFM results). Thus the obtained ρ ratio (0.60) for the complex can be ascribed to both an inhomogeneous radial density distribution and the expansion of corona due to water incorporation or swelling. (see Figure 4.23)

Further information on the particle structure can be obtained by small-angle neutron scattering (SANS). Figure 10 shows the combined SANS and SLS data and the pair distance distribution function resulting from indirect Fourier Transformation (Figure 4.22). It reveals particles with a maximum dimension of about 650 nm, that is, a "geometrical radius" of 325 nm. The radius of gyration of this P(r) is $R_G = 195$ nm, which is good agreement with the Guinier extrapolation result of the light scattering data ($R_G =$ 190 nm). The P(r) can then further be deconvoluted into a radial density profile of the spherical particle, as shown in Figure 11c. It shows basically a two-step profile with a higher scattering length density in the inside, the core exhibiting a radius of about 140 nm and an outer shell with substantially lower scattering length density with a thickness of about 210 nm and about 1/10 of the density of the inner part.

Hence, the core-shell structure predicted based on the R_G/R_H from light scattering is confirmed. While this morphology as such was also indicated by the AFM images of the particles deposited onto a surface, the radii obtained from scattering are substantially

larger. This can in part be attributed to the different average that is measured in both methods, that is, the relative contribution of larger particles in a polydisperse sample is larger in scattering. Yet dynamic light scattering revealed not too broad distributions so that this is likely not the only explanation. Changes of the self assembled structure upon drying on the surface are likely to happen. This may lead to some shrinking, in particular of the looser outer shell. Accordingly, the shrinkage of the core shell-spheres at $\lambda = 1$ upon drying on the surface is more extended than the one of the more solid spheres at $\lambda = 0.1$. Nevertheless, both in solution and on a surface some type of core-shell architecture was observed.

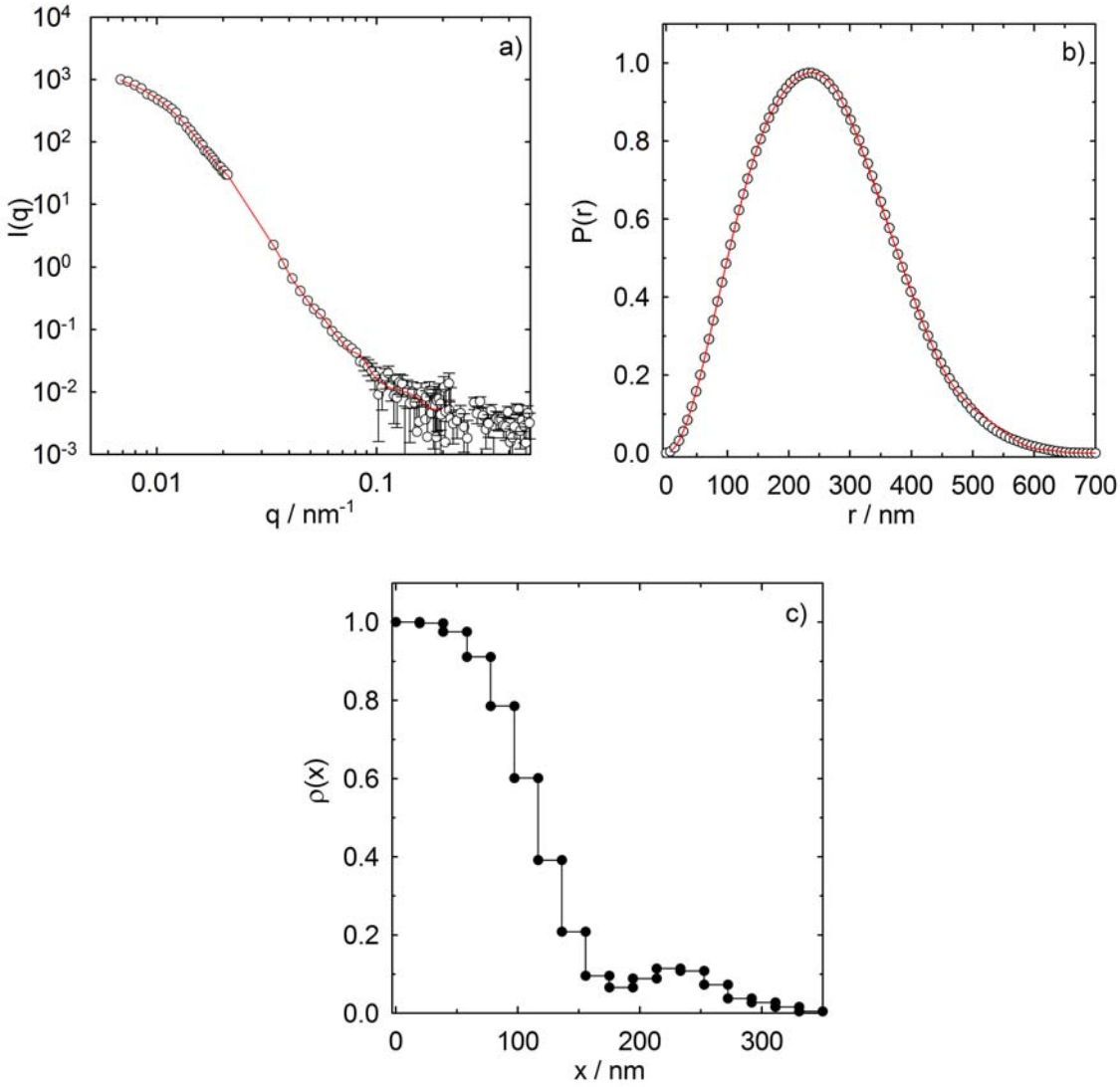

Figure 4.22. Small-angle neutron scattering results for the PD4-PY sample with λ = 1.0: a) Experimental SLS and SANS scattering curve I(q) (symbols) and fit to the data (red line), b) pair distance distribution function P(r) according to the fit in a) (symbols) and fit to the data (red line), c) radial density profile ρ(x) according to the fit in b).

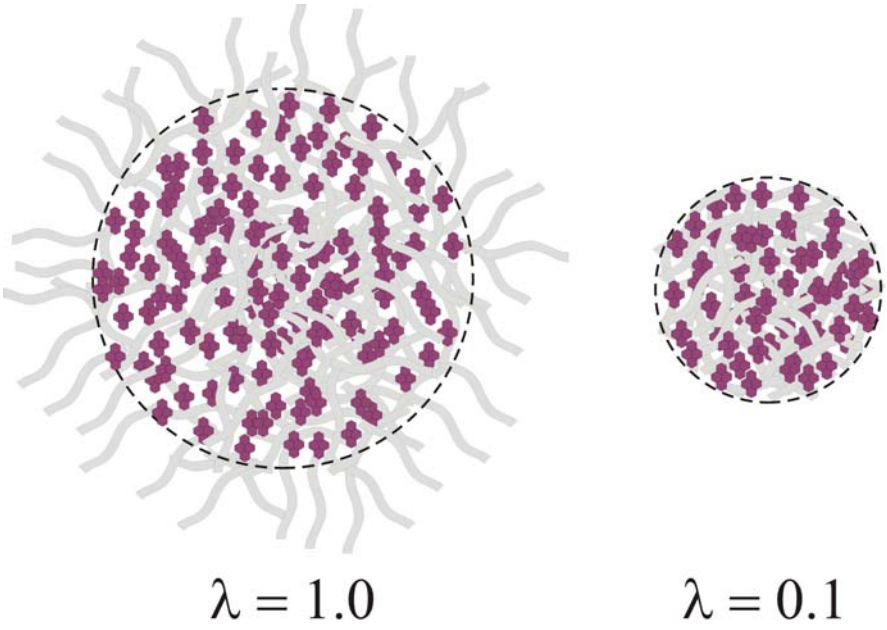

Figure 4.23. Proposed model of PD4-PY particles at λ = 0.1 and λ = 1.0

For λ>1, D_{app} distributions at various λ are depicted in Figure 4.19b. A significant decrease in R_H with inceasing amount of added polyelectrolyte has been observed. Even in the presence of very small excess of ionenes (λ = 1.1) R_H has decreased to 90 nm and it reaches 50 nm for λ = 2.0. Possible reason for the size decrease can be the smaller amount of "linking" multivalent dye molecules per polymer chain. As clearly seen from corresponding AFM images in this region, geometrically undefined particles are present rather than spherical aggregates, which is in accordance it the broad size distribution observed in DLS. It may also be that the reason lies in less probe-probe interactions which provide stability of resultant nanospheres. Due to the excess of host sites of ionenes at λ>1, dye molecules may be bound to ionenes according to the unspecific site binding mechanism rather than cooperative binding. One may interpret the results such that probe-probe interactions are prerequisite to obtain well defined supramolecular particles from PD4-PY complexes.

4.3.2 PD6-PY Complexes

PD6-PY agregates have also been investigated by light scattering methods. For variying λ, R_G and R_H are given in Table 4.2. In contrast to the previous system there is no clear correlation between λ and size of the complexes in solution evident. As it can be seen from the images of the complexes are stucturless interconnected precipitates (flocculants) rather than well defined objects. Light scattering investigations show that PD6-PY complexes vary in size as a result of variation in charge ratio. Figure 4.25 shows the distribution of apparent diffusion coefficients (D_{app}) as a function of scattering vector square (q^2) for various charge ratio. R_G values of complexes have been obtained from the Zimm plots (Figure 4.25c). These results reveal that at $\lambda \leq 1$ region, PY in excess binds high number of chains together and therefore the aggregation may increase and even macroscopic flocculation may occur (interconnected aggregates). However in the case where λ equals 1 aggregation level decreases significantly due to balance in oppositely charged species. Accordingly, it may be concluded that stoichiometric complexes of PD6-PY lower the aggregation level but higher the surface roughness of complexes.

Table 4.2. R_H, R_G of PD6-PY samples at various λ

λ	R_H / nm	R_G / nm	D_z / 10^{-12} m^2s^-
0.1	360	280	0.64
0.5	1000	280	0.25
1.0	110	130	2.0
2.0	26	-	8.3

As we have already discussed, complex formation between polyelectrolyte and oppositely charged molecules are predominantly governed by strong Coulomb interactions. Resulting structures of complexes may vary depending on the nature of polyelectrolyte as well as differences in the local structures such as arrangement,

proximity and stereochemistry of ionic sites. At this stage it may be considered that inter-charge distances play a decisive role in the case of self-assembly of structurally similar dyes and polyelectrolytes. As clearly indicated by corresponding AFM and fluorescence microscopy results these two ionenes yield an entirely different aggregates in size and topology (see page 69). These significant variations in particle size and morphology of resultant aggregates can be attributed to the differences in binding behavior of PY to the ionenes due to the charge density and flexibility of host molecules. Obviously, the number of positive charges is proportional to the degree of polymerization in linear ionenes. Considering the PD4 and PD6, we may assume that numbers of charged groups are equal since molecular weights and correspondingly degrees of polymerization are nearly the same. In this case effects of inter-charge distances ionenes are more pronounced on the resulting structures of complexes. Theoretical calculations deduce that inter-charge distances between adjacent DABCO as 0.55 nm and 0.88 nm for PD4 and PD6 respectively (see Figure 4.24).

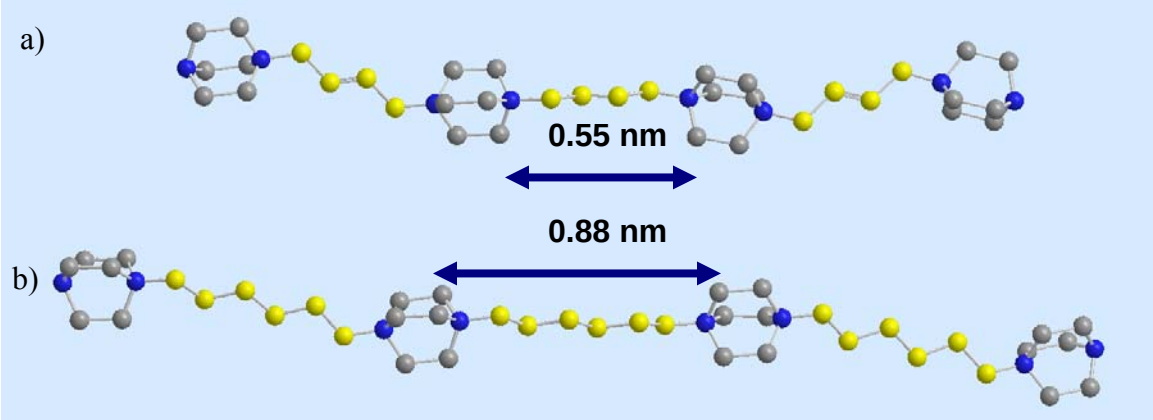

Figure 4.24. Inter-charge distances for a) PD4, b) PD6

Accordingly, on a local scale PD4 may enhance the probe-probe interactions (π–π interactions) due to close proximity between the successive charged units but rigid trans buten group between the charged unit limits the spatial adaptation of PD4 upon complexation and may disrupt the formation of extended PY-PY aggregates.

It may be concluded that macroscopic aggregates form a precipitate from aqueous solution as a result of the strong aggregation tendency of PY molecules on ionene backbone.

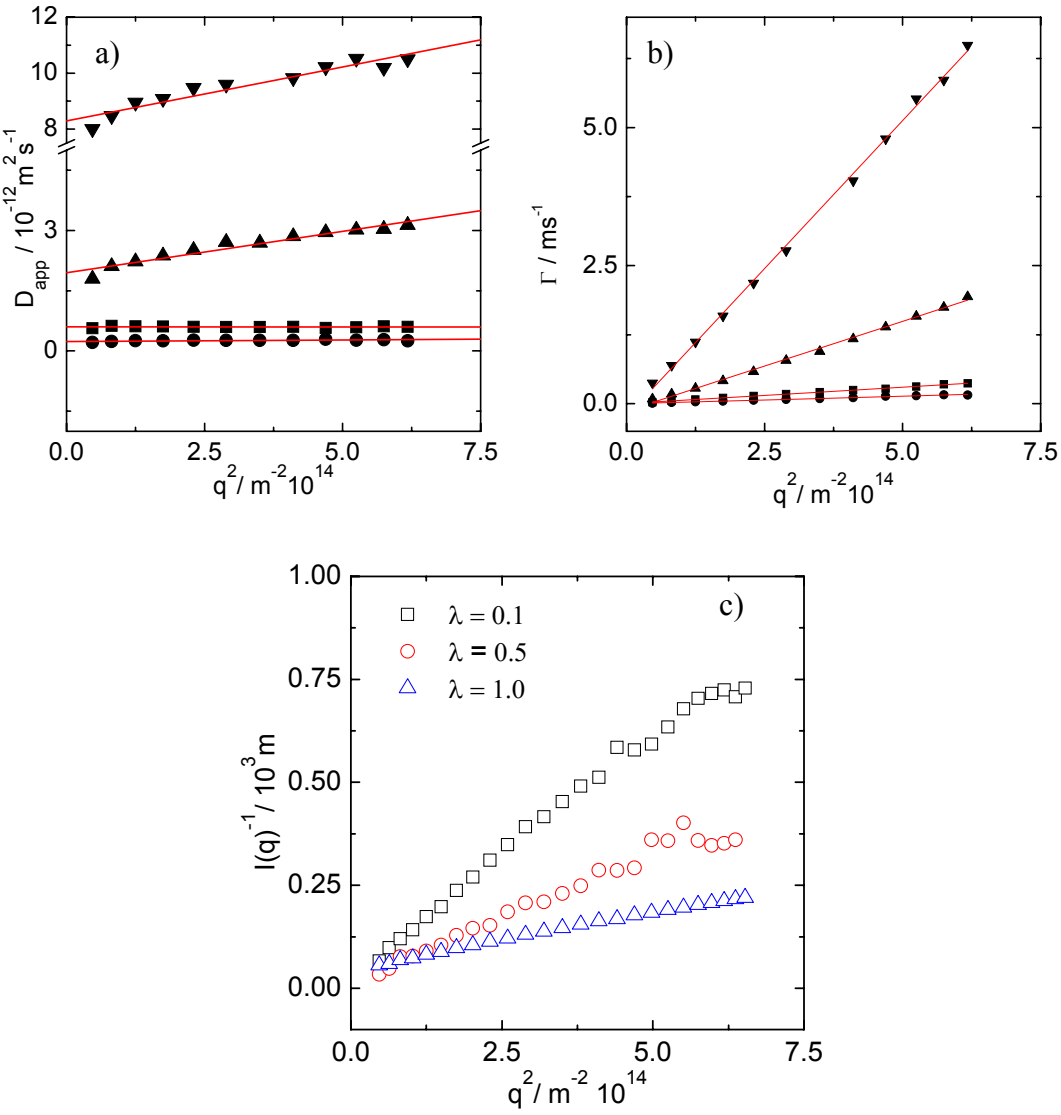

Figure 4.25. Diffusion coefficients of PD6-PY complexes at as a function of scattering vector square (■:λ=0.1,●:λ=0.5,▲:λ=1.0,▼:λ =2.0) b) Decay rate as a function of scattering vector square (■:λ=0.1,●:λ=0.5,▲:λ=1.0,▼:λ =2.0 c) Reciprocal scattering intensity (I^-) as function of scattering vector square (q^2)

4.3.3 Influence of Preparation Conditions and Added Salt

Static and dynamic light scattering reveal the PD4-PY precipitates in form of as spherical structures. As we discussed in previous sections, the aggregation is mainly controlled by the concentration of components and colloidal stability against the further coagulation is provided via electrostatic repulsion. Although the stability of particles is effectively preserved by electrostatic interactions, it may still be manipulated by external stimuli such as ionic strength. The effect of ionic strength (salt addition) on the course of complex formation may cause different processes that may take place during the complexation. In general addition of salt could cause dissolution of the supramolecular assemblies due to screening or formation of macroscopic flocculation ("salting out").

To elucidate the general tendencies of the influence of the salt on aggregates formation we have investigate the complexation reaction by light scattering method in the presence of low molecular mass salt. The dependence of hydrodynamic radius R_H and diffusion coefficients on charge ratio λ have already been presented in Figure 4.26 and

Table 4.3. R_H, D_{app} values of PD4-PY in 0.4 M KBr solution.

λ	R_h / nm	D_{app} / 10^{-12} m^2 s^-
0.1	80	0.3
0.5	130	1.6
1.0	190	1.1
2.0	150	1.4

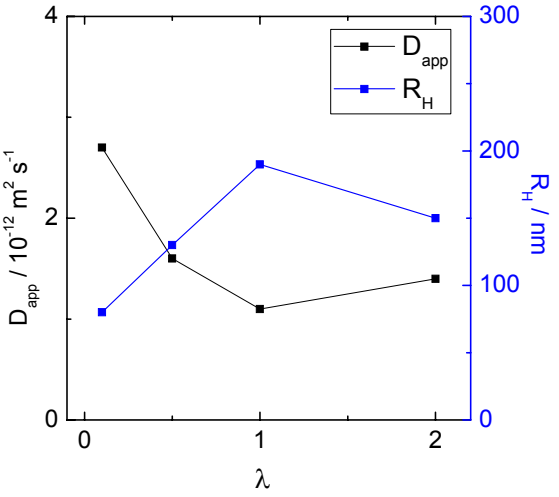

Figure 4.26. Diffusion coefficients and R_H of PD4-PY complexes at as a function of λ in 0.4 M KBr solution.

The PD4-PY complex formation is sensitive to the presence of salt. Presence of salt decreases the size of aggregates as compared to complexes that prepared in pure water substantially. The reason for the decrease in R_H may be a drop in the level of aggregation due to the screening of electrostatic interaction between dye and polyelectrolyte. As clearly indicated by Figure 4.27, particles formed by PD4 and PY in pure water have a significantly different hydrodynamic radii as the ones formed in the presence of salt. The R_H of particles at $\lambda = 0.1$ is increased from 64 nm to 80 nm which may be a consequence of partial dissolution of particles due to screening of surface charged groups. Hydrodynamic radii of particles at λ is 0.5 and 1.0 were 130 and 190 nm, respectively, whereas in pure water R_H is 230 nm, at $\lambda = 0.5$ and 320 nm at $\lambda = 1.0$. The drop in R_H is nearly 40% in the presence of salt. In order to understand this response, one may consider the possibility for local spatial adaptation of the ionenes chain. It is clear that higher chain flexibility and more coiled structure make the conformational adaptation of chain easier and subsequently leads to lower level of aggregation of multiple chains. Accordingly, increasing the ionic strength induces both screening of Coulomb interactions between dye and ionenes and conformational changes along ionenes chains.

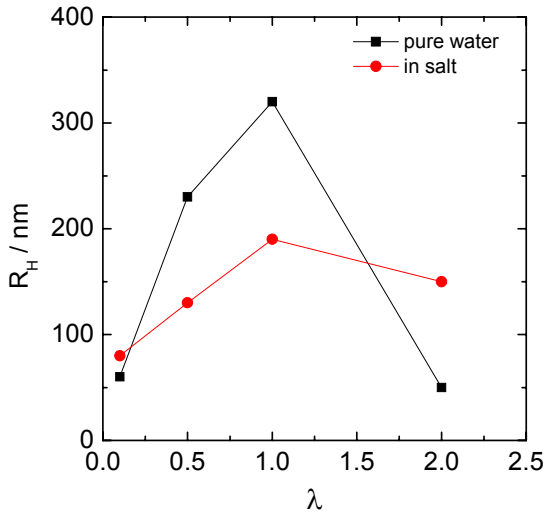

Figure 4.27. Diffusion coefficients and R_H of PD4-PY complexes at as a function of λ in pure water and in KBr solution (0.4 M).

Although the size aggregates are affected substantially by the presence of low molecular mass salt, the dependence on λ brings the identical trend as observed in pure water that is a larger hydrodynamic radii of resulting particles for larger λ. According to this trend, the particle size reaches a maximum R_H for λ =1.0 and beyond this point a drastic decreases in R_H are observed. In other words, both in pure water and salt solution, particles become smaller when λ exceeds 1.0. However in contrast to pure water, the decrease in hydrodynamic radius at λ equals 2.0 less expressed in salt solution (see Figure 4.27). This may be a consequence of the formation of more loosely packed, particles in the presence of salt. On the course of particle formation, salt causes a transition to a more coiled and flexible structure of polyelectrolytes and weakens the ionic binding of oppositely charged molecules. Accordingly, particles which are enriched by polyelectrolyte chains rather than dye molecules as a requirement of λ = 2.0 composition, may easily expand and yield larger hydrodynamic radii as compare to particles formed in pure water.

Another interesting question is: the response of pre-built particles to subsequent addition of salt. Light scattering investigation shows that subsequent addition of salt causes substantial decrease in diameter of PD4-PY particles. After addition of KBr

solution in to solution of PD4-PY (where $\lambda = 1.0$) D_z of complexes was found as 9.7 x 10^{-13} m^2 s^{-1} (see Figure 4.28a) and inset graph in Figure 4.28 shows that diffusion process is translational. R_H and R_G are deduced as 220 and 120 nm, while these values are 320 and 190 nm respectively in pure water. This result indicates a decrease in the level of aggregation or a disintegration of complexes. The disintegration mechanism of such complexes is predominantly governed by screening of Coulomb repulsion between the charged molecules. As proposed in previously, complexes consist of a core which is made of stoichiometric complex of PD4 and PY and surrounding loose shell. It may be that addition of salt screens the charges and induces disintegration of outer chains.

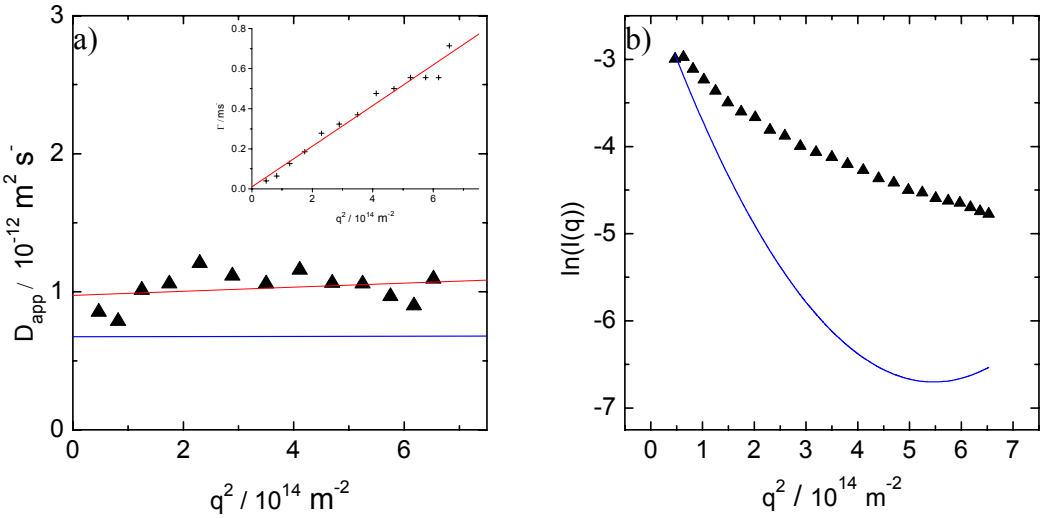

Figure 4.28. a) Diffusion coefficients of PD4-PY complexes at as a function of scattering vector square at $\lambda = 1.0$. b) Guinier plot of PD4-PY at $\lambda = 1.0$ in KBr solution (0.4 M). Blue lines represent the corresponding curves of PD4-PY complexes where $\lambda = 1.0$ in pure water.

5 Self-assembly of Water-Soluble Polythiophene with Nucleotides and Oligonucleotides

The performance of organic electronic devices such as light-emitting diodes[161] solar cells[162] and field effective transistors[163] strongly correlates with the nanoscopic order in π-conjugated systems. Self-assembly of conjugated polymers has the potential to provide a precise structure and controlled interchain interactions on the nano scale, and thereby to modify crucial electrical and optical propreties of resulting materials.[164,165] In last decades several strategies have been developed to produce ordered conjugated systems by the association of the small building blocks. One approach is through rod-coil block copolymers which however require tedious synthetic steps.[166-168]

In this chapter we present an alternative and facile method to fabricate self-organized π-conjugated supramolecular aggregates based on water soluble polythipohene: As pointed out in the introduction part electrostatic self-assembly in aqueous solution. It is meanwhile established that the self-assembly of oppositely charged ionic species can lead to highly organized bulk materials[17,21,169] Recently it was shown that also well defined supramolecular structures in solution can be formed through this route.[170-175] Our strategy is to prepare supramolecular polythiophene assemblies by providing a suitable ionic template which can induce conformational changes in the polythiophene and thereby directs its aggregation. The structure of polythiophene carrying positive charges is shown in scheme 1. Adenosine triphosphate and oligonucleotide of 51 bases are used as negatively charged species that can induce alignment of the polythipohene via electrostatic interaction and additional π interaction.

5.1 Synthesis of Water Soluble Thiophene Monomer (2)

Water soluble polythiophene based polyelectrolyte was prepared according to scheme1. Synthesis of compound 1 was reported elsewhere[177]. Detail of the synthesis of compound **2** is given in appendix.

Poly (3-alkoxy-4methylthiophene) (PT) was prepared according to a general procedure employed for the synthesis of water soluble polythiophenes.[177] Comparing NMR spectra of the polymer and monomer reveals, peak broadening and disappearance of the aromatic hydrogen peaks of thiophene (see Figure 5.1). These confirm a successful polymerization and suggest that the molecular weight lies in the same range as reported values[178] (6-10 kDa and polydispersity index of about 1.2-2.9).

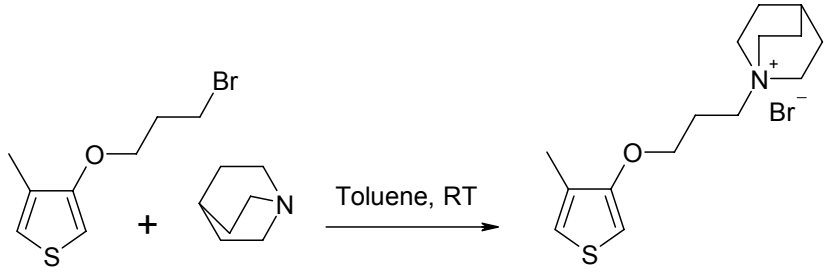

1 **2**

Scheme 5.1. Synthesis of water soluble thiophene monomer (2)

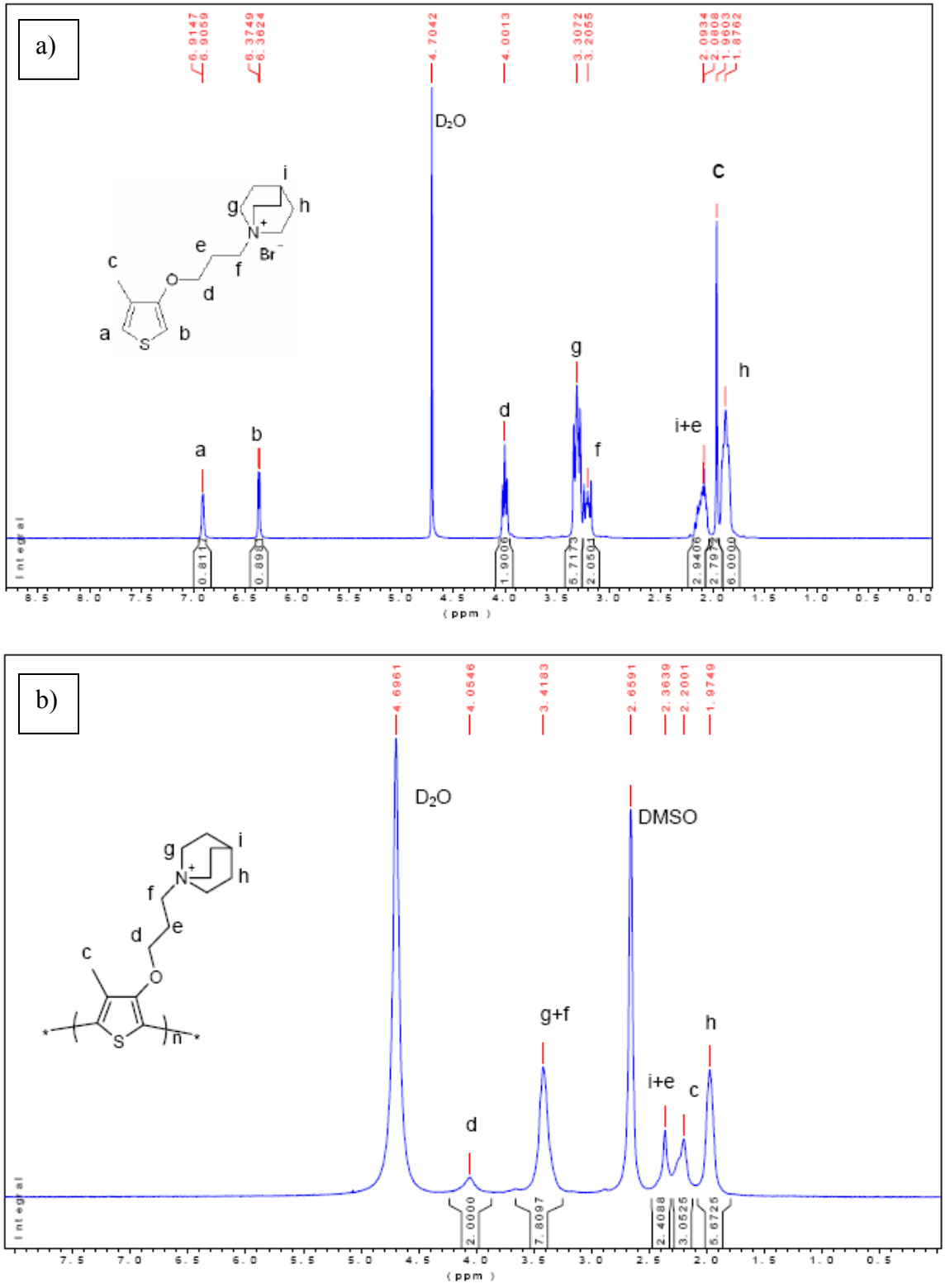

Figure 5.1. ^{1}H NMR spectrum of water soluble thiophene monomer, b) ^{1}H NMR spectrum of PT(polythiophene)

5.2 Polythiophene-Adenosine triphosphate (ATP) complexes

PT has been selected as a model conjugated polymer to monitor the complex formation with negatively charged molecules such as adenosine triphosphate. Complex formation is mainly driven by coulombic forces between the ionic groups. However π-π stacking of polythiophene backbone provides a cooperative contribution to the complex formation and colloidal stability of complex. It is known that the conformation of PT is sensitive to external stimuli as a result of the presence of sterically demanding side chains. Therefore the changes in the π-π* transitions that arise from the conformational alternations in the PT backbone upon the formation of a complex can be monitored by absorption spectroscopy. ATP has been selected as a ligand due to its biological relevance and fairly noninterfering UV absorbtion maximum with the PT.

Titration of PT with ATP was performed in water at 20^{o} C. As shown in Figure 5.2 the absorption maximum of PT in water appears at 400 nm and it is associated with random coil conformation of the PT derivatives. Upon adding increasing amount of ATP, the absorption maximum is gradually red shifted to 540 nm with an observed dramatic color change from yellow to red. This distinct shift and the appearance of the two vibronic bands are characteristic for aggregation of the PT backbone.

More remarkably, PT-ATP complexes are responsibve to temperature changes. As shown in Figure 5.3 variation of temperature ranging between 20 to 70 ^{o}C causes significant color change and corresponding alternation in the state of the complexes. As pointed out by Leclerc chromic effects are obviously the consequences of the main chain conformation (and / or interchain interactions), it is also has been found that these thermochromic properties are strongly dependent upon the nature and the position of the side chains along the backbone. More precisely, it has been suggested that these optical effects are driven by a delicate balance between repulsive steric interactions and attractive interchain (or interchain due to chain folding) interactions; the latter being necessary to get a planar conformations in the case of thermochromic polythiophenes. Accordingly the response of our system to temperature is the consequence of disintegration / reformation of PT-ATP ionic complexes by heating and cooling. More explicitly, the planar conformation of the PT backbone which is provided by

complexation reaction, transforms in to the random coil conformation by heating due to the disintegration of complexes. As indicted by the Figure 5.3c temperature triggered geometry transformation on PT backbones is a reversible process with low degree of hysterisis. It can be concluded that the PT-ATP system is a dynamic system which is able to recover itself as soon as external stimuli is removed. This system can be good candidate for stimuli responsive materials.

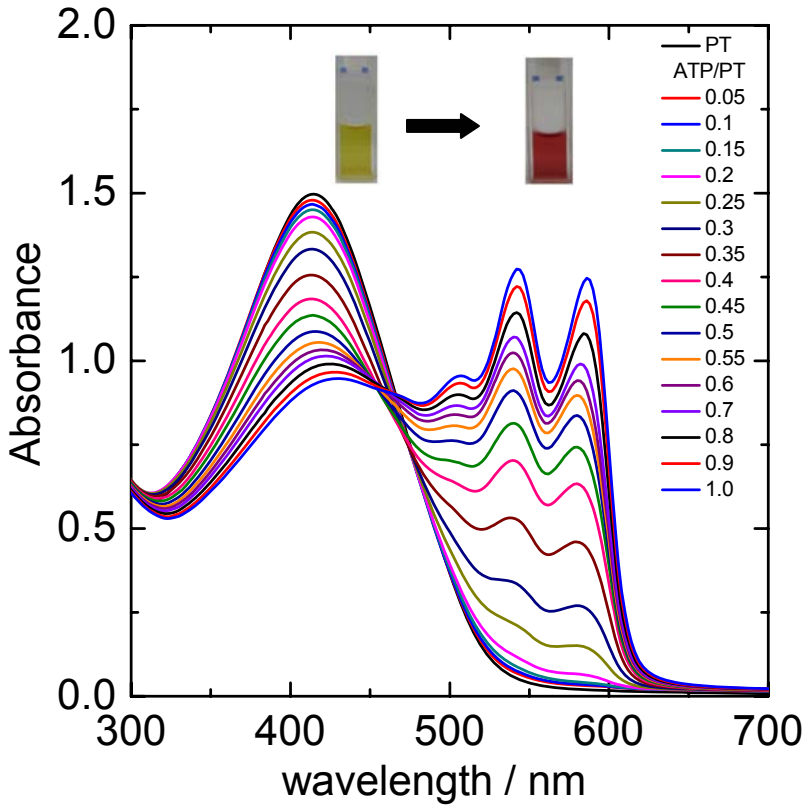

Figure 5.2. UV-Vis absorption spectra of titration of PT solution with ATP

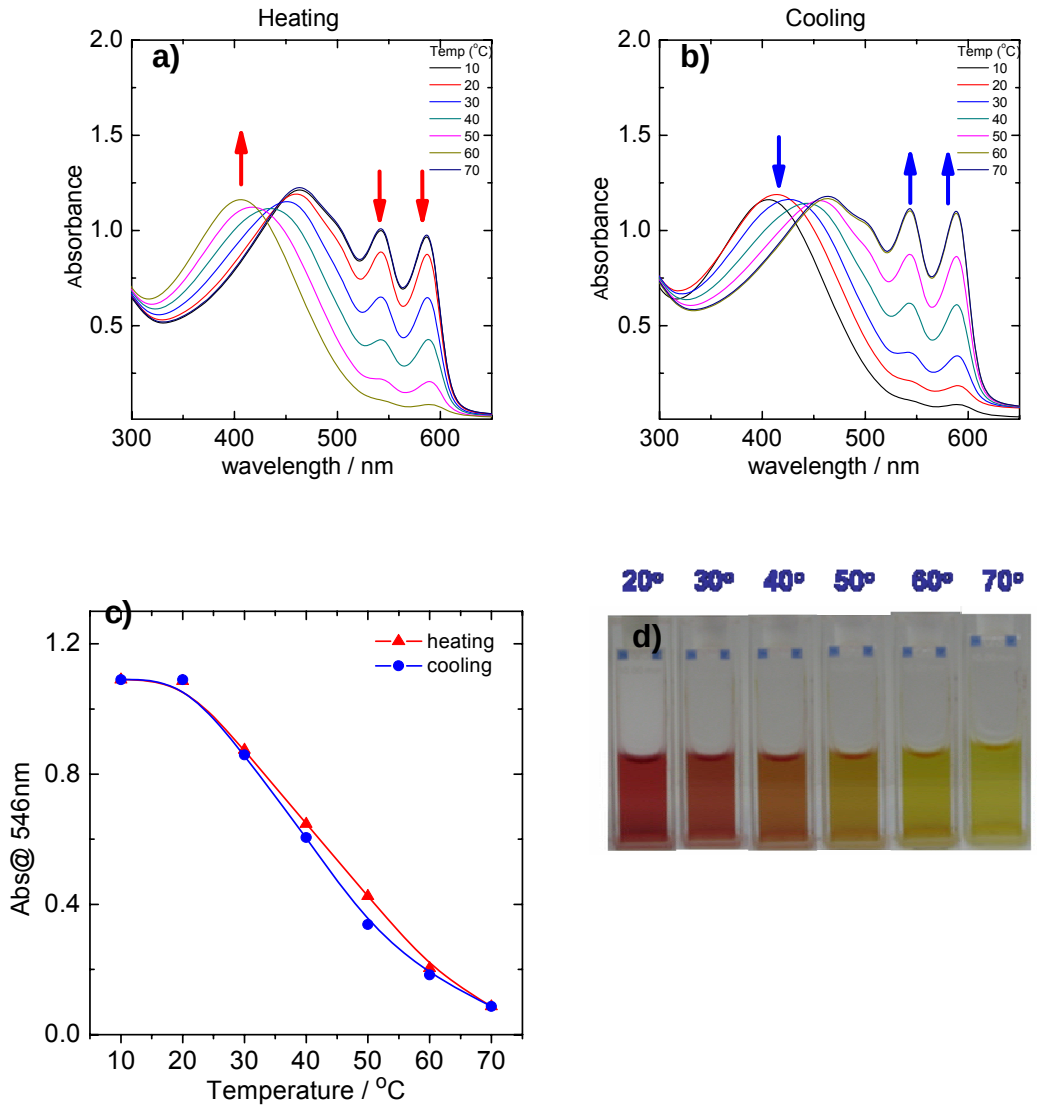

Figure 5.3. a) Temperature dependent UV-Vis absorption spectrum of PT-ATP complex in water upon heating b) Temperature dependent UV-Vis absorption spectrum of PT-ATP complex in water upon cooling c) Absorbance intensity of at 546 nm upon heating and cooling d) color change of solution of PT-ATP complex.

The solution structure of both PT and PT-ATP complexes were investigated by dynamic light scattering. The average diffusion coefficient $\langle D_z \rangle$ which is a z-average was determined by extrapolation of the apparent diffusion coefficient towards to zero scattering vector q. D_z values were calculated as 1.1 x 10^{-11} m^2 s^{-1} and 1.3 x 1.0. x 10^{-12} m^2 s^{-1}(see figure). Significant increase in hydrodynamic radius arises from the complex formation. Corresponding D_z values yield R_H 18 and 170 nm for PT and PT-ATP complexes respectively i.e. size of the complexes are much different than polytiophene itself.

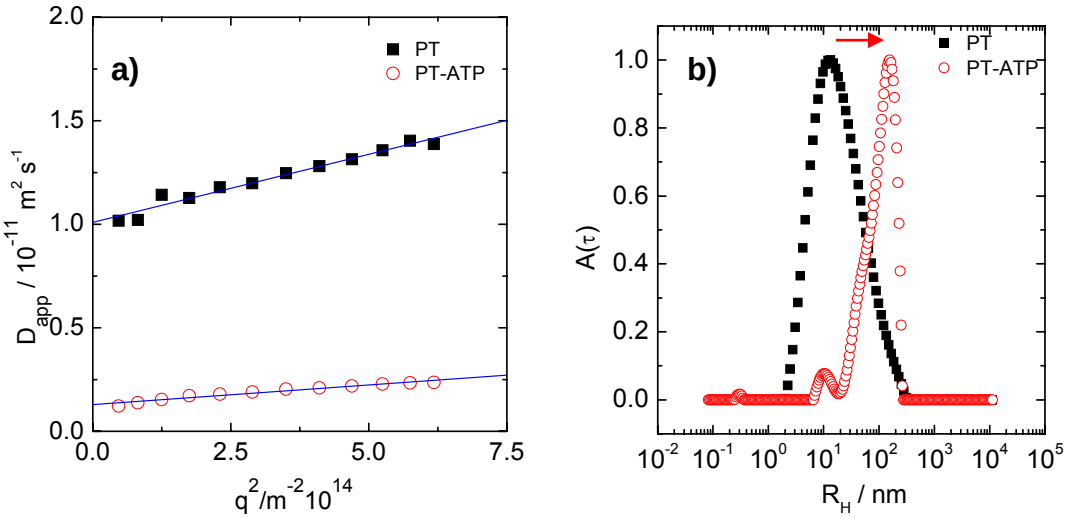

Figure 5.4. a) Distribution apparent diffusion coefficients of PT and PT-ATP complexes as a function of scattering vector square (in 0.1 M LiBr solution at room temperature) b)Hydrodynamic radius distribution of PT and PT-ATP complex

The significant size and color changes suggest that PT-ATP complexation is a consequence of aggregation of many PT chains with APT molecules due to both ionic interactions between opposite charges and hydrophobic interactions between the PT backbones. More remarkably PT-ATP complexes are responsive to temperature changes since increasing temperature induces the spatial transformation on the PT backbone. In addition to this, PT-ATP complexes may switch their states from highly aggregated states to non-aggregated states with increasing temperature and this is a fully reversible process. (It has to be considered that solvent quality may be affected by temperature gradient i.e

solvent at elevated temperature is good solvent for PT-ATP complexes but it may behave as bad solvent at low temperature.)

5.3 Polythiophene-Oligonucleotide Complexes

The response of polythiophene based polyelectrolyte to oppositely charged small molecules was adressed in the previous section; The poly (3-alkoxy-4methylthiophene) backbone transforms into amore planar conformation upon complexation. This unique property of PT has been further investigated by using an oligonucleotide instead of adenosine triphosphate as second building block. The strategy is to prepare supramolecular polythiophene assemblies through an ionic template which can induce aggregation of PT in to different geometry.

The PT-oligoucleotide (51 bases (5'-CGC CCA TCA CCA TCA CCA TCA CCA TCG ATC CCG GGG TTG AGG AAG AAT AAA-3')) complex formation reaction has been monitored UV-vis absorption spectroscopy. Upon addition of oligonucleotide to PT solution a significant color change from yellow to red is observed. Figure 5.5a shows UV-Vis spectra of PT with different amounts of added oligonucleotide. PT in water exhibits an absorption maximum at around 410 nm which corresponds to a random-coil conformation or a less conjugated (nonplanar) conformation.[179] Upon adding increasing amounts of oligonucleotide, absorption maximum gradually shifts to 521nm which refers to a highly conjugated planar conformation. The shift in the UV-Vis spectrum demonstrates that with the rigid oligonucleotide structures the PT backbone is forced in to a more planar conformation due to complexation. An isosbestic point proves the existence of two conformations of PT in solution. However they may occur on the same PT backbone or on different chains.[180] Figure 5.5b shows the fluorometric detection of PT and PT-oligonucleotide complex in aqueous solution. While PT has fluorescence maximum at 530 nm, fluorescence intensity is quenched and red shifted to 550 nm due to planar aggregated form of PT in the oligonucleotide complex. As the absorption spectrum gradually changes until a charge ratio of oligonucleotide:PT = 1:1 is reached and then stays constant, it can be concluded that PT can bind oligonucleotide (at least) up to

charge ratio of 1:1. In the following we therefore focus on the characterizations of the 1:1 complex in particular its nano scale structure.

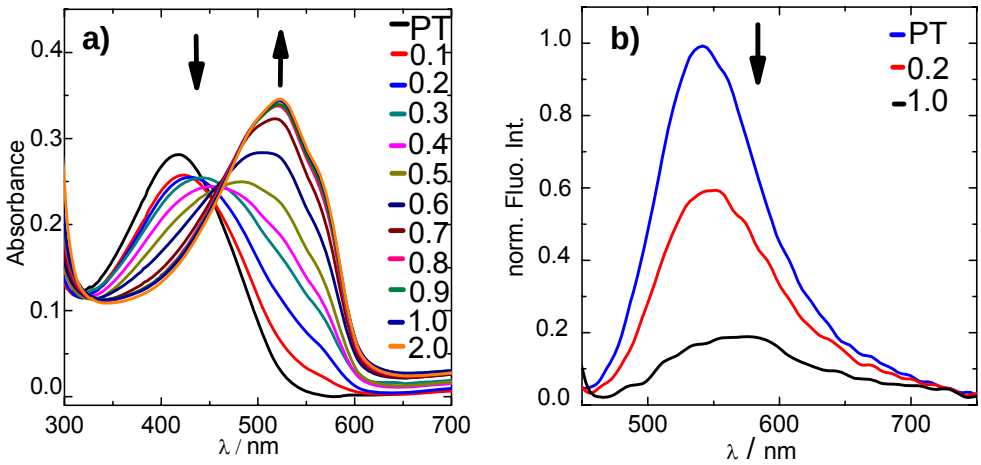

Figure5.5. Absorption spectra of PT (concentration of repeat unit $5.4x10^{-4}$M) in water increasing concentration of oligonucleotide (negative charges). b) Fluorescence spectrum of a PT solution ($5.4x10^{-4}$M concentration of repeat unit or positive charges)

A first impression of the supramolecular structure after deposition o to a surface has been obtained by Atomic force microscope. Figure 5.6 a, c shows the morphology of the PT component only as, prepared by deposition on hydrophilic mica surface: globular structures are found. The hydrophobic PT backbones may tend to form a more compact structure and reduce the contact area with mica.[181] The measured mean diameter and height are 24 and 3 nm, respectively. The AFM of the complex of PT with the 51-base-oligonucleotide in the stoichiometric ratio 1:1 is shown in Figure 5.6 b, d. It obviously differs from the globular structure of the PT molecules: the complexes show a cylindrical morphology. Narrowly distributed height and width are observed, while the length of the assemblies shows a moderately broad distribution. The narrow height and width distribution however indicate that the structure of the polythiophene-oligonucleotide complex is well defined. The measured average length, width and height are 151 nm, 36 nm and 2 nm, respectively where of course the convolution of the AFM tip plays a role in the evaluation of particle size.[182,183] The low height of the aggregtes may be caused by the intersection with the mica surface or upon drying. Also the morphology may have

changed upon sample preparation. However, the clear morphology and size difference between polymer and complex strongly supports the hypothesis that PT forms supramolecular "wires" with oligonucleotide.

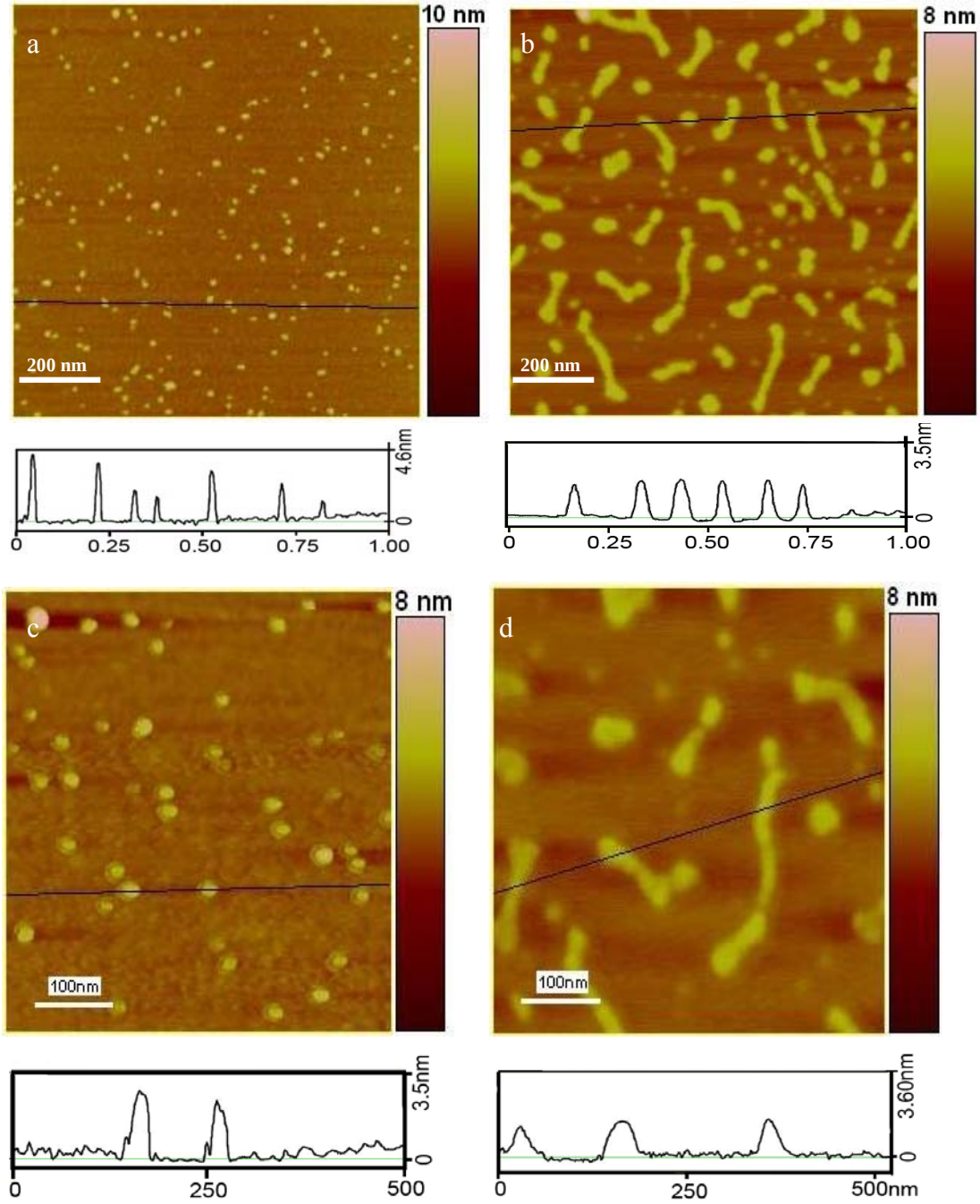

Figure 5.6. AFM images of a, c) polythiophene and b, d) polythiophene-oligonucleotide complexes on bare mica.

The solution structure of the nanoscale assemblies can be directly studied by scattering methods. The self assembled 1:1 complex of PT-oligonucleotides in aqueous solution was investigated by light scattering. Measurement of diffusion coefficient, extrapolation to zero angle and using Stoke's equation yields hydrodynamic radius of R_H = 68 nm. Static light scattering results are presented in Figure 5.7a as reciprocal total static scattering intensity $Kc/R(\theta)$ as a function of square of scattering vector q^2 (Zimm representation). It yields an apparent radius of gyration of the complex of R_G has been calculated as 86 nm. In a different data representation, static light scattering data elucidate the morphology of the complex in solution. The double logarithmic representation in Figure5.7b at high q shows a slope of -1 indicating "one-dimensional" rod like (or worm like) species.

The ratio $\rho = R_G / R_H$ is calculated to be 1.25 which may indicate short cylindrical species in solution. From the onset of the -1 slope in figure 3b the cylinder length appears to even longer (300-400 nm). The hydrodynamic radius can be further be compared with the AFM results and corresponds to larger ones of the cylinder (300 nm), which is understandable as the larger particles contribute more to the scattering intensity.

It should be noted that the length of the cylinder (av.150 nm up to 300nm) is longer than the countour length of the components (oligonucleotide ~ 20nm, PT~ 25nm) thus the oligonucleotide is able to connect many PT molecules into longer wires. More remarkably, the diameter indicates that several polymer chains associate also in diameter (about 7-10 by simple volume consideration), yet the diameter is very well defined. This may be due to the delicate interplay of electrostatic attraction and entropically favoured release of continuous upon association on the one hand and the energetically and entropically disfavoured conformation change upon planaization the other hand.

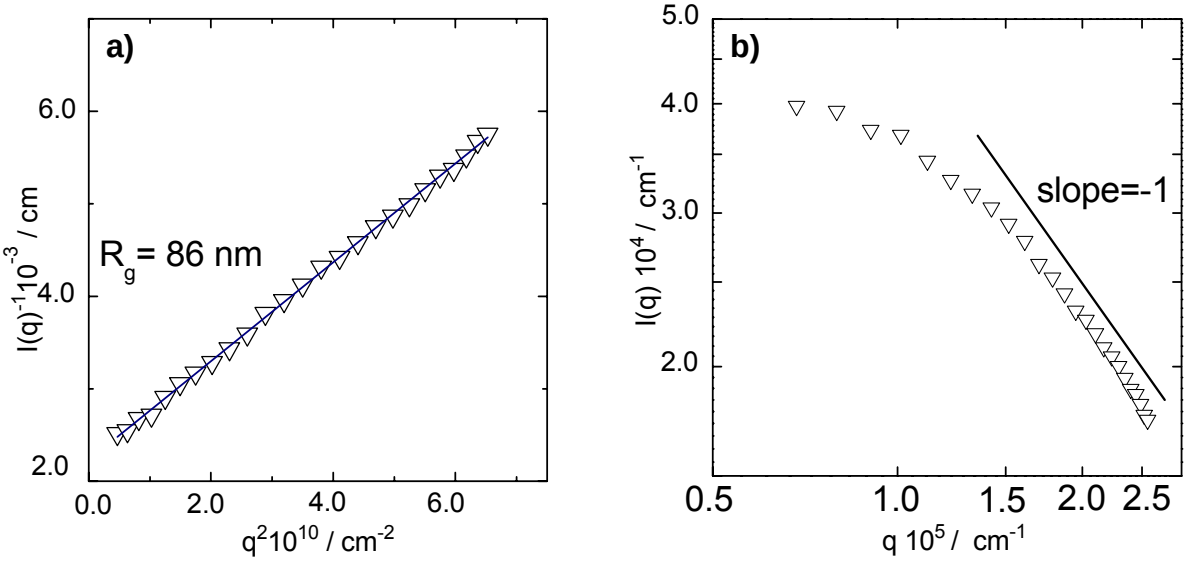

Figure 5.7. a)Reciprocal static light scattering intensity $I(q)^{-1}$ as a function of square of scattering vector q; b) Double logarithmic representation of the scattering curve

5.4 Conclusion

On the basis of these examples it has been clearly shown that the optical properties of polythiophene based polyelectrolyte can be dramatically altered by external stimuli such as temperature and ligand binding. Moreover, the result obtained with oligonucleotide-PT allows to prepare supramolecular "wires" with a well defined diameter by "electrostatic self-assembly" in aqueous solution. The cylindrical morphology formed in solution remains intact upon deposition on a mica surface and drying. This approach may thus simplify the fabrication of organic nanowires of conjugated polymers. Obviously, variation of the template is expected to diversify the characteristic of the resultant architectures, e.g. allow for the formation of longer wires.

6 General Conclusion

In this work the association of different cationic ionenes with sodium pyrene tetrasulfonate was investigated. It is found that the ionic complexes of PD4-PY self organize into nanospheres in dilute aqueous solutions. The complex formation, that is size and architechture of the resulting particles depend on chemical structure of ionenes, mixing ratio, ionic stenght and can be tuned in the range of 50 nm to 300 nm in radius. Due to large number of parameters that effect the complex formation, there is no general mechanistic or kinetic model explaning these architechtures. Nevertheless, dye-polyionen interactions can be considered as a special example of complex formation between oppositely charged polyelectrolytes. Polyelectrolyte-polyelectrolyte as well as dye-polyelectrolyte complex formation is mainly governed by Coulombic forces between the ionic sites of the components; however additional interactions in-between the dye molecules play a decisive role in the case of PE-dye complexation. The complex formation is a kinetically controlled process which is based on the formation of electrostatic “bonds” between the ionic species. The particle formation can be considered as the consequences of fast phase separation in a system containing polyions and oppositely charged molecules.

Although it does not entirely fit the whole experimental findings that are discussed here, formation of spherical aggregates may be considered with regard to “complex coacervation”. The concept of complex coacervation is based on the energy driven phase separation of an originally one-phase polymer solvent system in to polymer rich gel phase and sol phase of low polymer concentration due to the desolvation and aggregation of the polymer chains.[184] As proposed by Nakajima; coacervation may reasonably be interpreted by a free energy equation taking into account contributions from the entropy of mixing, enthalpy of mixing and electrostatic free energy.[184] According to his approach in the case of a two component system composed of water and oppositely charged polyelectrolytes in which polyelectrolytes are equimolar, have identical volume fraction φ_r / 2 chain length r, and charge density σ, the free energy of mixing ΔF can be written as follows:

$$\frac{\Delta F}{N_r kT} = \varphi_w \ln \varphi_w + \frac{\varphi_r}{r} \ln\left(\frac{\varphi_r}{2}\right) - \alpha(\sigma\varphi_r)^{3/2} + \chi_{12}\varphi_w\varphi_r \qquad (1)$$

where, N_r is the total number of lattice sites having the volume corresponding to one water molecule *v*, φ_w is the volume fraction of the water, χ_{12} is the interaction parameter between water and polyelectrolytes and α is the electrostatic interaction parameter which is given by the following equation: $\alpha = e^2 / 3\varepsilon\,(4\pi e^2 / \varepsilon kTv)^{1/2}\,(1 / kT)$ in which ε is the dielectric constant and e is the elementary charge. In accordance with the equation 1, phase separation occurs when the second derivative of free energy of mixing with respect to volume fraction of polyelectrolyte is zero or less than zero i.e. depending on the parameters such as concentration of species, chain length of polyions, charge density, ionic strength and hydrophobic effects liquid-liquid like phase separation occurs and polyion chains aggregate to form coacervate droplets by increasing the polyion concentration in droplets.

Obviously, on the one hand the above-mentioned parameters make the complex formation process complicated; on the other hand, some of these parameters can be used to control the size and geometry of resultant complexes. First of all, it can be stated that the size of the ionenes-dye aggregates can be varied with the ratio of components. According to our observation the increase in the ionenes concentration in PD4-PY system is reflected by a increase in particle size. The size of PD4-PY particles vary between 50 and 300 nm depending on the concentration of PD4. In addition to size control, resultant particles have certain colloidal stability. The stability of nanoparticles results simply from the interplay of ionic and hydrophobic forces. Obviously these nanoparticles consist of a charge neutralized core surrounded by a shell of attached chains of ionenes which stabilize the particles against further coagulation via electrostatic repulsion. In other words, the finite size "colloid-like" particles are stabilized by repulsive forces which are provided by unique core-shell particle architechture. Furthermore it should be noted that the function this parameter differs in the case of PD6-PY system and shows discontinuous in particle size increase by concentration of polyionen.

Concerning the ionenes components, PD4 and PD6, the intercharge distances or charge density was found to be decisive parameters in determining aggregate size and packing density. As indicated by calculations the intercharge distance in PD6 is larger

than PD4, in other words, the charge densities of these two ionenes are significantly different. Current understanding about polyelectrolyte complexes points out that the packing density of quasi-soluble complexes shows a general tendency to increase with the charge density. This statement is in good agreement with our observation: PD6 with a distance of 6 CH_2-groups forms almost macroscopic aggregates at charge stoichiometry, while the polymer PD4 with only 4 CH_2-groups spacer including a double bond can form compact spherical nanoparticles with core-shell architecture. It is obvious that the charge density of polyionen component has major importance in determining the size and geometry of complexes.

Another decisive influence on the structure of particles is the ionic strength. A prediction of the effects of the presence of salt is very difficult because of the complicated processes of structure formation and interplay with the specific characteristics of the components. However, it can be concluded that subsequent addition of salt or complexation in the presence of salt causes the formation of less aggregated complexes where decreased aggregation is the consequences of screening of Coulombic forces by salt molecules.

It can be concluded that the systems studied in this thesis can lead fluorescent composite nanoparticles the size of which can be tuned via choice of components and medium. Such particles may have potential in optical applications, but in particular represent a model system that allows to study binding of the same probe to various polyelectrolytes/conditions, which may be important in the context of drug delivery and DNA detection.

7 Appendix

Synthesis of PD6.

To a 100 ml round bottom flask 0.038 M solution of 1-4 Diazabicyclo[2.2.2] Octane (DABCO) in DMF/MeOH and the solution 0.038 M 1-6 dibromohexane were added . The clear mixture was stirred during 96 hours at ambient temperature. Polymer was precipitated in acetone and further washed in excess acetone during two hours. White precipitate were filtrated and dissolved in Milli Q water. Subsequently this solution was extracted with ether many times and water phase collected. Solution was freeze dried and polyionen PD6 were obtained as white powder (Yield: 100%). Proton and Carbon NMR spectrum were recorded by Bruker 300MHz NMR spectrometer.

Synthesis of PD4, PD4-2.

For the synthesis of PD4 and PD4-2 same synthetic procedure in the preparation of PD6 were followed.(Yield: 100%) Proton and Carbon NMR spectrum were recorded by Bruker 300MHz NMR spectrometer.

Synthesis of PD4coPD6.

To a 100 ml round bottom flask 0.038 M solution of 4-Aza-1-azoniabicyclo [2.2.2] octane, 1.1'(1.6-hexanediyl)-bis-,dibromide[43] in DMF/MeOH and the solution 0.038 M trans-1,4-dibromo-2-butene were added . The clear mixture was stirred during 96 hours at ambient temperature. Polymer was precipitated in acetone and further washed in excess acetone during two hours. White precipitate were filtrated and dissolved in Milli Q water. Subsequently this solution was extracted with ether many times and water phase collected. Solution was freeze dried and polyionen PD4coPD6 were obtained as white powder (Yield: 100%).

Molecular Weight Determination of Ionenes by Size Exclusion Chromatography (SEC)

Determination of the molecular weight of the ionenes were performed on a Water GPC equipped with a Novema 100A^o and 300 A^o column mounted in series (PSS Company Mainz). The eluent was a solution of 0.1 M NaCl and 0.1 % trifluoroacetic acid and flow rate was 0.5 ml min^{-1}. Ionenes samples were dissolved in eluent and stirred one day at room temperature and injected. Pullulan (-1,4'- ;-1,6- Glucan) (PSS company Mainz) were used as standard. Corresponding M_n and M_w values of ionenes are shown in table 2.1.

Synthesis of Polythiophene

All chemicals were purchased from Aldrich and Merck and were used without further purification. The oligonucleotide, "hisAfor" with 51 bases (5'-CGC CCA TCA CCA TCA CCA TCA CCA TCG ATC CCG GGG TTG AGG AAG AAT AAA-3') was purchased from Eurofins MWG GmbH , Ebersberg (Germany).

Solution of 1-Azabicyclo[2.2.2]octane (1 g, 9 mmol) in 10 mL toluene was added in to solution of 3-(3-bromo)propoxy-4-methylthiophene (1) (0.3 g, 1.2 mmol) in 20 mL toluene. The mixture was stirred 24 h at room temperature and then filtered. The white crude product was washed many times with toluene and diethyl ether successively. The product (white hydroscopic powder) was dried in oven at 40^{o}C for one day. NMR:^{1}H-NMR(D_2O,250 MHz) δ 6.90 (d, 1H), 6.36(d, 1H), 4.00 (t, 2H), 3.30 (t, 6H), 3.47 (t, 8H), 3.20 (p, 2H).

Polymerization:

500 mg (1.45 mmol) of **2** and 930mg (5.8 mmol) of anhydrous $FeCl_3$ were mixed in 25 mL of dry chloroform, and stirred for 24 hours at 0^o C under N_2 atmosphere. The solid was filtered and washed with methanol many times. The crude product was dissolved in methanol by adding a few drops of hydrazine and was precipitated by addition of a saturated solution of tetrabutlyammonium chloride in acetone. The Black-red product

was washed with acetone and dried in oven. NMR:^{1}H–NMR (D_2O –DMSO, 250 MHz) δ 3.98 (2H), 3.47(8H), 3.47(8H), 2.29(3H), 2.12(3H), 1.90(6H).

Instrumentation and Sample Preparation

Absorption spectra were recorded by a UV-VIS Perkin-Elmer Lambda2 spectrometer. Stock PY solution were prepared in range of 1.8 10^{-4} M and titrated with corresponding polyionen solution of which concentration is 1mg/L. The fluorescence spectra were recorded on a Xe-lamp equipped spectrofluorometer (SPEX Fluorolog II (212)). Sample was excited at 350 nm. Identical solutions were used with the UV-Vis experiment. For polythiophene samples: A stock polymer solutions in range of 5.4 10^{-4} mol/L (based on the repeat unit concentration) was prepared and titrated with oligonucleotide (hisAfor) solution with a molar concentration of negative charges 1.1 10^{-2}M.

AFM images were recorded on a MultiMode Nanoscope IIIa Atomic Force Microscope (Veeco Instruments, California, USA) in tapping mode at room temperature. Silicon cantilever (OMCLAC 160 TS-W, Olympus, Japan) with 42 Nm^{-1} spring constant was used. The tip was 160 μm long, 50 μm wide and 4.6 μm thick, the height of the tip was 7~15 μm, the radius of the tip was less than 10 nm. Typical imaging parameters used were: (1) working frequencies, 300~400 kHz; (2) working oscillation amplitude, 1~1.5 V; (3) scan rate, 1 Hz; (4) image resolution, 512x512 pixels. The raw topography data was processed by flatting to remove the background slope.

For imaging ionenes, PD4 and PD6 solutions (1mg/L in 0.1 M KBr) were diluted hundred fold and 1μl aliquot dropped plasma cleaned positively doped silicon surface, then blown dry with N_2 immediately. For imaging PD4- PY and PD6-PY complexes, stock solution of PY was mixed with corresponding amount of ionenes solution (1mg/L) by charge ratio 1:1, and 1:10 (Ionenes:Dye) the complex solution was incubated at room temperature for 30 min, then diluted by 100 fold. A 1 μL of diluted complex solution was deposited on plasma cleaned positively doped silicon surface by drop casting, then blow dry with N_2 immediately.

For imaging polythiophene, a 3 μL polymer aliquot (18.7 mg/L) was dropped on freshly cleaved mica surface, then blow dried with N_2 immediately; For imaging

polythiophene-oligonucleotide complexes, a 51 bases oligonucleotide stock solution was mixed with polythiophene solution (18.7 mg/L) by charge ratio 1:1, the complex solution was incubated at room temperature for 5 min, then diluted 100 fold. 3~5 μL of diluted complex solution was deposited on freshly cleaved mica by drop casting, then blown dried with N2 immediately.

Confocal Laser Scanning Microscopy was performed at a commercial *s*etup (Carl Zeiss, Jena, Germany) consisting of the module LSM 510 and an inverted microscope model Axiovert 200. In all experiments described bellow we employed a C-Apochromat 40x objective (Carl Zeiss, Jena, Germany) with numerical aperture (NA) of 1.2. The imaging was done by excitation at laser wavelength of 457 nm and after filtering with a long pass LP505 emission filter.

Light scattering measurements were performed on a commercially available ALV spectrometer consisting of goniometer and an ALV 5000 full digital correlator (320channels) equipped with a red laser (He-Ne laser, λ=632.8nm).All measurements were carried out at temperature T= 20^{o} C. All solutions were prepared by using ultra pure Milli Q water. All solutions were clarified with filter (MilliPore-Millex-HA). All polymers were dissolved in ultrapure water (Milli-Q water with a conductivity ≤18.2MΩ cm) during several hours.

Small Angle Neutron Scattering. Samples for SANS were prepared in D_2O and transferred into optical quality quartz cells with 2 mm path length. SANS studies were performed at the FRM II, Munich, Germany and at Institute Laue Langevin (ILL), Grenoble, France. Data shown result from the KWS 1 instrument of the Jülich Center for Neutron Science at FRM II using three configurations with the neutron wavelengths λ and sample-detector distances d of λ = 0.45 nm / d = 1.6 m, λ = 0.45 nm / d = 7.6 m and λ = 1.2 nm / d = 7.6 m. A total scattering vector range of 0.034 nm^{-1} < q < 3.0 nm^{-1} was covered. Data were corrected for empty quartz cell scattering, electronic background and detector uniformity, and converted to an absolute scale using secondary standards. The data were further corrected by subtracting the contributions from solvent scattering and incoherent background. All measurements and data treatment have been performed according to common procedures. After combination with the static light scattering data,

the scattering curve I(q) was Fourier transformed into the three-dimensionally averaged pair distance distribution function P(r) via the relationship

$$I(q) = 4\pi \int_{r=0}^{\infty} P(r) \frac{\sin(qr)}{qr} dr$$

(1)

where r is the radial distance and q is the scattering vector magnitude. The indirect transformation method is applied in order to minimize termination effects using the program ITP, *Indirect Transformation for the calculation of P(r)*, by O. Glatter which includes smoothing of the primary data by a weighted least square procedure (estimation of the optimum stabilization parameter based on a stability plot), desmearing and transforming into real space simultaneously.[185-187] The actual calculations dealing with the experimental scattering curves accounted for the measured beam profile and the wavelength distribution of the experimental setup. The P(r) was further numerically deconvoluted into a radial density profile ρ(x), with x = 2r.

UV-Vis (Cooperative Binding) Supplement

The dimerization constant K_d of PY was estimated in the absence of polycations. The following equation is generally accepted:[78]

$$\left[(\varepsilon_A - \varepsilon)/C_A^0\right]^{1/2} = (2K_D/\Delta\varepsilon)^{1/2}\left[\Delta\varepsilon - (\varepsilon_A - \varepsilon)\right] \qquad 1$$

where C_a^0 is the total mass in concentration of the dye and ε, ε_a and ε_D denote the extinction coefficients at 283 nm of the solution, pure monomer, and pure dimer, respectively and $\Delta\varepsilon = \varepsilon_A - \varepsilon_D$. Accordingly, a plot of $\left[(\varepsilon_A - \varepsilon)/C_A^0\right]^{1/2}$ versus $\left[(\varepsilon_A - \varepsilon)\right]$ should yield a straight line with intercepts $(2K_D/\Delta\varepsilon)^{1/2}$ on the ordinate and $\Delta\varepsilon$ on the abscissa. To determine the K_D and ε_D, first ε_A should be estimated by a plot of ε versus log C_a^o. From the intercept on the ordinate axis ε_A was estimated as 96.000 $M^{-1}cm^{-1}$ (Figure A.1).

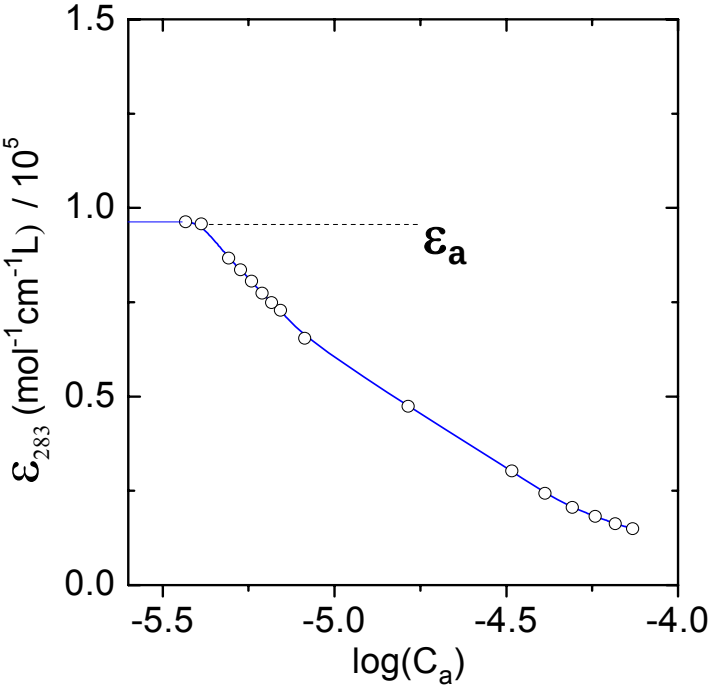

Figure A.1. Molar extinction of PY solutions as a function of the total monomer concentration of dye C_a^0.

Thereafter the parameters ε_d and K_d are determined easily from the plot $\left[(\varepsilon_a - \varepsilon)/C_a^0\right]^{1/2}$ versus $\left[(\varepsilon_a - \varepsilon)\right]$ as 5.1 x 10^3 $M^{-1}cm^{-1}$, 5.0 x 10^4 L mol^{-1} respectively(see Figure A.2).

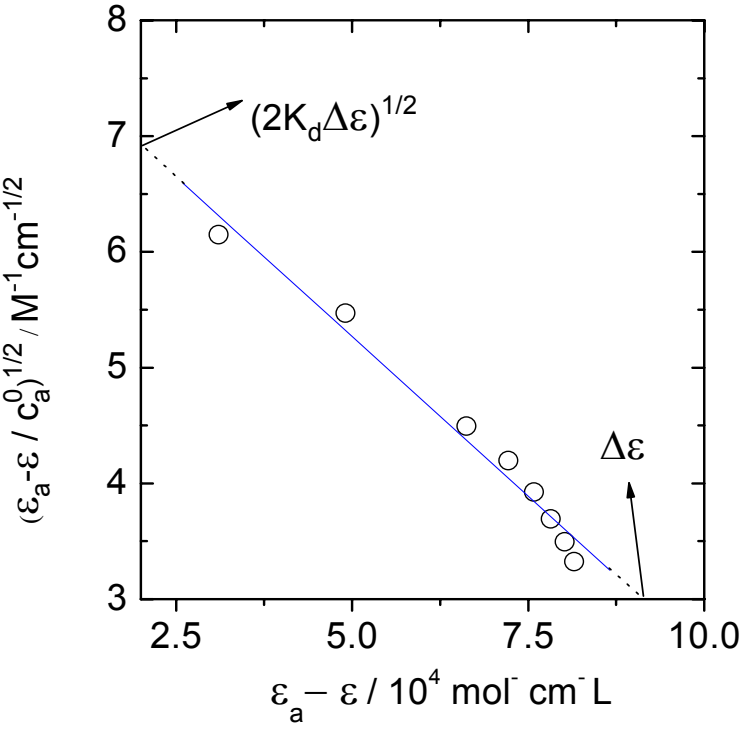

Figure A.2. Plots to determine dimerization constants (K_d) and intrinsic extinction coefficients (ε_a,ε_d) for PY solutions with no polycations.

Addition of polycation solution to PY solution caused metachroism at 288 nm. This observation shows that PY molecules stack on the polycations. Therefore, it is necessary to determine the extinction coefficient ε_{st} of the stacked dye molecules. For the extinction coefficient of solution ε containing stacked dye molecules it is:

$$\varepsilon = \gamma_a \varepsilon_a + 2K_d C_a^0 \gamma_a^{\,2} \varepsilon_d + \theta g p \varepsilon_{st} \qquad 2$$

where γ_a is the fraction of free monomeric dye, θ is the fraction of the occupied sites, g is the number of the binding sites per monomer segment of polymer (PD6 and PD4coPD6) λ is polymer / dye ratio . Quantitative estimations shows that the second term of the right hand side can be neglected. After further derivations, the following the following equation is obtained.

$$\varepsilon = \varepsilon_{st} + (\varepsilon_A - \varepsilon_{st})(s/K)C_A^{0^{-1}} \qquad 3$$

where K is the cooperative binding constant and s = KC_a (C_a concentration of the free monomeric dye). If the parameter s becomes almost constant with respect to changes of C_a^0 a plot ε versus $(C_a^0)^{-1}$ at constant P / D (λ) should eventually result in a straight line (Figure A.3a). Extrapolation of $(C_a^0)^{-1}$ to 0 yields ε_{st}=1.5 10^4 $M^{-1}cm^{-1}$. From another plot (Figure A.3b) the same value was obtained as ε_{st} = 1.5 $10^4 M^{-1}cm^{-1}$. The procedure was followed for PD4coPD6 and PY system as well and ε_{st} was estimated as 1.5 $10^4 M^{-1}cm^{-1}$ (see Figure A.4a,b)

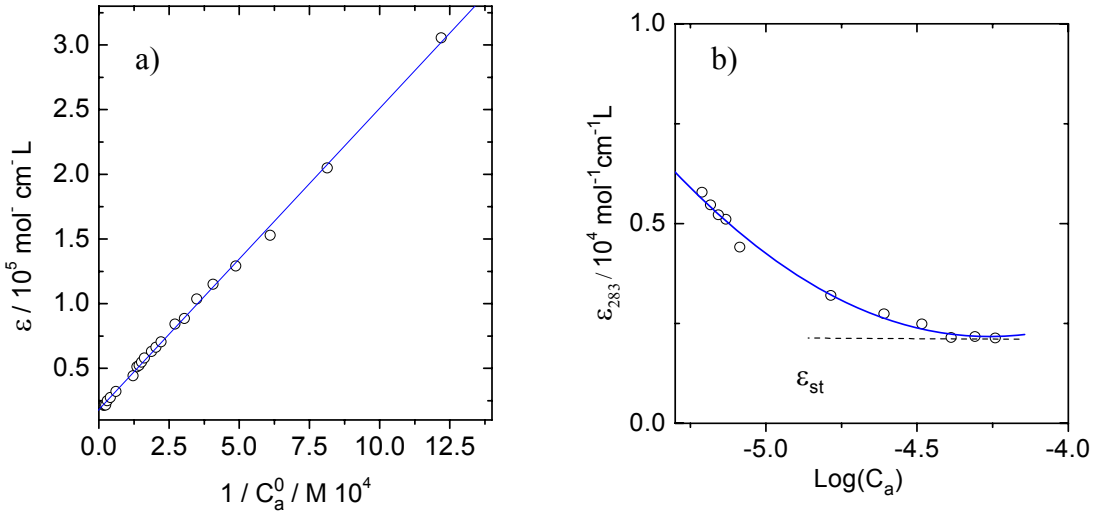

Figure A.3. a) Molar extinction of PD6 and PY solutions as a function of the reciprocal value of the total weighing in concentration of the dye ($1 / C_a^0$) b) Molar extinction of PY solutions as a function of logarithm of the total mass in concentration of the dye ($\log / C_a^0$)

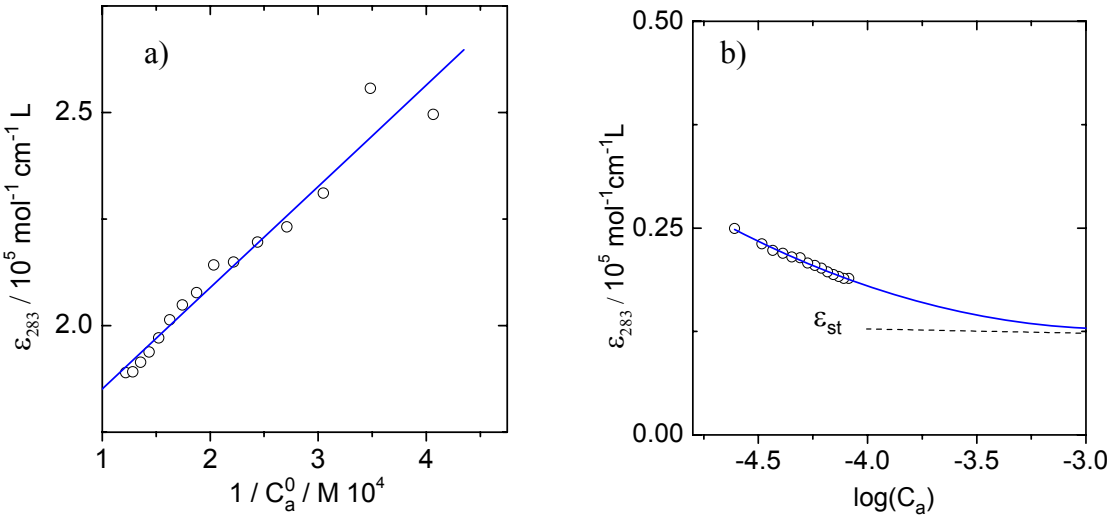

Figure A.4. a) Molar extinction of PD4co6 and PY solutions as a function of the reciprocal value of the total mass in concentration of the dye (1 / C_a^0) b) Molar extinction of PY solutions as a function of logarithm of the total weighing in concentration of the dye (log / C_a^0)

With increasing C_a^0 (at constant p) greater and greater fractions of the dye will be bound , hence $\varepsilon \to \varepsilon_{st}$. Another derivation yields the following relations:

$$\gamma_a^* + \theta g p = 1 \qquad 4$$

$$\gamma_a^* = \gamma(1 + 2K_d C_a^0 \gamma_a) \qquad 5$$

$$\gamma_a = (s / K) C_a^{0-1} \qquad 6$$

$$K = (\gamma_a^{0*} C_a^0)^{-1} + 2K_d \qquad 7$$

where $\gamma_a^{0\,*}$ denotes the γ_a^* at the intersection point. Using Eqn.3, 5 and 6 the value of γ_a^* was calculated and plotted against the p (P/D) at constant C_a^0. From the intercept on the p axis of the common limiting straight line for small p, we obtained g = 0.72 for PD6/PY system (Figure A.5.a) and 0.76 for PD4coPD6/PY (Figure A.5.a). From the value of γ_a^* of the intersection point of the experimental curve and the auxiliary curve line with the half of the slope of the first one in the figure the value of K (cooperative binding constant) was determined as 6.4 x 10^6Lmol^{-1} (using Eqn.7)

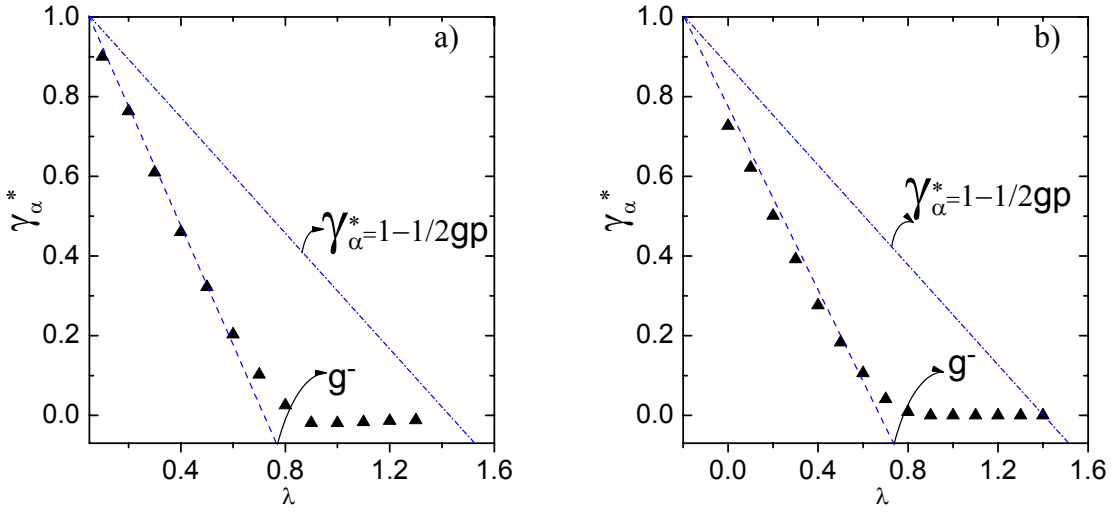

Figure A.5. a) PD6-PY system, b) PD4coPD6-PYsystem: fraction of free dye (γ_α^*) as a function of polymer to dye ratio (p).

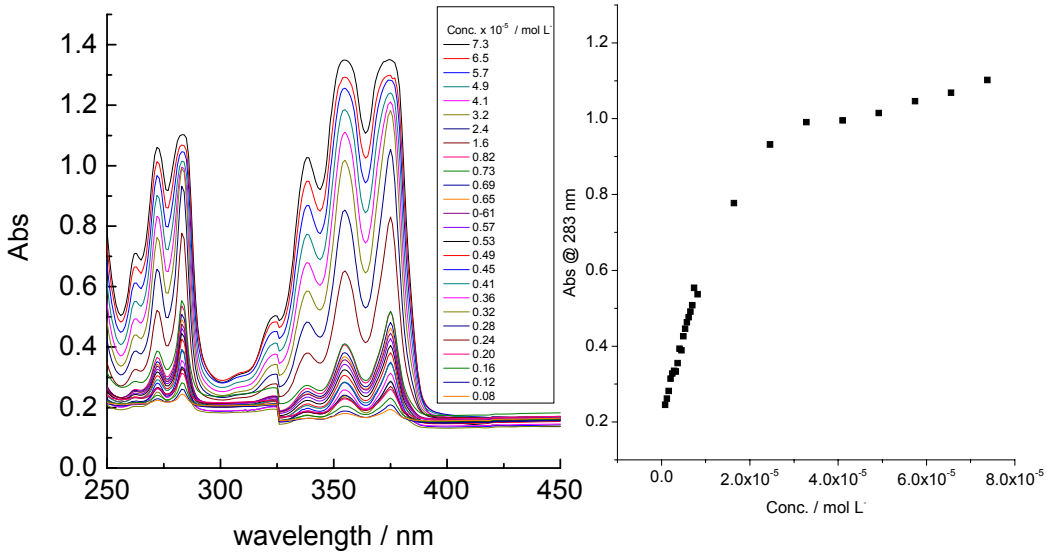

Figure A.6. Concentration dependent absorption spectrum of PY dye in aqueous solution

Light Scattering Supplement

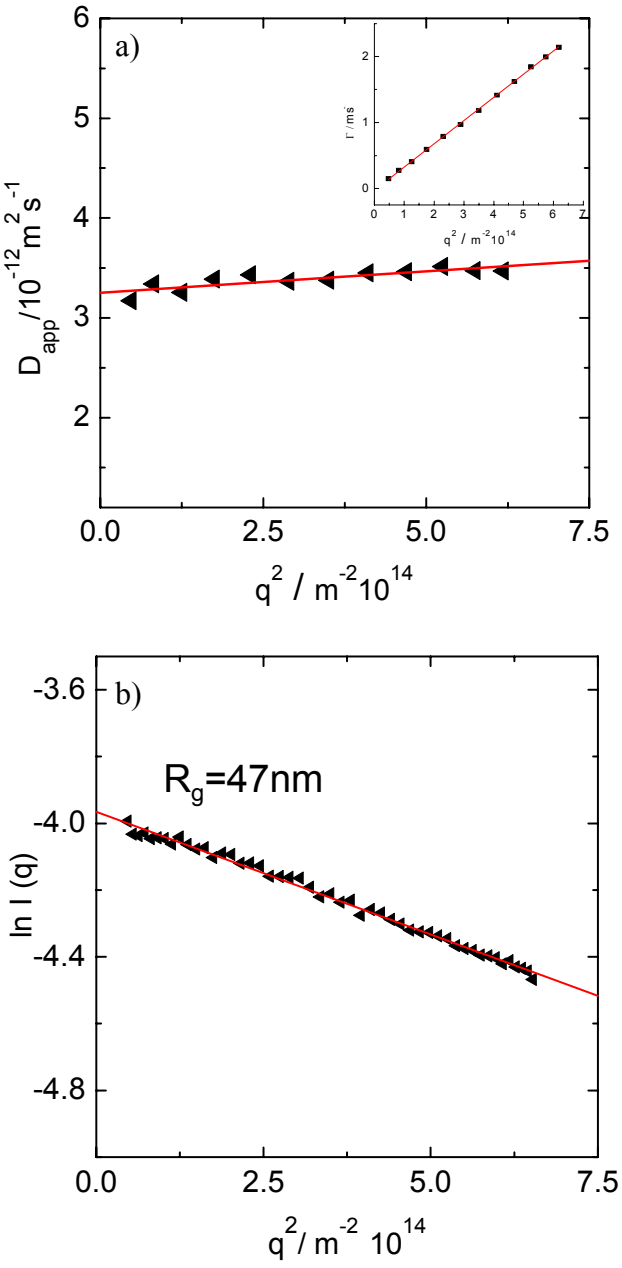

Figure A.7. a) Diffusion coefficients of PD4-PY complexes at as a function of scattering vector square at λ = 0.1 b) Guinier plot of PD4-PY at λ = 0.1.

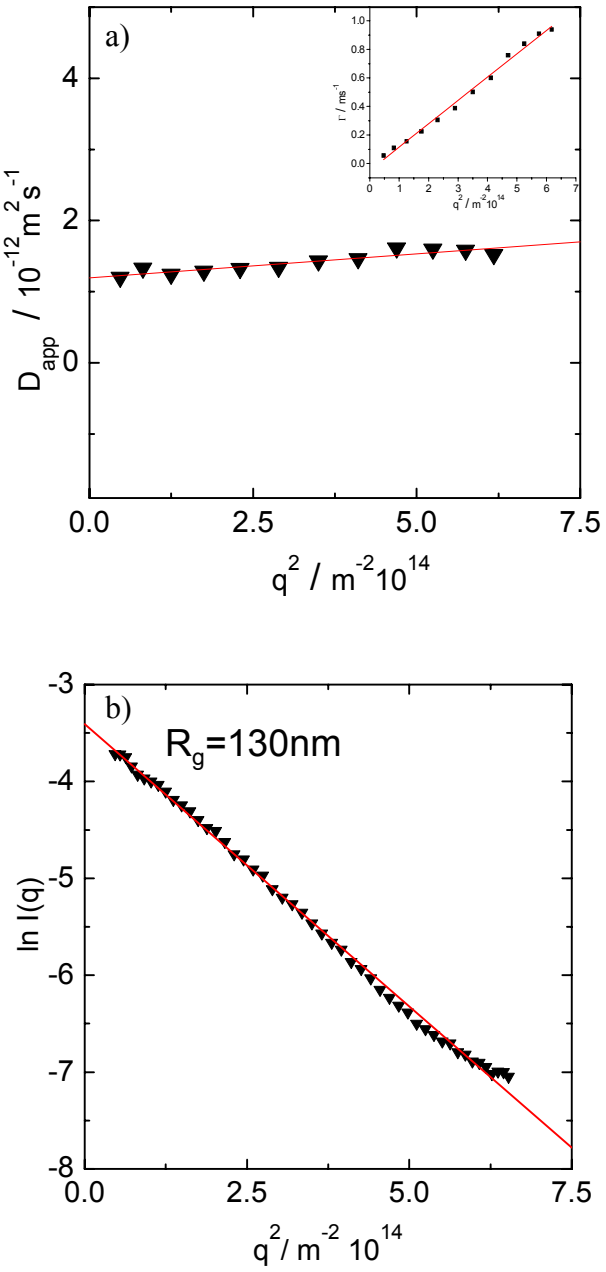

Figure A.8. a) Diffusion coefficients of PD4-PY complexes at as a function of scattering vector square at λ = 0.3 b) Guinier plot of PD4-PY at λ = 0.3.

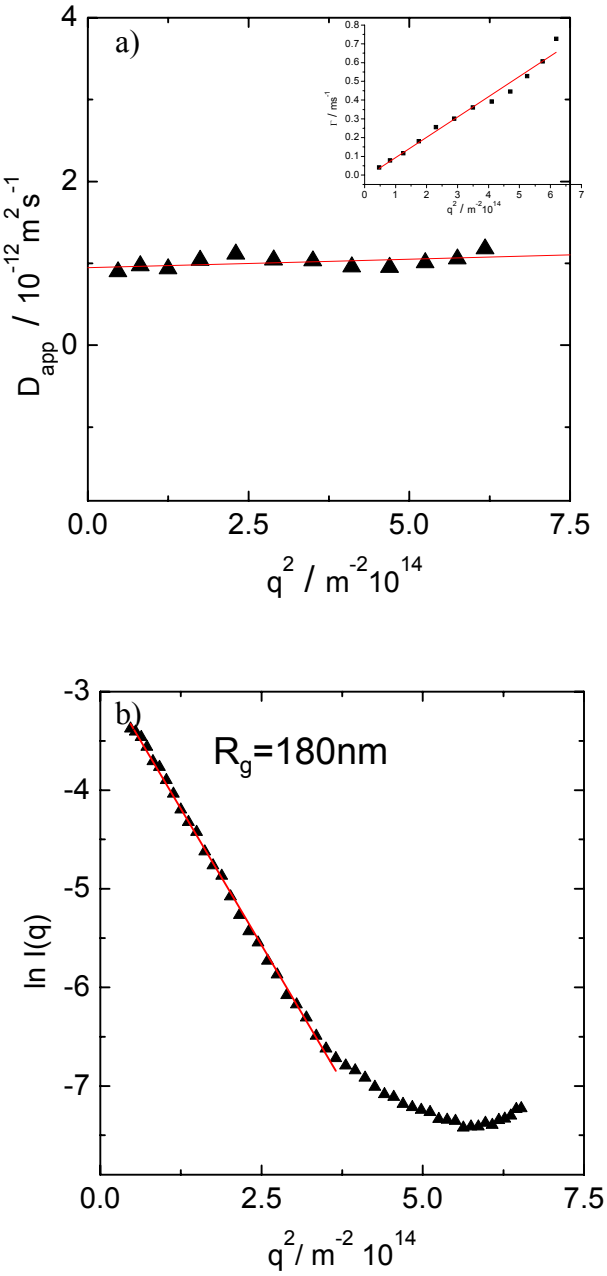

Figure A.9. a) Diffusion coefficients of PD4-PY complexes at as a function of scattering vector square at λ = 0.5 b) Guinier plot of PD4-PY at λ = 0.5.

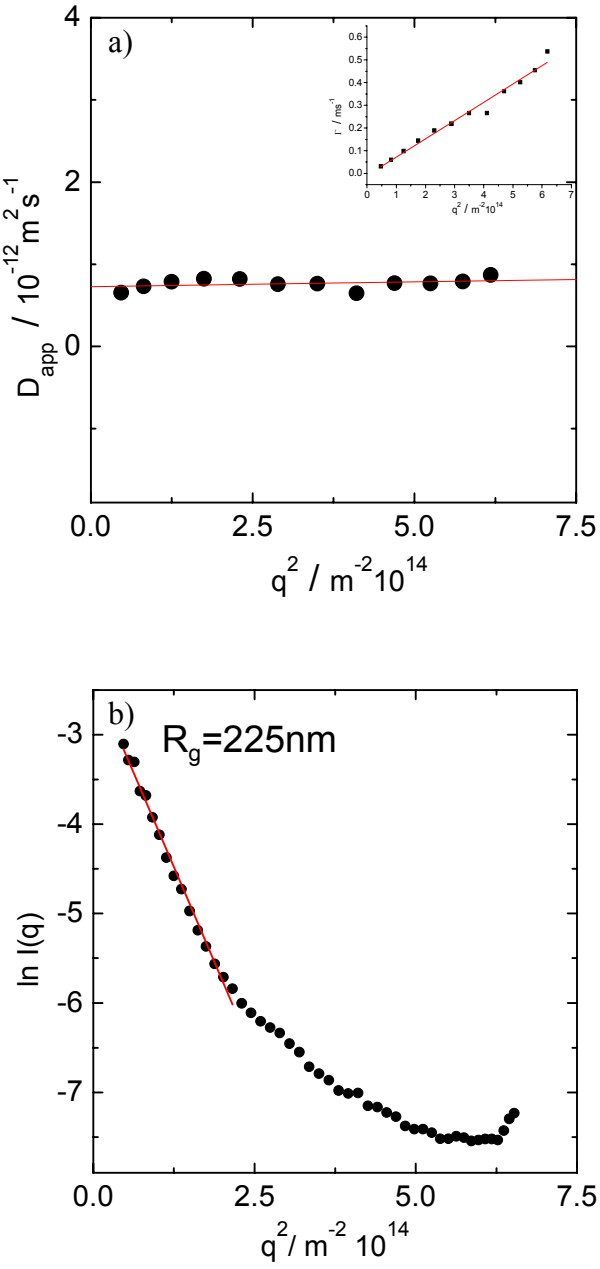

Figure A.10. a) Diffusion coefficients of PD4-PY complexes at as a function of scattering vector square at λ = 0.7 b) Guinier plot of PD4-PY at λ = 0.7.

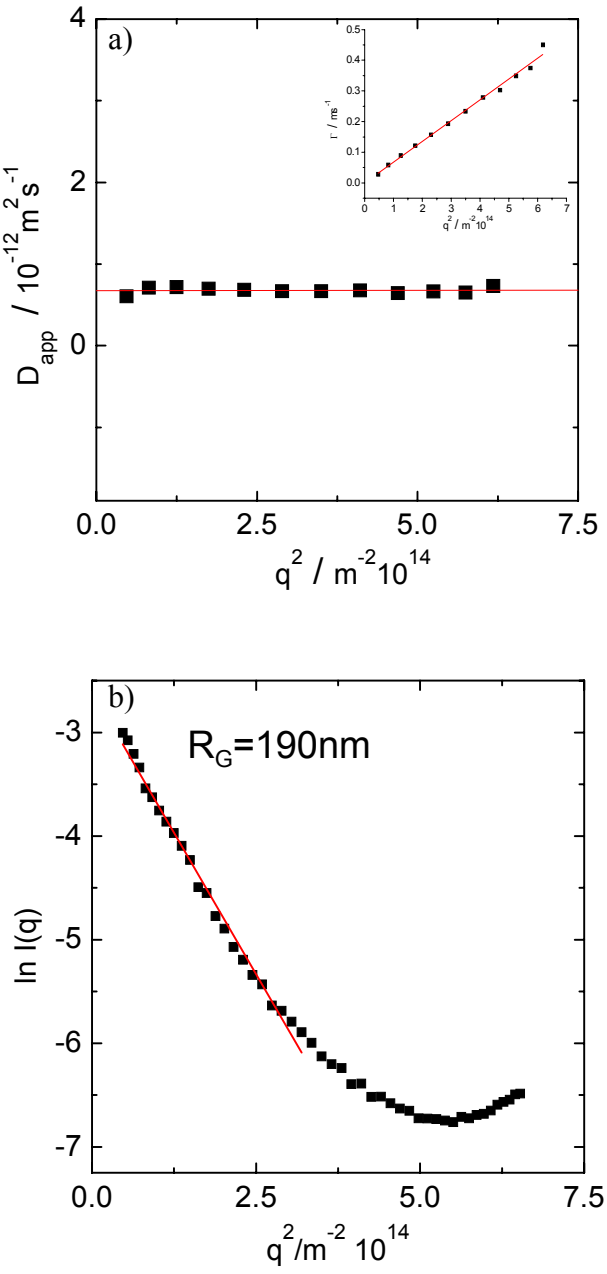

Figure A.11. a) Diffusion coefficients of PD4-PY complexes at as a function of scattering vector square at λ = 1.0. b) Guinier plot of PD4-PY at λ = 1.0

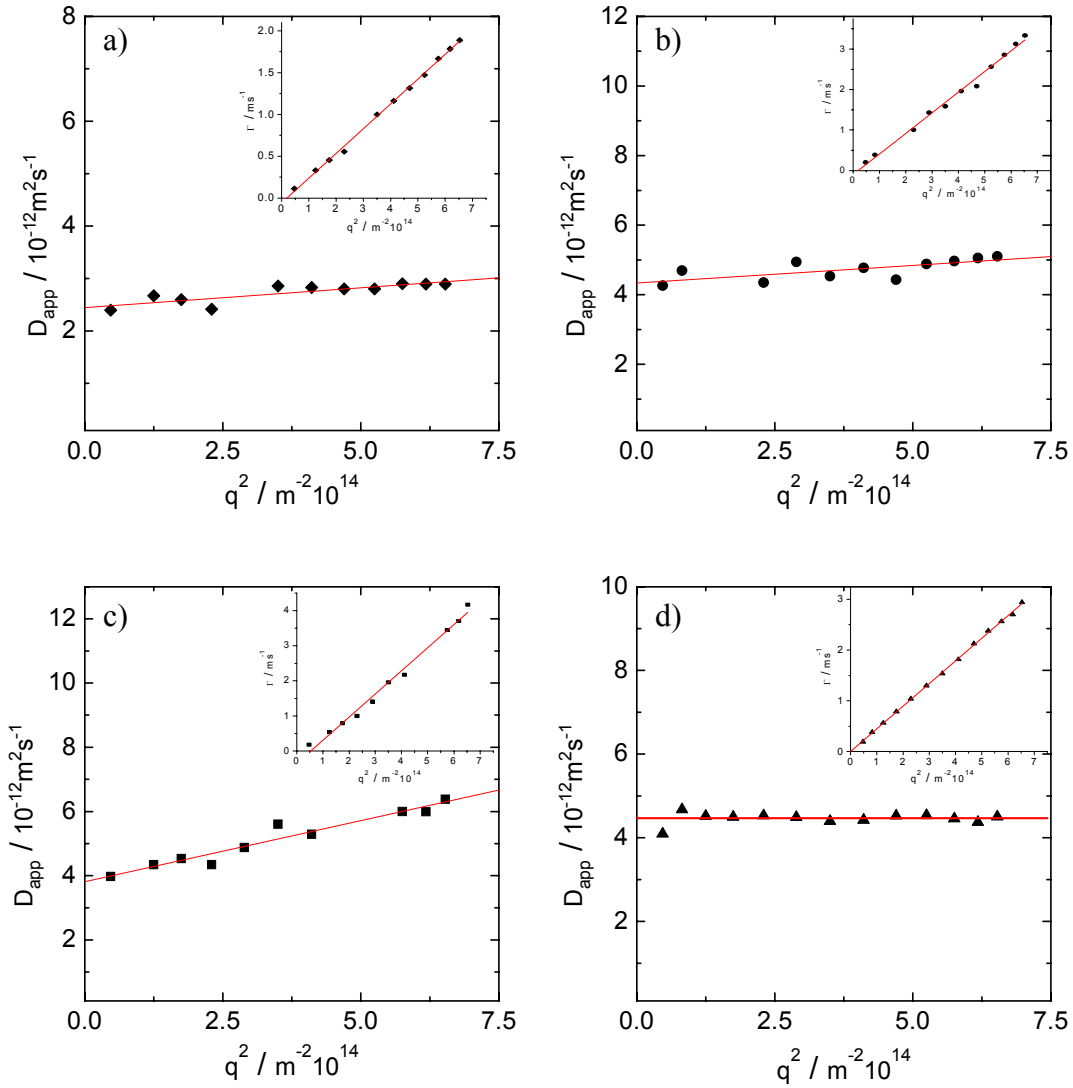

Figure A.12. a) Diffusion coefficients of PD4-PY complexes at as a function of scattering vector square at various λ. a) λ = 1.1, b) λ = 1.5, c) λ = 1.2, d) λ = 2.0

8 References

1. *Intermolecular and Surface Forces: With Applications to Colloidal and Biological Systems* Israelachvili, Jacob *N.* Elsevier Science & Technology Books,**1992**
2. Tanford, Charles. *The Hydrophobic Effect: Formation of Micelles and Biological Membranes*. New York, NY: John Wiley & Sons Inc. **1973**
3. Z. Y. Ou and M. Muthukumar, *J. Chem. Phys* **2006***, 124*, 154902 .
4. Willerich, I.; Groehn, F. Chemistry--A European Journal **2008,** 14(30)
5. Groehn, F.; Klein, K.; Brand, S. Chemistry--A European Journal **2008**, 14(23), 6866-6869
6. Li Y, Yildiz, U. H.; Müllen, K.; Gröhn, F. *Biomacromolecules*, **2008**, accepted
7. Ushio, H.; Yasunaga, T.; Sano, T.; Tsuji, Y. *Bioploymers*, **1976**, *15*, 187-201.
8. Horn, D. *Prog. Colloid Polym. Sci.* **1978,** *65,* 251-264.
9. Tscharner, V.; Schwarz, G. *Biophys. Struct. Mechanism* **1979**, *5*, 75-90.
10. Handel, T. M.; Cohen, H. L.; Tan, J. S. *Macromolecules* **1985**, *18*, 1200-1206.
11. Vishalakshi, B. *J. Polym. Sci., Polym. Chem. Ed.* **1995**, *33*, 365-371.
12. Kossel, A. Hoppe Seiler's *Z Physiol. Chem.* **1896,** *22,* 176
13. Willststaetter, R.; Rohdewald, M. *Hoppe Seiler's Z Physiol. Chem.* **1934**, *225*, 103
14. Michaels A. S.; Mieakka, R. G.; *J. Phys. Chem.* **1961,** *65*, 1765.
15. Michaels A. S.; Mir, I.; Schneider, N. S. *J. Phys. Chem.* **1965,** *69*, 1447.

16. Thünemann, A. *Prog. Polym Sci.* **2002**, *27*, 1473.

17. Ober, C. K.; Wegner, G. *Adv. Mater*. **1997**, *9*, 17.

18. Antonietti, M.; Thünemann, A. *Current Opinion In Colloid & Interface Sci.* **1996** *21*, 319

19. Zhou, S.; Chu, B. *Adv. Mater*. **2000**, *12*, 545.

20. MacKnight W. J.; Ponomarenko, E. A.; Tirrel, D. *A. Acc. Chem. Res.* **1998**, *31,* 781

21. Faul, C.; Antonietti, M. *Adv. Mate*r. **2003**, *15*, 673.

22. Antonietti, M.; Henke, S.; Thünemann, A. *Adv. Mater*. **1996**, *8*, 41.

23. Bertrand, P.; Jonas, A.; Laschewsky, A. *Macromol. Rapid. Comm*. **2000,** *21*, 319.

24. Radtchenko, I. L.; Sukhorukow, G. B.; Mohwald, H. *Colloids & Surfaces A-Physico-chemical & Engineering Aspects,* **2002**, *202,* 127

25. Caruso, F. *Adv. Mater.* **2001,** *13,* 11

26. Antonietti, M.; Conrad, J.; Thünemann, A. *Macromolecules* **1994**, *27,* 6007.

27. Hayakawa, K.; Kwak, J. C. T. *J. Phys. Chem*. **1982**, *86*, 3866

28. Hayakawa, K.; Kwak, J. C. T. *J. Phys. Chem*. **1983**, *87*, 506

29. Tsuchide, E.; Osada, E.; Samada, K. *J.Polym. Sci. A1,* **1972**, 3397.

30. Tsuchide, E.; Osada, E.; Ohno, H. *Macrom. Sci.* **1980**, *B17*, 683.

31. Kabanov, V. A. *Macromolecular Complexes in Chemistry and Biology,* ed. By Dubin, P. et al.; Springer Verlag Berlin, New York, **1994**, *Chapter 10*, 151.

32. Kabanov, V. A.; Zezin, A. B. *Macromol. Chem. Suppl.* **1984**, *10*, 259

33. Dautzenberg, H. *Physical Chemistry of Polyelectrolytes, Surfactant science series, Vol. 99* T. Radeva, Ed., Marcel Dekker, Inc. **2001**, p.743

34. Philipp, B.; Dawydoff, W.; Linow, K. J. *Zeitschrift fur Chemie* **1982**, *22*, 1

35. Goddard, E. D. *Colloid and Surfaces* **1986**, *19*, 301

36. Antonietti, M.; Burger, C.; Effing, J. *Adv. Mater*. **1995**, *7*, 751.

37. Antonietti, M.; Burger, C.; Conrad, J.; Kaul, A. *Macromol. Symp.* **1996**, *106*, 1.

38. Thünemann, A. F.; Schnoller, U.; Nuyken, O.; Voit, B. *Macromolecules* **1999**, *32*, 7414.

39. Thünemann, A. F.; Schnoller, U.; Nuyken, O.; Voit, B. *Macromolecules* **2000**, *33*, 5665.

40. Thünemann, A. F.; Ruppelt, D; Burger, C.; Mullen, K. *J. Mater. Chem.* **2000**, *10*, 13.

41. Thünemann, A. F.; General, S. *Macromolecules* **2001**, *34*, 6978.

42. Ruokolainen, J.; Makinen, R.; Torkkeli, M.; Makela, T.; Serimaa, R.; Tenbrinke, G.; Ikkala, O. *Science* **1998**, *280*, 557.

43. Hayakawa, K.; Kwak, J.C.T In *Cationic Surfactants*; Rubingh, D. N., Holland, P. M., Eds.; Marcel Dekker; New York, **1991**; p 189

44. Goddard, E. D. In *Interactions of Surfactants with Polymers and Proteins*; Goddard E.D., Ananthapadamananabham, K. P., Eds.; CRC Press, Boca Raton, FL, **1993**; p 171.

45. Bloor, D. M.; Wan-Yunus, W. M. Z.; Wan-Bandhi, W. A.; Li, Y.; Holzwarth, J. F.; Wyn-Jones, E. *Langmuir* **1995**, *11*, 3395.

46. Bloor, D. M.; Li, Y.; Wyn-Jones, E. *Langmuir* **1995**, *11*, 3378.

47. Olofsson, G.; Wang, G. *Pure Appl. Chem.* **1994,** *66*, 527.

48. Wang, G.; Olofsson, G. *J. Phys. Chem.* **1995**, *99*, 5588.

49. Fox, G. J.; Bloor, D. M.; Holzwarth, J. F.; Wyn-Jones, E. *Langmuir* **1998**, *14*, 1026

50. Seng, W. P.; Tam, K. C.; Jenkins, R. D.; Bassett, D. R. *Macromolecules* **2000**, *33*, 1727

51. Seng, W. P.; Tam, K. C.; Jenkins, R. D.; Bassett, D. R. *Langmuir* **2000**, *16*, 2151

52. Persson, K.; Wang, G.; Olofsson, G. *J. Chem. Soc. Faraday Trans*. **1994**, *90,* 3555.

53. Thuresson, K.; Nystorm, B.; Wnag. G.; Lindmann, B. *Langmuir* **1995**, *11*, 3730.

54. Fares, H.; De Schryver, F. C.; Sein, A.; Bijma, K.; Kevelam, J.; Engberts, J. B. F. N. *Macromolecules* **1996**, *29*, 3873.

55. Wang, Y.; Han, B.; Yan, H.; Kwak, J. C. T. *Langmuir* **1997,** *13*, 3119.

56. Wang, C.; Tam, K. C. *Langmuir* **2002**, *18*, 6484.

57. Wang, M.; Silva, G. L.; Armitage, B. *J. Am. Chem. Soc*. **2000**, *122*, 9977.

58. Xie, A.; Liu, B.; Hall, J.; Barron, S.; Higgins, D. *Langmuir* **2005**, *21*, 4149.

59. Xiao, S.; Lu, X.; Lu, Q.; Su, B. *Macromolecules* **2008**, *41*, 3884-3892.

60. Ma, T.; Li, C.; Shi, G. *Langmuir* **2008**, *24*, 43.d) Chen, J.; Dong,W.;

61. Möhwald, M.; Krastev, R. *Chem. Mater*. **2008**, *20*, 1664.

62. Peyratout, C.; Donath, E.; Daehne, L. *J. Photochem. Photobiol. A.* 2001, *142*, 51

63. Wang, L.; Wang, X.; Xu, M.; Chen, D.; Sun, J. *Langmuir* **2008**, *24*, 1902.

64. Qi, B.; Tong, X.; Zhao, Y. *Macromolecules* **2006**, *39*, 5714.

65. Rousseau, E.; Van der Auweraer, M.; De Schryver, F. C. *Langmuir* **2000**, 16, 8865

66. Kometani, N.; Nakajima, H.; Asami, K.; Yonezawa, Y.; Kajimoto, O. *J. Phys. Chem.B* **2000**, 104, 9630.

67. Peyratout, Claire S.; Daehne, Lars. *Angew. Chem. Int. Ed.* **2004**, *43*, 3762

68. Mano, Joao F. *Adv. Eng. Mater.* 2008, *10*, 515.

69. Ai, Hua; Jones, Steven A.; Lvov, Yuri M. *Cell Biochem. Biophys.* **2003**, *39*, 23.

70. Liu, B.; Bazan, *Proc. Natl. Acad. Sci.USA* **2005** *102*, 589

71. Liu, B.; Bazan, G. C. *Chem. Mater.* **2004**, *16*, 4467

72. Buey, J.; Swager, T.M *Angew. Chem. Int. Ed*. **2000** *39*, 608

73. Cacialli, F. et al. *Nat. Mater*. **2002**, *1*, 160.

74. Li, C.; Numata, M.; Bae, A.-H.; Sakurai, K.; Shinkai, S. *J. Am. Chem. Soc*. **2005**, *127*, 4548

75. Morikawa, M.; Yoshihara M.; Takeshi, E.; Kimizuka, N. *J. Am. Chem. Soc*. **2005**, *127*, 1358.

76. Sakai, N.; Sisson, A. L.; Bürgi, T.; Matile, S *J. Am. Chem. Soc*. **2007**, *129*, 15758.

77. Sisson, A. L.; Sakai, N.; Banjeri, N.; Fürstenberg, A.; Matile, S. *Angew Chem. Int. Ed*. **2008** *47*, 3727

78. Schwarz, G.; Klose, S.; Balthasar, W. *Eur. J. Biochem*. **1970**, *12*, 454.

79. Littmann, E., R.; Marvel, C., S.; *J. Am. Chem. Soc.* **1930**, *52*, 287.

80. Gibbs, C. F.; Littmann, E., R.; Marvel, C., S.; *J. Am. Chem. Soc.* **1933**, *55*, 753.

81. N. Menschutkin, *Z. Phys. Chem Steochem Verwandtschaftsl*. **1890,** *5*, 589

82. N. Menschutkin, *Z. Phys. Chem Steochem Verwandtschaftsl*. **1890,** *6*, 41

83. Casson, D.; Rembaum, A. *Macromolecules* **1972,** *5*, 75.

84. Noguchi, N.; Rembaum, A. *Macromolecules* **1972**, *5*, 253.

85. Rembaum, A.; Noguchi, N. *Macromolecules* **1972**, *5*, 261.

86. Parker, A. J. *J. Chem. Soc.* **1961**, 4396.

87. Ross, S. D.; Barry, J. E.; Peterson, P. C. *J. Am. Chem. Soc.* **1961**, *83*, 2133.

88. Parker, A. J. *Adv. Phys. Org. Chem.* **1967**, *5*, 173.

89. Brown, H. C.; Eldred, N. R. *J. Am. Chem. Soc.* **1949**, *71*, 2133.

90. Bird, M. L.; Hughes, C. D.; Ingold, C.K. *J. Chem. Soc.* **1954**, 634.

91. Laidler, K. J.; Hinshelwood, C. N. *J. Chem. Soc.* **1938**, 858.

92. Ando, T.; Tanabe, H.; Yamataka, H. *J. Am. Chem. Soc.* **1984**, *106*, 3094.

93. Davis, R. E. *J. Am. Chem. Soc.* **1965**, *87*, 3010.

94. Katritzky, A. R.; Tarr, S. M.; Rasmussen, J. K. and Krepski, L. R. *J. Polym. Sci. Poly. Chem. Ed.* **1988**, *26*, 3323.

95. H. Shirakawa, E.J. Louis, A.G. MacDiarmid, C.K. Chiang, A.J. Heeger, *J. Chem. Soc. Chem. Commun*. **1977**, 578.

96. C.K. Chiang, C.R. Fischer, Y.W. Park, A.J. Heeger, H. Shirakawa, E.J. Louis, S.C. Gau, A.G. MacDiarmid, *Phys. Rev. Letters*, **1977,**39 1098.

97. G. Wegner, *Angewandte Chemie* **1981,**20, 361.

98. A.F. Diaz, *Chem. Scr*. 17 1981 142.

99. G. Tourillon, F.J. Garnier, *J. Electroanal. Chem.* **1982**, 135, 173.

100. A.F. Diaz, K.K. Kanazawa, G.P. Gardini, *J. Chem. Soc., Chem. Commun.* **1979** 635.

101. G. Grem, G. Leditzky, B. Ullrich, G. Leising, *Adv. Mater*. **1992,** 4, 36.

102. J.H. Burroughes, D.D.C. Bradley, A.R. Brown, R.N. Marks, K. MacKay, R.H. Friend, P.L. Burn, A.B. Holmes, *Nature* **1990** ,347, 539.

103. J. Rault-Berthelot, J. Simonet, *J. Electrochem. Soc.* **1985,**182, 187.

104. A.G. MacDiarmid, A.J. Epstein, *Faraday Discuss. Chem. Soc*. **1989,** 88, 317.

105. Ruini, F. Rossi, U. Hohenester, E. Molinari, R.B. Capaz, and M.J. Caldas, *Synthetic Metals*, **2001**, 119, 257.

106. D. Kumar, R.C. Sharma, *Eur. Polym. J.*, **1998,** 34, 1053.

107. J. A. Rogers, Z. Bao, V. R. Raju, *Appl. Phys. Lett*., **1998,** 72 2716.

108. N. Toshima, O. Ihata, *Synth. Me*t. **1996,** 79 165-172.

109. H. Yan, M. Kajita, N. Toshima, *Macromol. Mater. Eng*. **2002,**287 503-508.

110. Z.C. Sun, Y. H. Geng, J. Li, X. H. Wang, X. B. Jing, F. S. Wang, *J. Appl. Polym. Sci*., **1999**, 72 1077-1084.

111. J. Roncali, *Chem. Rev*., **1992** ,92, 711.

112. Huglin, M. B. *Light Scattering from polymer solutions* Academic Press London and New York, **1972**

113. McIntyre, D. and Gornick F. *Light Scattering from polymer dilute solutions***,** Gordon and Breach, New York and London. **1964**

114. Kratochvil, P. *Classical light scattering from polymer solutions*, Elsevier, Amsterdam **1987**,

115. Burchard, W. *Macromol. Chem. Makromol Symp*. **1988**, *18*, 1

116. Berne, B. J. and Percora, R. *Dynamic light scattering.* Wiley*,* NewYork **1976**

117. Chu, B. Laser light scattering. Academic Press, New York **1974**

118. Cummins, H. Z. and Pike, E. R. Photon correlation spectroscopy and light beating spectroscopy. Plenum Press London and New York, **1974**

119. Schmitz, K. S. Dynamic light scattering by macromolecules Academic Press New York, **1990**

120. Schmidt, M. Dynamic light scattering the method and some applications, chapter 8 p.372-406 edited by Brown, W. Clarendon Press Oxford **1993**

121. Burchard, W., Schmidt, M., Stockmayer, W. H., *Macromolecules* **1980**, *13*, 1265

122. Casson, D.; Rembaum, A. *Macromolecules* **1972**,*5*, 75.

123. Noguchi, N.; Rembaum, A. *Macromolecules* **1972**, *5*, 253.

124. Rembaum, A.; Noguchi, N. *Macromolecules* **1972**,*5*, 261.

125. Salamone, J, C.; Snider, B. *J. Polym. Sci., Part A: Polym. Chem. Ed.* **1970**, *8*, 3495.

126. Wang, J.; Meyer, H.; Wegner, G. *Macromol. Chem. Phys.* **1994**, *195*, 1777

127. Tscharner, V.; Schwarz, G. *Biophys. Struct. Mechanism* **1979**, *5*, 75.

128. Ushio, H.; Yasunaga, T.; Sano, T.; Tsuji, Y. *Bioploymers*, **1976**, *15*, 187.

129. Vishalakshi, B. *J. Polym. Sci., Polym. Chem. Ed.* **1995**, *33*, 365.

130. Handel, T. M.; Cohen, H. L.; Tan, J. S. *Macromolecules* **1985**, *18*, 1200.

131. Trukhanova, E. S.; Litmanovich, A. A.; Paraschuck, V. V.; Sybatchin, A. V.; Izumrudov, V. A. *Macromolecules* **2003**, *36*, 2066.

132. Thalberg, K.; Lindman, B. in *Surfactants in Solutions*; *Vol: 11* Mittal, K. L. Ed.; Plenum: New York, **1991**.

133. Behr, J. P. *Bioconjugate Chem.* **1994**, 5, 382

134. Kabanov, A. V.; Kabanov, V. A. *Biocojugate Chem.* **1995**, *6*, 7.

135. Izumrudov, V. A.; Bronich, T. K.; Saburova, O. S.; Zezin, A. B.; Kabanov, A. V. *Macromol. Chem. Rapid Commun*. **1988**, *9*, 7

136. Gao, X.; Huang, L. *Gene Ther.* **1995,** 2, 710

137. Monkkonen, J.; Urtti, A. *Adv. Drug Delivery Rev.* **1998**, *34*, 37.

138. Chen, J.; Dong, W.; Möhwald, H.; Krastev, R. *Chem. Mater*. **2008**, *20*, 1664.

139. Beyer, S.; Mak, W. C.; Trau, D. *Langmuir* **2007**, *23*, 8827.

140. Yan, Y.; Besseling, N. A. M.; de Keizer, A.; Marcelis, A. T. M.; Drechsler, M.; Stuart, M. A. C. *Angew Chem. Int. Ed*. **2007**, *46*, 1807.

141. Yu, C.; Wang, K.M.C.; Chan, K.H.Y.; Yam, V. W-W. *Angew Chem. Int. Ed*. **2005** *44*, 791

142. Dähne, L.; Leporatti, S.; Donath, E.; Möhwald, H. *J. Am. Chem. Soc*. **2001**, *123*, 5431.

143. Kurth, D. G.; Caruso, F.; Schuler, C. *Chem. Comm*. **1999**, *16*, 1579.

144. Winnik, M. F. *Chem. Rev.* **1993**, *93*, 587.

145. Todesco, R. V.; Basheer, R. A.; Kamat, P. V. *Macromolecules* **1986**,*19*, 2390

146. Yamazaki, I.; Winnik, F.; Winnik, M. A.; Tazuke, S. *J.Phys. Chem.* **1987,** *91*, 4213

147. Winnik, F.; Winnik, M. A.; Tazuke, S. Ober, C. K. *Macromolecules* **1987**,*20*, 38.

148. Caruso, F.; Donath, E.; Möhwald, H.; Georgieva, R. *Macromolecules* **1998**, *31*, 7365.

149. Stramel, R. D.; Nguyen, C.; Webber, S. E.; Rodgers, M. A. *J.Phys. Chem.* **1988,** *92*, 2934

150. Herkstroeter, W. G.; Matric, P. A.; Hartmann, S. E.; Williams, J. L. R.; Farid, S. *J. Polym. Sci. Part A : Polym. Chem.Ed.* **1983**, *21*, 2473.

151. de Melo, S. S.; Costa, T.; Oliveira, N.; Schillen, K. *Polym. Int.* **2007**, *56,* 882.

152. Schillen, K, Anghel, D. F.; Miguel, M. G.; Lindman, B. *Langmuir* **2000**, *16*, 10528.

153. Thünemann, A.; General S. *Journal of Controlled Release* **2001**, *75*, 237

154. Zheng, G.; Pan, C. *Macromolecules* **2006**, *39*, 95.

155. Matejicek, P.; Uchman, M.; Lokajova, J.; Stepanek, M.; Prochazka, K.; Spirkova, M. *J. Phys. Chem. B* **2007**, *111*, 8394

156. Li, X.; Ji, J.; Shen, J. *Macromol. Rapid Commun.* **2006**, *27*, 214

157. Jada, A.; Hurtrez, G.; Siffert, B.; Riess, G. *Macromolec. Chem. Phys.* **1996**, *197*, 3697.

158. Yang, M.; Wang, W.; Yuan, F.; Zhang, X. W.; Li, J. Y.; Liang, F. X.; He, B. L.; Minch, B.; Wegner, G. *J. Am. Chem. Soc*. **2005**, *127*, 15107.

159. Regenbrecht, M.; Akari, S.; Förster, S.; Möhwald, H. *Surf. Interface Anal.* **1999**, *27*, 418.

160. Kunz, D.; Thurn, A.Burchard, W. *Colloid&Polymer Sci.* **1983**, *261*, 635.

161. J.H. Burroughes, D.D.C. Bradley, A.R. Brown, R.N. Marks, K. MacKay, R.H. Friend, P.L. Burn, A.B. Holmes, *Nature* **1990** ,347, 539.

162. Sariciftci, N. S.; Smilowitz ,L.; Heeger, A. J. and Wudl ,F. *Science* **1992**, *258*, 1474.

163. Gelinck, G. H.; Geuns, T. C. T. and de Leeuw, D. M. *Applied Phys. Lett*. **2000**, *77*, 1487.

164. Donat-Bouillud, A.; Mazerello, L.; L.; Gagnon, P.; Goldenberg, L.; Petty, M. C.; Leclerc, M. *Chem. Mater.* **1997**, *9,* 2815.

165. Langeveld-Voss, B. M. W.; Janssen, R. A. J.; Christiaans, M. P. T.; Meskers, S. C. J.; Dekkers, H. P. J. M.; Meijer, E. W. *J. Am. Chem. Soc.;* **1996**, *118*, 4908.

166. Klok, H.A.; Lecommandoux, S. *Adv. Mater*. **2001**, *13*, 1217.

167. Liu, J.; Sheina, E.; Kowalewski, T.; McCullough, R. D. *Angew. Chem. Int. Ed.* **2002** *41*, 329

168. Wang, H.; Wang, H. H.; Urban,V. S.; Littrell, K. C.; Thiyagarajan, P.; Yu, L. P. *J. Am. Chem. Soc.* **2000**, *122*, 6855.

169. Thuenemann, A. F.; Kubowicz, S.; Burger, C.; Watson, M. D.; Tchebotareva, N.; Muellen, K. *J. Am. Chem. Soc*, **2003**, *125*, 352.

170. Canilho, N.; Kasemi, E.; Mezzenga, R.; and Schluter, D. *J. Am. Chem. Soc.* **2006**, *128*, 13998.

171. Buey, J.; Swager, T. M.; *Angew. Chem. Int. Ed.* **2000**, *39*, 608

172. Li, C.; Numata, M.; Bae, A.-H.; Sakurai, K.; Shinkai, S. *J. Am. Chem. Soc*. **2005**, *127*, 4548.

173. Cacialli, F. et al. *Nat. Mater*. **2002**, *1*, 160.

174. Bjork, P.; Herland A.; Scheblykin, I. G.; Inganas, O. *Nano Lett*. **2005**, *5*, 1948.

175. Nillson, K. P. R.; Inganas, O. *Nat. Mater*. **2003**, *2*, 419

176. Li, C.; Numata, M.; Bae, A.-H.; Sakurai, K.; Shinkai, S. *J. Am. Chem. Soc*. **2005**, *127*, 4548.

177. Hoang-Anh, H.; Boissinot, M.; Bergeron, M. G.; Corbeil, G.; Doré, K.; Boudreau, D.; Leclerc, M. *Angew. Chem. Int. Ed.* **2002**, *41*, 1548

178. Lukkari, J.; Salomaki, M.; Viinikanoja, A.; Aaritalo, T.; Paukunnen, J.; Kocharova, N.; Kankare, J. *J. Am. Chem. Soc*, **2001**, *123*, 6083.

179. Leclerc M. *Adv. Mater*. **1999**, *11*, 1491

180. Leclerc, M. and Faid, K. *Hand Book of Conducting Polymers 2nd ed*. Marcel Dekker; New York; **1997**, 695-706

181. Kim B.S. *European Polymer Journal* **2001**; Greve D.R. *Synthetic Metals* 1999

182. Cacialli, F. et al. *Nat. Mater.* **2002**,*1*,160.

183. McIntire, T. M.; Brant, D. A. *J. Am. Chem. Soc*. **1998**, *120*, 6909.

184. Nakajima, A.; Sato, H. *Colloid & Polymer Sci.* **1974**, *252*, 294

185. Glatter, O. *J. Appl. Crystallogr.* **1977,** *10,* 415-421.

186. Glatter, O. *J. Appl. Crystallogr.* **1980,** *13,* 577-584.

187. Lindner, P., Zemb, T., Eds. Neutrons, X-rays, and Light: Scattering Methods Applied to Soft Condensed Matter; Elsevier: Amsterdam, 2002.